Alma Mater Studiorum
Università degli Studi di Bologna

Scuola di Scienze

Corso di Laurea Magistrale in Astrofisica e Cosmologia

Dipartimento di Fisica e Astronomia

Asymmetric drift and halo flattening in disk galaxies: analytical models

Elaborato finale

Candidato:
Christophe Smet

Relatore:
Chiar.mo Prof. Luca Ciotti

Co-relatore:
Silvia Posacki

Sessione I
Anno Accademico 2013-2014

Abstract/Sommario

Abstract

The main result in this work is the solution of the Jeans equations for an axisymmetric galaxy model containing a baryonic component (distributed according to a Miyamoto-Nagai profile) and a dark matter halo (described by the Binney logarithmic potential).

The velocity dispersion, azimuthal velocity and some other interesting quantities such as the asymmetric drift are studied, along with the influence of the model parameters on these (observable) quantities. We also give an estimate for the velocity of the radial flow, caused by the asymmetric drift.

Other than the mathematical beauty that lies in solving a model analytically, the interest of this kind of results can be mainly found in numerical simulations that study the evolution of gas flows. For example, it is important to know how certain parameters such as the shape (oblate, prolate, spherical) of a dark matter halo, or the flattening of the baryonic matter, or the mass ratio between dark and baryonic matter, have an influence on observable quantities such as the velocity dispersion.

In the introductory chapter, we discuss the Jeans equations, which provide information about the velocity dispersion of a system. Next we will consider some dynamical quantities that will be useful in the rest of the work, e.g. the asymmetric drift. In Chapter 2 we discuss in some more detail the family of galaxy models we studied. In Chapter 3 we give the solution of the Jeans equations. Chapter 4 describes and illustrates the behaviour of the velocity dispersion, as a function of the several parameters, along with asymptotic expansions. In Chapter 5 we will investigate the behaviour of certain dynamical quantities for this model. We conclude with a discussion in Chapter 6.

Sommario

Il risultato principale di questa tesi è la soluzione delle equazioni di Jeans per un modello galattico costituito da una componente barionica (distribuita secondo un profilo di densità Miyamoto-Nagai) e un alone di materia oscura (distribuito secondo il modello di potenziale logaritmico di Binney).

Studiamo la dispersione di velocità, la velocità azimutale e alcune altra quantità interessanti, come l'asymmetric drift. Studiamo inoltre l'influenza dei parametri dei modelli su queste quantità osservabili. Diamo una stima della velocità del radial flow, che è una conseguenza dell'asymmetric drift.

Risolvere un modello analiticamente non ha solo una bellezza matematica. Questi risultati possono essere utili per fare delle simulazioni numeriche. Infatti, è importante sapere come alcuni parametri, per esempio la forma dell'alone (oblato, prolato, sferico), lo schiacciamento del disco o il rapporto tra la massa barionica e oscura, possono avere un'influenza sulle quantità osservabili.

Nel primo capitolo descriviamo le equazioni di Jeans, che danno informazioni sulla dispersione della velocità di un sistema, e consideriamo alcune quantità dinamiche che saranno utili nel resto della tesi, come l'asymmetric drift. Nel Capitolo 2 discutiamo con più dettagli i modelli galattici che abbiamo considerato. Nel Capitolo 3 diamo la soluzione delle equazioni di Jeans per questo modello. Il Capitolo 4 consiste soprattutto di grafici delle quantità trovate come funzione dei parametri, e ci sono anche delle espansione asintotiche. Nel Capitolo 5 guardiamo l'andamento di alcune quantità dinamiche per questo modello. Concludiamo con il Capitolo 6.

Contents

Chapter 1

Introduction

1.1 Preliminaries

Analytical galaxy models are often used as starting points for more elaborate investigations. In general, galaxies are thought of, in first approximation, as systems in equilibrium. The proper approach to describe a (multi-component) collisionless system is to use the phase-space distribution. However, this approach, even though physically based, is in the vast majority of cases quite difficult, due to the need to solve the Poisson equation: this difficulty increases considerably for non-spherical systems. The alternative approach is to use the Jeans equations, i.e. to solve for the first velocity moments of the distribution function, see e.g. [3].

Of course, in this approach there is no guarantee that the distribution function of the model is positive, and often some educated guess is needed to impose the closure relation (for example a prescribed anisotropy).

In the epoch of computers, it is tempting to ask why bother with analytical models of galaxies, when more realistic models could be constructed by using directly numerical methods (or even N-body numerical simulations). The fact is that solvable models, even if quite idealized, offer the unique advantage of a first-hand understanding of the role of parameters and assumptions on the obtained results. These insights can then be used to interpret the more complicated (and realistic) numerical or observational data.

In the literature, there is a quite large number of spherically symmetric galaxy models (one and two-components) with Jeans equations that can be fully solved analytically. This is not a surprise since in this case the describing equations are ordinary differential equations depending only on r. The class of axisymmetric models is by far less populated, and only a handfull of two-component axisymmetric galaxy models are presently known. Some examples are the Miyamoto-Nagai selfgravitating model (see [19] and [18]).

In this work we show that, quite remarkably, the Jeans equations for the

Miyamoto-Nagai model embedded in the Binney logarithmic potential [4] can be solved analytically for general choices of the parameters.

Among the obvious applications of the models (in addition to test numerical codes dedicated to the solution of the Jeans equations), we recognize the possibility to use these models for hydrodynamical simulations of gas flows in early type galaxies, where the knowledge of the stellar velocity fields is fundamental for the description of the thermalisation of the interstellar medium, injected by the stellar feedback [20], [25].

Another simple application is to determine the effects of the relative shape of the stellar and dark matter distribution in disk galaxies on the vertical kinematics of stars. In fact, this quantity is used to infer properties of dark matter near the equatorial plane in our galaxy [26].

Finally, we propose an interesting application of the obtained functions for the asymmetric drift (AD). In general, it is expected (e.g., by chemical evolution studies) that disk galaxies host *radial* flows in their disk. These flows are expected to influence the chemical gradient of stellar populations in the disk, so that from the study of chemical and age gradients in the disk it is expected to gain information on galaxy formation. The problem is *how* such radial flows are sustained. In fact, in case of angular momentum conservation, such flows cannot exist. Various explanations use (for example) gravitational effects due to non-perfect axisymmetry (e.g., bars, spiral arms, etc.) or gas accretion from above and below the disk of material with a smaller specific angular momentum, so that after the mixing the gass falls toward the center (as the angular momentum J of circular orbits in the equatorial plane decreases for decreasing R in stable disks). All these hypotheses are realistic and may be at play. However, one could look also at "inner", more "regular" mechanisms that can lead to radial gas flows. One possibility is represented (in principle) by considering the coupling between stellar mass losses and AD. In fact, at each radius, the gas injected by the stars has (due to AD) a smaller specific J than the gas rotating with the local circular velocity, and this will produce a radial inflow. We use our models to get some quantitative estimates of this effect.

1.2 The Jeans equations and their application in simple models

Galaxies can, in good approximation, be regarded as systems in equilibrium. This equilibrium situation allows the use of the Jeans equations to describe the dynamics of a galaxy. These equations are interesting since they give relations between observationally accessible quantities such as the velocity dispersion components. Here we will merely state the Jeans equations, the derivation, as is done in [4], is given in Appendix A. We give the equations in the particular case of spherical symmetry and in the axisymmetric case.

1.2.1 Spherical case

In spherical coordinates there is only one Jeans equation, most often written as

$$\frac{d(\rho\sigma_r^2)}{dr} + 2\frac{\beta}{r}\rho\sigma_r^2 = -\rho\frac{d\Phi}{dr}, \tag{1.1}$$

where

$$\beta = \frac{2\sigma_r^2 - \overline{v_\varphi^2} - \overline{v_\theta^2}}{2\sigma_r^2} \tag{1.2}$$

is the anistropy parameter, a degree for the radial anisotropy. Since there is only one such equation, it is in general not possible to obtain β and σ_r^2 from a known ρ and Φ: the equations are not closed. In the special case of an ergodic distribution function $f(H)$ however, where H is the Hamiltonian of the system and $H = E$, we know that $\beta = 0$ and the equation can be solved for σ_r.

We give an example of a spherically symmetric model for which the Jeans equation can be solved. The Plummer sphere has potential-density pair

$$\Phi(r) = -\frac{GM_*}{\sqrt{r^2 + b^2}}, \tag{1.3}$$

$$\rho(r) = \frac{3M_*b^2}{4\pi(r^2 + b^2)^{5/2}}. \tag{1.4}$$

It is easily checked that the total mass is indeed given by M_*. The parameter b is a characteristic radius, in the sense that a sphere with radius b and uniform density $\rho(0)$ would have the same mass M_*.

If we assume an ergodic distribution function, straightforward integration of the Jeans equation (1.1) gives

$$\sigma_r^2 = \frac{GM_*}{6\sqrt{r^2 + b^2}}. \tag{1.5}$$

As a second example, we will look at the influence of a central black hole on the velocity dispersion in a galaxy, modelled by a Plummer sphere, this will be done in Section 4.3.

1.2.2 Axisymmetric case

In the axisymmetric case there are two Jeans equations:

$$\frac{\partial\rho_*\sigma^2}{\partial z} = -\rho_*\frac{\partial\Phi}{\partial z} \tag{1.6}$$

and

$$\frac{\partial\rho_*\sigma^2}{\partial R} + \rho_*\frac{\sigma^2 - \overline{v_\varphi^2}}{R} = -\rho_*\frac{\partial\Phi}{\partial R}. \tag{1.7}$$

The derivation of these equations is given in Appendix A.

Notice that in the special case of spherical symmetry, formal integration of eq. (1.6) shows that also σ has spherical symmetry, i.e. $\sigma = \sigma(r)$.

In order to determine the azimuthal velocity we adopt the Satoh [27] k-decomposition

$$\overline{v_\varphi}^2 = k^2(\overline{v_\varphi^2} - \sigma^2), \tag{1.8}$$

and then it follows

$$\sigma_\varphi^2 \equiv \overline{v_\varphi^2} - \overline{v_\varphi}^2 = k^2\sigma^2 + (1-k^2)\overline{v_\varphi^2}, \tag{1.9}$$

where $0 \leq k \leq 1$. This implicitly assumes that the supporting distribution function is a Satoh distribution function $f(E, J_z; k)$. The case $k = 1$ corresponds to the isotropic rotator while for $k = 0$ no net rotation is present and all the flattening is due to the azimuthal velocity dispersion σ_φ. In principle, k can be a function of (R, z), bounded above by the function $k_{\max}(R, z)$, so that $\sigma_\varphi^2 = 0$ [6]. From eq. (1.7) it easily follows that in the spherical limit of a two-integrals distribution function $\overline{v_\varphi^2} = \sigma^2$, and, if in addition the distribution function is of the Satoh family, then the spherical limit is isotropic.

In Chapter 2 we will introduce the Miyamoto-Nagai model and the Binney model. Both are axisymmetric and we will solve the Jeans equations for these models.

Evans [8] used a result by Lynden-Bell [17], which states that the even part of the distribution function can be recovered from $\rho(R, \Phi)$ by a double Laplace inversion. Since the density for this model, obtained from the potential by Poisson's equation, can be written as a function of R and Φ (instead of the usual R and z), this leads to an explicit and remarkably simple form for the distribution function:

$$F(E, J_z^2) = (AJ_z^2 + B)e^{\frac{4E}{v_0^2}} + Ce^{\frac{2E}{v_0^2}} \tag{1.10}$$

with

$$A = \left(\frac{2}{\pi}\right)^{5/2} \frac{1-q^2}{Gq^2v_0^3}, \qquad B = \left(\frac{2}{\pi^5}\right)^{1/2} \frac{R_0^2}{Gq^2v_0}, \qquad C = \frac{2q^2-1}{4\pi^{5/2}Gq^2v_0}. \tag{1.11}$$

1.3 The model we consider

We use the Miyamoto-Nagai density profile (which will be discussed in detail in the next chapter) to describe the baryonic matter in a galaxy. The parameters in this model allow for a large range of different-looking models. In [18] the authors point out that this model mimics the observed density distribution in disk galaxies surprisingly well, and that the same model with

different parameters can also be used to describe the bulge of a galaxy. We will not use this latter feature in our model.

However if we want to discuss properties such as velocity dispersion, we cannot restrict ourselves to the baryonic matter. Also dark matter has an influence - and as we will see, quite an important one. Nowadays there is an overwhelming amount of evidence for the existence of this still mysterious dark matter. We give a short overview.

- A galaxy rotation curve shows the rotation velocity of stars in a galaxy as a function of their distance to the center. If all the matter were in the baryonic form, the bulk of it would be contained in the galactic bulge. Hence the rotaton velocity outside the bulge should decrease in an almost Keplerian way. However observations indicate that the velocity curve remains almost flat, even at a distance well beyond the bulge, indicating that matter is distributed almost uniformly up to large distances.

- The velocity dispersion in a galaxy is much larger than what could be explained by the baryonic matter alone, an observation our model will agree with.

- X-ray emissions originating from the gas within galactic clusters is also a probe for the mass distribution: their energy is related to the density and pressure of the gas and, assuming equilibrium, this is an indication of the gravitational effect [6].

- Gravitational lensing is the phenomenon where light from a very distant source gets gravitationally bent by a massive intermediate object along the line of sight, such as a galaxy cluster. The strength of this effect is proportional to the mass of the intermediate object and the discrepancy between the thus measured mass and the observed luminosity is an indication for 'missing' mass, i.e. dark matter.

- Fluctuations in the cosmic microwave background (CMB) spectrum reveal a lot of information. Since baryonic and dark matter have different effects on density perturbations, the characteristics of the CMB power spectrum (locations and intensity of the peaks) are another confirmation of the existence of dark matter.

- The large-scale structure of the universe points in the direction of a hierarchical (bottom-up) structure growth. Without dark matter it would have been impossible to create structures that are as large as we observe today.

These indirect observations of dark matter point towards the existence of dark matter, structured in almost spherical, smooth, virialized haloes.

However it remains difficult to deduce the density distribution. Dark matter density estimates in the solar neighbourhood are given in [26]. We chose to model the dark matter using Binney's logarithmic potential, which will be discussed in more detail in the next chapter. The parameter q in this model allows for both oblate ($q < 1$) and prolate ($q > 1$) halo shapes. The concept of a prolate halo may be surprising, but this seems to be the case for the Andromeda galaxy [13]. Recent work on the shape of the dark matter halo can be found in [9] and [10].

1.4 Asymmetric drift and thermalisation temperature in galactic gas flows

Asymmetric drift (AD) is the phenomenon where stars rotate in a galaxy at a mean velocity $\overline{v_\varphi}$ which is smaller than the circular velocity v_{circ} at this radius. Here we will look at the cause of this phenomenon, its consequences, and how its observation can improve galaxy density models.

The circular velocity is the velocity a test particle would have in a circular orbit in the equatorial plane at radius R. Since in this case the centrifugal force

$$F = -\frac{v_{\text{circ}}^2(R)}{R} \tag{1.12}$$

should be exactly balanced by the attractive force induced by the potential,

$$F = -\nabla\Phi(R) = -\frac{d\Phi}{dR}, \tag{1.13}$$

we find that

$$v_{\text{circ}}^2 = R\frac{d\Phi}{dR}. \tag{1.14}$$

We recognize this term, up to a factor, in the right-hand side of the radial Jeans equation (1.7), so by multiplying this equation by R/ρ_* and evaluating at $z = 0$, we obtain

$$v_{\text{circ}}^2 - \overline{v_\varphi}^2 = \sigma_\varphi^2 - \sigma^2 - \frac{R}{\rho_*}\frac{\partial\rho_*\sigma^2}{\partial R}. \tag{1.15}$$

Hence in the case of an isotropic rotator this further simplifies to

$$v_{\text{circ}}^2 - \overline{v_\varphi}^2 = -\frac{R}{\rho_*}\frac{\partial\rho_*\sigma^2}{\partial R}. \tag{1.16}$$

Since the quantity $v_{\text{circ}}^2 - \overline{v_\varphi}^2$ is the one that most easily follows from the previous discussion, we adopt it as our definition for the asymmetric drift:

$$\text{AD} = v_{\text{circ}}^2 - \overline{v_\varphi}^2. \tag{1.17}$$

Notice that in [4] the authors use the definition $v_\mathrm{a} = v_\mathrm{circ} - \overline{v_\varphi}$. The connection between both definitions is obvious:

$$\mathrm{AD} = v_\mathrm{a}(v_\mathrm{circ} + \overline{v_\varphi}) = v_\mathrm{a}(2v_\mathrm{circ} - v_\mathrm{a}) \simeq 2v_\mathrm{a}v_\mathrm{circ}, \tag{1.18}$$

where the last approximation holds if v_a is considerably smaller than v_circ.

The asymmetric drift is an important phenomenon, for several reasons. As there are only very few analytically solved models, most galaxy models rely on numerical simulations. A better understanding of the importance and the effect of the asymmetric drift could considerably enhance the accuracy of these simulations.

The asymmetric drift can also provide a clue to the shape of the dark matter halo of a galaxy. From cosmological N-body simulations [7], [1] we know that these haloes are not spherical. However, they are not expected to be disk-shaped, either. A better knowledge of the halo shape would obviously improve the quality of both analytical models and numerical simulations [26]. For elliptical galaxies the halo shape can be probed using the effect of the dark matter on X-ray emission, but this is not possible in disk galaxies. Hence properties such as the asymmetric drift and the vertical velocity dispersion profile could tell us something on the halo shape.

Finally the asymmetric drift also has an important consequence on radial flows in a disk galaxy. Gas clouds which have an angular momentum corresponding to v_circ, get mixed because of the stars which, at the same radius, have a smaller velocity v_φ. This causes the gas to obtain a smaller velocity than the one required for the radius it moves on, and as a result the gas falls inward, creating radial flows.

We will calculate the importance of the asymmetric drift in Chapter 5.

Another possible application of this kind of results is in determining the flattening of the dark matter halo. This quantity is not easily measured, but as we will see several observable quantities in our model depend significantly on the flattening parameter. Hence measuring these quantities could give more insight in the degree of flattening of the dark matter halo.

Another application, not treated in this work, lies in the possibility to calculate in a simple way the thermalisation of stellar winds interacting with the gas flows in early-type galaxies (see, e.g. [5], [6], [22], [24], [21], [20]). We can define, as in [25], the equivalent temperature of stellar motions as

$$T_* = T_\sigma + \gamma_\mathrm{th} T_\mathrm{rot}, \tag{1.19}$$

where

$$T_\sigma = \frac{\mu m_\mathrm{p}}{3k_\mathrm{B}M_*} \int \rho_* \mathrm{Tr}(\sigma^2) dV \tag{1.20}$$

is the contribution of random stellar motions (here k_B is Boltzmann's constant, μ is the mean molecular weight at solar abundance and m_p is the

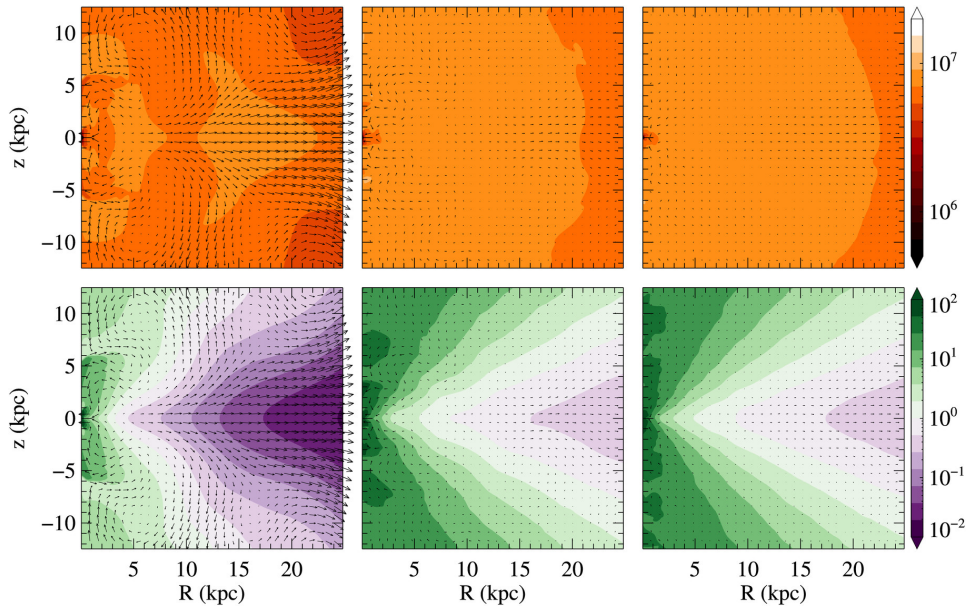

Figure 1.1: Temperature (top panels) and heating over cooling time ratio (bottom panels) for a velocity dispersion supported E7 galaxy at different ages (from left to right: 2.4 Gyr, 8 Gyr, 13 Gyr).

proton mass), $\gamma_{\rm th}$ is a parameter that can be estimated by using the results of numerical simulations, and

$$T_{\rm rot} = \frac{\mu m_{\rm p}}{3 k_{\rm B} M_*} \int \rho_* \overline{v_\varphi}^2 dV \tag{1.21}$$

is the contribution of stellar streaming motions.

Our models are important in this respect because it has been shown that gas flows in galaxies of identical structure but different kinematical support are characterized by different ISM velocity fields, with important consequences both for their X-ray emission and for accretion phenomena on their central black holes. This can be seen in Figures 1.1 and 1.2, taken from [21]. In both figures the top panels show the temperature, the bottom panels show the heating over cooling time ratio, at different ages (from left to right: 2.4 Gyr, 8 Gyr, 13 Gyr). In both cases an E7 galaxy was simulated, both simulations have an identical mass profile. However, the galaxy in Figure 1.1 is velocity dispersion supported (hence $k = 0$ in eq. (1.8) in the Satoh approach) so the flattening is caused by σ_φ. The galaxy in Figure 1.2 on the other hand is an isotropic rotator, so $k = 1$, and the flattening is due to the rotation.

The great flexibility of our models in principle allows for a fast exploration of parameter space.

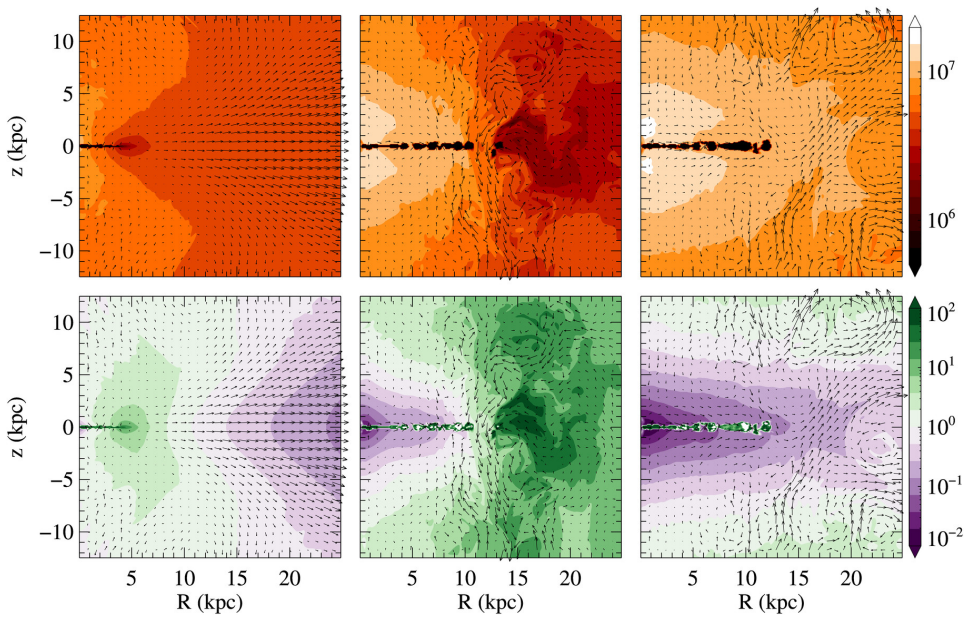

Figure 1.2: Temperature (top panels) and heating over cooling time ratio (bottom panels) for an isotropic rotator E7 galaxy at different ages (from left to right: 2.4 Gyr, 8 Gyr, 13 Gyr).

Chapter 2

The models

2.1 The Miyamoto-Nagai model

The Miyamoto-Nagai potential-density pair is

$$\Phi(R,z) = -\frac{GM_*}{\sqrt{R^2+(a+\zeta)^2}}, \tag{2.1}$$

$$\rho(R,z) = \frac{M_* b^2}{4\pi}\frac{aR^2+(a+3\zeta)(a+\zeta)^2}{\zeta^3[R^2+(a+\zeta)^2]^{5/2}}, \tag{2.2}$$

where $\zeta = \sqrt{z^2+b^2}$ and (R,φ,z) are the standard cylindrical coordinates. The absence of φ in the formulae indicates that it is an axisymmetric model. The ratio $s = a/b$ is the flattening parameter. For $a = 0$, so $s = 0$, the model reduces to the Plummer sphere [23]. For $b = 0$, so $s \to \infty$, we obtain the Kuzmin razor-thin disk [16]. Positive finite values of s give oblate models. It can easily be checked that the total mass is indeed given by M_*.

Figures 2.1-2.3 show how the density varies as a function of z and R, for certain values of the flattening parameter s. It is clear that with increasing s one goes from a spherical model at $s = 0$ to an ever more flattened model. As s tends to infinity (so b tends to zero while a is positive), we obtain a superficial density.

Direct integration of the first Jeans equation (1.6) leads to

$$\rho_*\sigma^2 = \frac{M_*^2 G b^2}{8\pi}\frac{(a+\zeta)^2}{\zeta^2[R^2+(a+\zeta)^2]^3} \tag{2.3}$$

and hence

$$\sigma^2 = \frac{M_* G}{2}\frac{\zeta(a+\zeta)^2}{[aR^2+(a+3\zeta)(a+\zeta)^2][R^2+(a+\zeta)^2]^{1/2}}. \tag{2.4}$$

At this point the solution of the second Jeans equation (1.7) is trivial: there

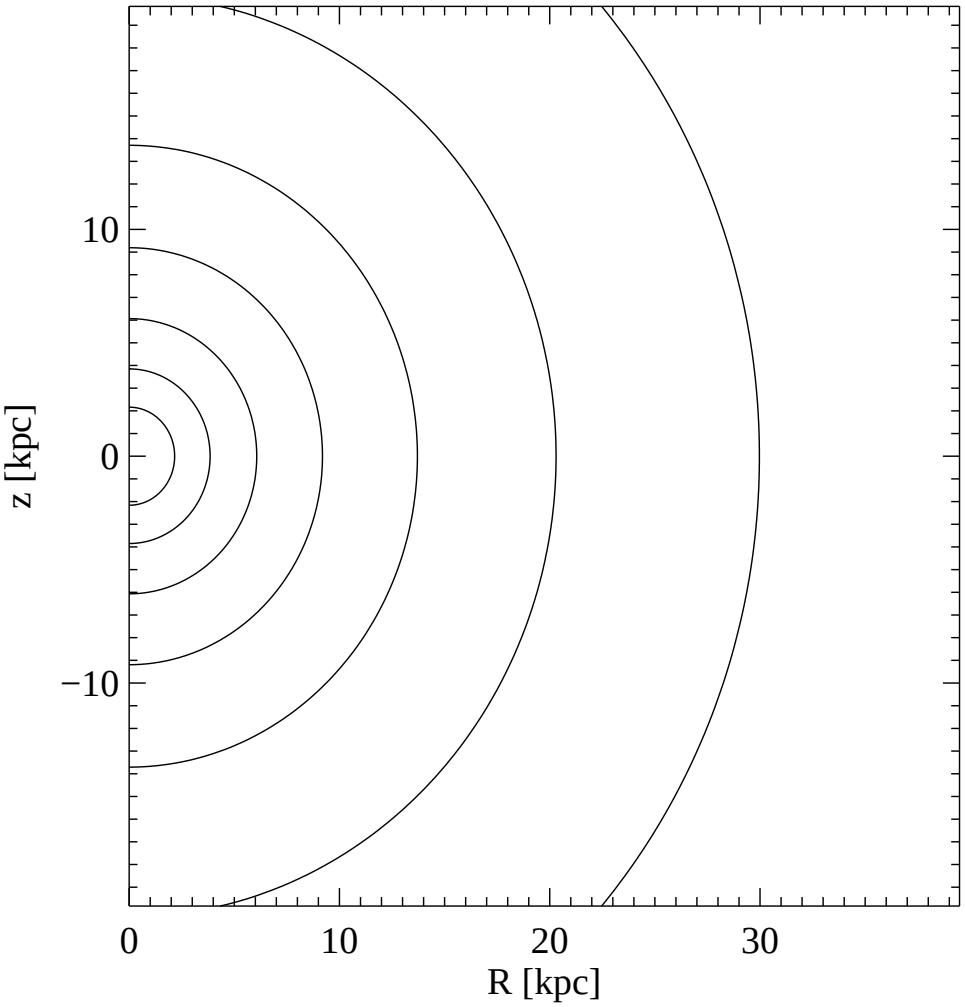

Figure 2.1: Isodensity contours for the Miyamoto-Nagai model for $s = 0$ (Plummer sphere).

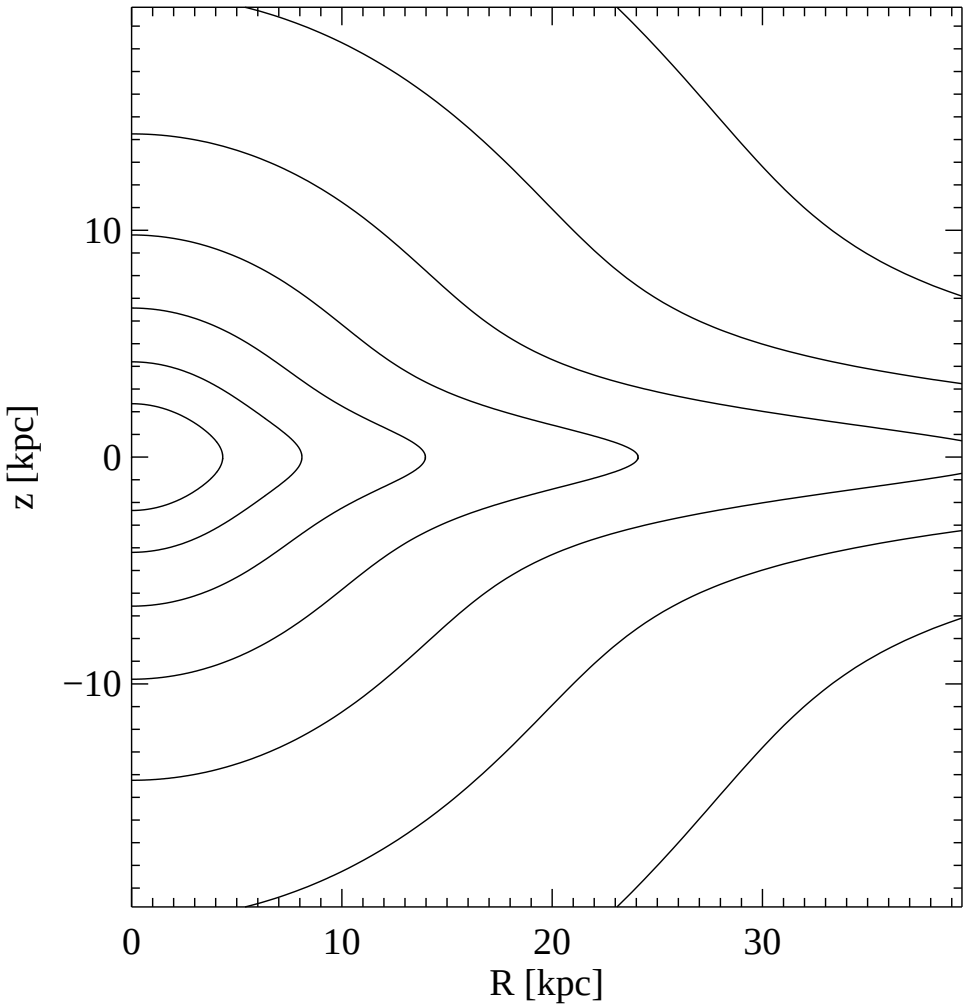

Figure 2.2: Isodensity contours for the Miyamoto-Nagai model for $s = 1$.

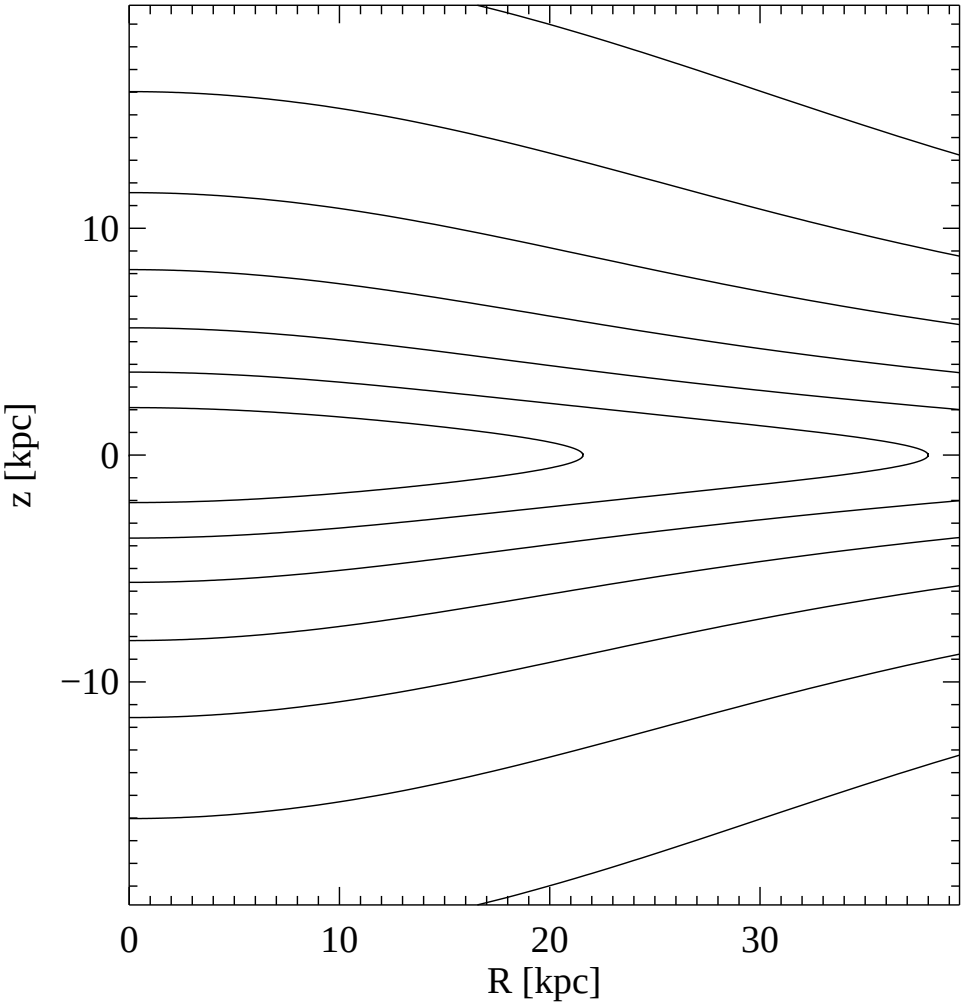

Figure 2.3: Isodensity contours for the Miyamoto-Nagai model for $s = 10$.

is no need for further integration. Solving for $\overline{v_\varphi^2}$ we obtain

$$\overline{v_\varphi^2} = \frac{M_* G}{2} \frac{\zeta(a+\zeta)^2 + 2aR^2}{[aR^2 + (a+3\zeta)(a+\zeta)^2][R^2 + (a+\zeta)^2]^{1/2}}. \tag{2.5}$$

We refer to Figures 3.1-3.3 where the black curve gives σ_* for the single component Miyamoto-Nagai model in the equatorial plane, for some different values of the parameters a and b. Notice that as the flattening parameter $s = a/b$ increases, σ_* decreases, especially in the central region.

As mentioned, if a tends to zero in the Miyamoto-Nagai model, we obtain the Plummer sphere. It is easily checked that putting $a = 0$ in the solution for the Miyamoto-Nagai model gives the result obtained in eq. (1.5) when we discussed systems with spherical symmetry.

Another option is to look at the two-component Miyamoto-Nagai model. This model was first considered in [18] as a model for our own galaxy, in an attempt to model the galactic rotation curve which has two peaks. A first analytical approach was presented in [6], where one component describes the stellar component and the other component describes a dark matter halo. In order to obtain some analytical results, it is necessary to choose two models with the same b parameter, but the a and M parameters can vary between the two components. Even with this simplifying condition it is not possible to solve the Jeans equations in only elementary functions, but some quantities such as the kinetic energy and the interaction energy betweens stars and halo can be exactly calculated. The authors calculate the virial interaction energy, given by $W = -\int \rho_* \langle \mathbf{x}, \nabla\Phi \rangle d^3\mathbf{x} = W_{**} + W_{*\mathrm{h}}$. They find that, with $s = a/b$,

$$W_{**} = \frac{GM_*^2}{8b}\left[\frac{\pi}{2s^2} - \frac{1-2s^2}{s(1-s^2)} - \frac{F(s)}{s^2(1-s^2)}\right], \tag{2.6}$$

where

$$F(s) = \begin{cases} \arccos(s)/\sqrt{1-s^2} & \text{if } 0 \le s < 1; \\ 1 & \text{if } s = 1; \\ \operatorname{arccosh}(s)/\sqrt{s^2-1} & \text{if } s > 1 \end{cases} \tag{2.7}$$

and so

$$W_{**}(0) = -\frac{3\pi M_*}{32}. \tag{2.8}$$

Near $s = 1$ we have that $F(s) = 1 + (1-s)/3 + \mathcal{O}(1-s)^2$ so that

$$W_{**}(1) = -\left(\frac{1}{3} - \frac{\pi}{16}\right) M_*. \tag{2.9}$$

As for the halo contribution, they find that, with $c = (s + s_{\rm h})/2$,

$$\frac{8b(1-c^2)^2}{GM_*M_{\rm h}}W_{*\rm h} = \frac{\pi}{2}\left(c-\frac{1}{c}\right)^2 - \left(2c+\frac{1}{c}\right) + \left(4-\frac{1}{c^2}\right)F(c) + s\left[\left(2c^2-1+\frac{2}{c^2}\right) - \pi\frac{(1-c^2)^2}{c^3} + \left(\frac{2}{c^3}-\frac{5}{c}\right)F(c)\right] \tag{2.10}$$

with

$$W_{*\rm h} = \frac{GM_*M_{\rm h}}{96b}(9\pi + 32s) \tag{2.11}$$

if $c = 0$ and

$$W_{*\rm h} = \frac{GM_*M_{\rm h}}{240b}\left[(15\pi - 32) + s(112 - 30\pi)\right] \tag{2.12}$$

if $c = 1$.

2.2 Binney logarithmic model

The Binney potential-density pair is

$$\Phi(R,z) = \frac{v_{\rm h}^2}{2}\ln\left(R_{\rm h}^2 + R^2 + \frac{z^2}{q^2}\right), \tag{2.13}$$

$$\rho(R,z) = \frac{v_{\rm h}^2}{4\pi G q^2}\frac{(2q^2+1)R_{\rm h}^2 + R^2 + (2-q^{-2})z^2}{(R_{\rm h}^2 + R^2 + z^2q^{-2})^2}. \tag{2.14}$$

Figures 2.4-2.7 show the isodensity contours for some different choices for the parameters q and $R_{\rm h}$. The parameter q is the axis ratio of the equipotential surfaces, which are ellipsoids. In this sense it is comparable to the parameter s in the Miyamoto-Nagai model: a smaller value for q results in a flatter distribution. Notice that q should be at least $1/\sqrt{2} \simeq 0.707$, else the density is no longer everywhere positive because of the term $2 - q^{-2}$. The value $q = 1$ gives a model with spherical symmetry. The parameter $R_{\rm h}$ mainly has an influence on the central behaviour: the density at the origin is a decreasing function of $R_{\rm h}$. If $R_{\rm h} = 0$, the central density diverges. At large distances, e.g. $R >> R_{\rm h}$, the influence of $R_{\rm h}$ is small.

The circular speed at radius R in the equatorial plane is

$$v_c(R) = \frac{v_{\rm h}R}{\sqrt{R_{\rm h}^2 + R^2}}. \tag{2.15}$$

It should be noted that this is an unphysical model: the mass outside any equipotential surface is infinite. Moreover, if $R_{\rm h} = 0$ then also the mass at the origin diverges. Despite this drawback, the model is very often used because it has a very easy analytical form.

The choice of parameters $R_\mathrm{h} = 0$ and $q = 1$ gives the well-known SIS (Singular Isothermal Sphere) model. In this case the density simplifies to

$$\rho(r) = \frac{v_\mathrm{h}^2}{4\pi G r^2}. \tag{2.16}$$

Other than having a singularity at the origin (since $R_\mathrm{h} = 0$) and having spherical symmetry (since $q = 1$), this model has the interesting property that it is isothermal: consider an isothermal gas at (constant) temperature T, composed of particles with mass m. This has equation of state $p = kT\rho/m$ where k is Boltzmann's constant. If this gas is in a state of hydrodynamical equilibrium, then balancing the pressure gradient with the gravitational force, we obtain

$$-\frac{GM(r)}{r^2}\rho = \frac{kT}{m}\frac{d\rho}{dr}, \tag{2.17}$$

where

$$M(r) = \int_{V(r)} \rho dV = \frac{v_\mathrm{h}^2 r}{G} \tag{2.18}$$

is the mass within a sphere with radius r (the integration is trivial). Solving the differential equation by separating the variables ρ and r, we obtain

$$-\frac{v_\mathrm{h}^2 m}{kT}\ln r = \ln\rho + C, \tag{2.19}$$

where C is an integration constant. Substitution of ρ as a function of r leads to

$$\left(2 - \frac{v_\mathrm{h}^2 m}{kT}\right)\ln r = \ln\left(\frac{v_\mathrm{h}^2}{4\pi G}\right) + C. \tag{2.20}$$

Since the right-hand side is independent of r, the coefficient of $\ln r$ should be zero, hence

$$v_\mathrm{h}^2 = \frac{2kT}{m}. \tag{2.21}$$

This explains the 'isothermal' in the name of this model, and it gives a further interpretation for the constant v_h.

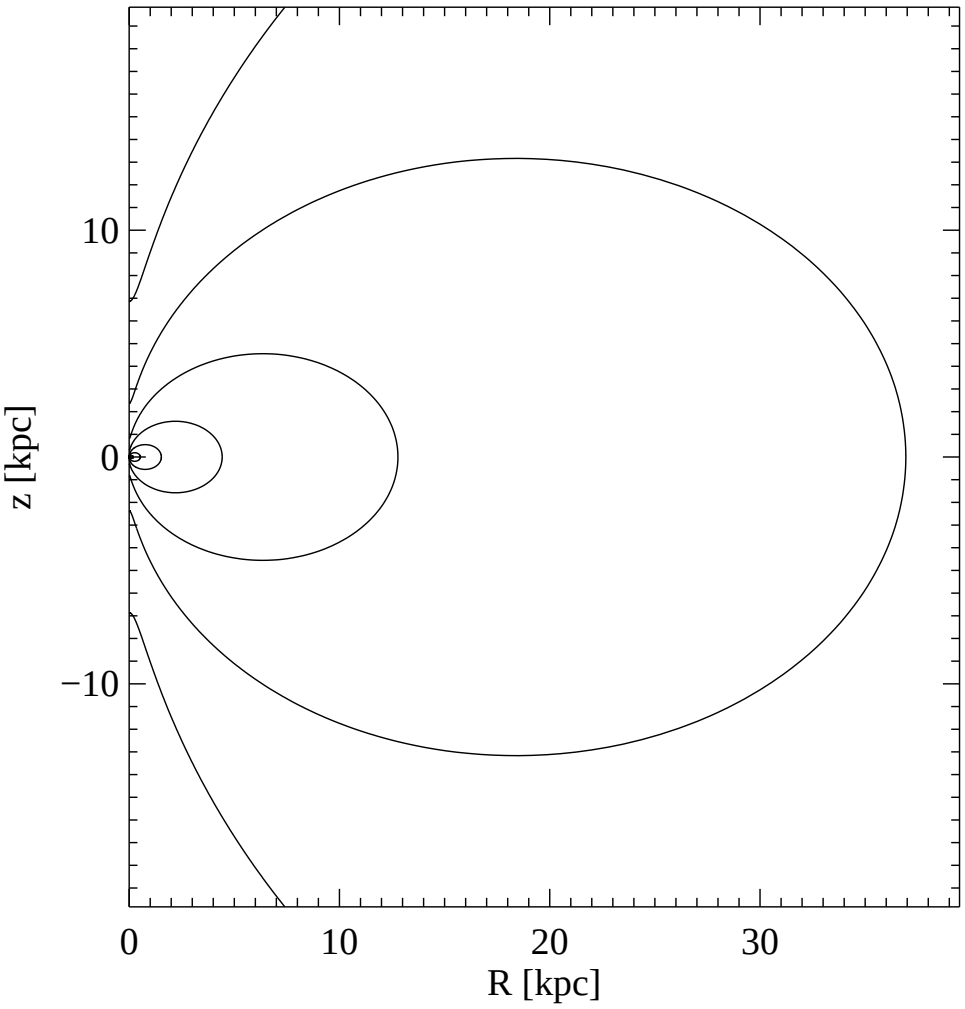

Figure 2.4: Isodensity contours for the Binney logarithmic model for $q = 0.71$, $R_{\rm h} = 0$.

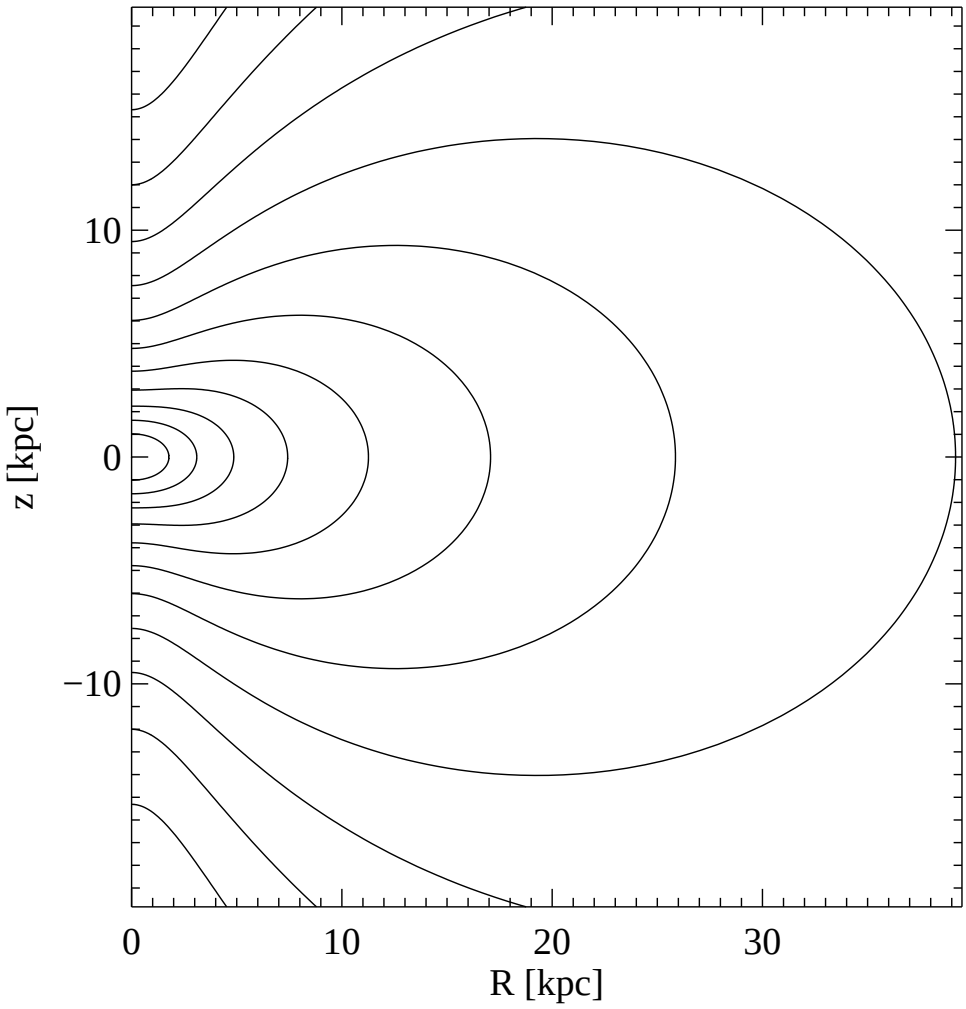

Figure 2.5: Isodensity contours for the Binney logarithmic model for $q = 0.71$, $R_{\rm h} = 1$.

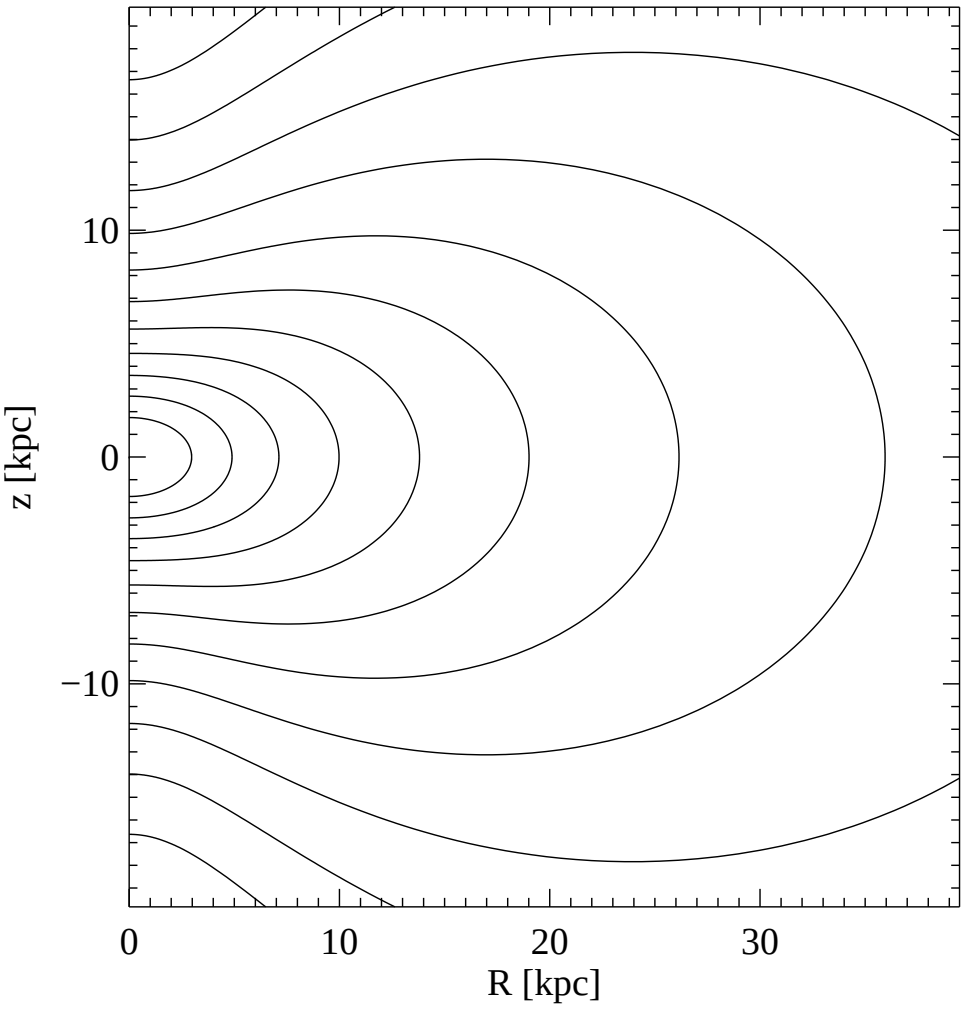

Figure 2.6: Isodensity contours for the Binney logarithmic model for $q = 0.71$, $R_{\rm h} = 2$.

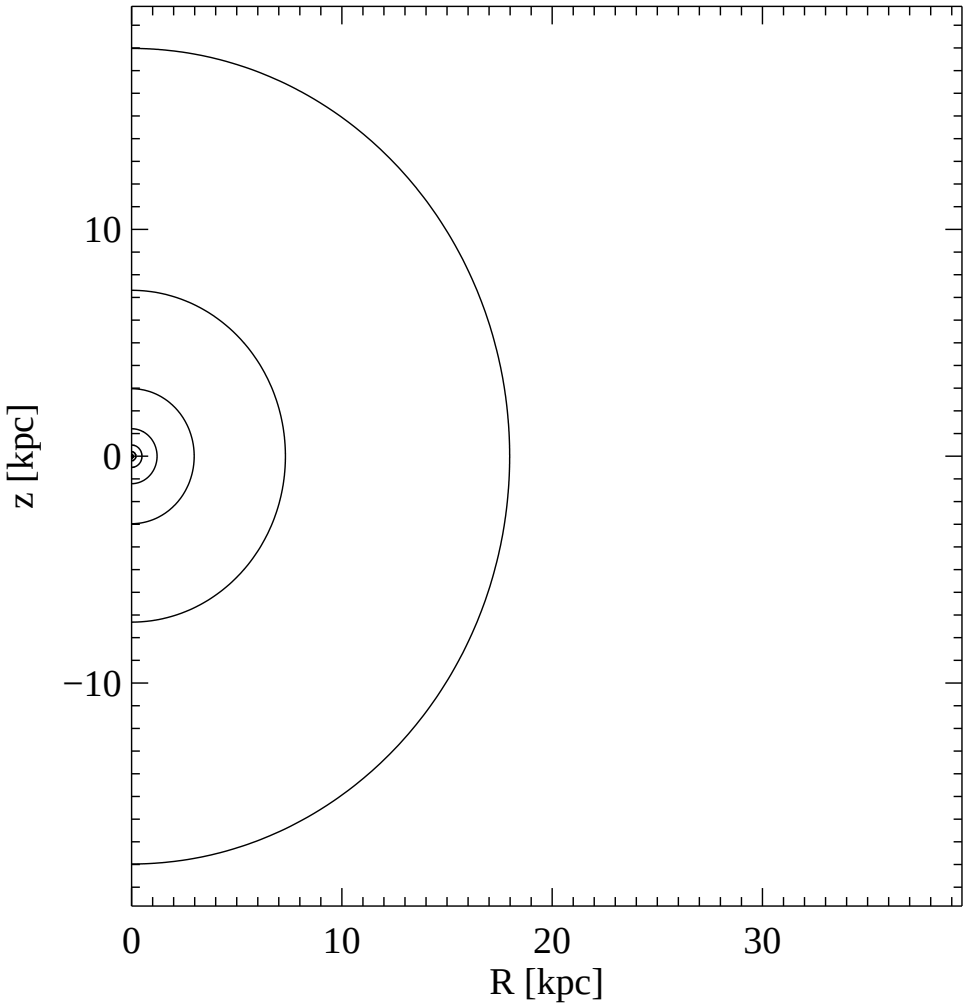

Figure 2.7: Isodensity contours for the Binney logarithmic model for $q = 1$, $R_{\rm h} = 0$ (SIS model).

Chapter 3

The solution of the Jeans equations

3.1 Solution of the vertical Jeans equation

3.1.1 The general case

We consider the model consisting of a baryonic component given by the Miyamoto-Nagai model and a dark matter component given by Binney's logarithmic potential, so the total potential is given by

$$\Phi_{\rm t} = \Phi_* + \Phi_{\rm h}, \tag{3.1}$$

where Φ_* is given by eq. (2.1) and $\Phi_{\rm h}$ is given by eq. (2.13).

The special cases $R = 0$ (z axis), $A = 0$ (critical cylinder) and $s = 0$ (spherical stellar density) are treated in Section 3.1.2. Note that all these special cases can be obtained as a limiting case of the general solution, but for the sake of simplicity we give the solution in these cases explicitly.

The contribution of the halo to the vertical and radial velocity dispersion is given by

$$\rho_*\sigma^2_{*\rm h} = \int_z^\infty \rho_* \frac{\partial \Phi_{\rm h}}{\partial z'} dz' = v_{\rm h}^2 \int_z^\infty \frac{\rho_* z'\, dz'}{A + 1 + z'^2} = \frac{M_* v_{\rm h}^2}{4\pi b^3} I, \tag{3.2}$$

where

$$A \equiv q^2(R^2 + R_{\rm h}^2) - 1 \tag{3.3}$$

and where the last identity is obtained by normalization of all the lenghts to b (in order to avoid cumbersome notation, from now on also R, $R_{\rm h}$ and z must be intended normalized to b). Note that, given q and $R_{\rm h}$, the minimum value for A is $q^2 R_{\rm h}^2 - 1$, a value reached on the z axis. The integral (3.2) is quite formidable, especially considering the fact that ρ_* contains two nested irrationalities. However, in the following we show that this integral can in fact be computed in terms of elementary functions.

Splitting the integral

We begin by removing the inner irrationality with the substitution $\zeta = \sqrt{1+z^2}$, so that

$$I \equiv \int_{\zeta}^{\infty} \frac{sR^2 + (s+3\zeta')(s+\zeta')^2}{\zeta'^2[R^2+(s+\zeta')^2]^{5/2}(A+\zeta'^2)} d\zeta'. \tag{3.4}$$

Note that $\zeta' \geq 1$, so that $A+\zeta'^2 \geq 0$ everywhere, where equality holds at the origin when $R_{\rm h} = 0$ (and so in particular for the SIS). In order to proceed with the integration, we now also remove the second irrationality with the change of variable $\mathrm{sh}\, x = (s+\zeta)/R$. Notice that this substitution is not valid if $R = 0$, however in this case the integrand in eq. (3.4) is a rational function of ζ' and its integration is elementary (see Section 3.1.2). If $R \neq 0$ we obtain

$$I = \frac{1}{R^2} \int_{\mathrm{arcsh}\,\lambda}^{\infty} \frac{\left[s + (3R\,\mathrm{sh}\, x - 2s)\mathrm{sh}^2 x\right]\, dx}{(R\,\mathrm{sh}\, x - s)^2[A + (R\,\mathrm{sh}\, x - s)^2](1+\mathrm{sh}^2 x)^2}, \tag{3.5}$$

where $\mathrm{arcsh}\, x = \ln\left(x + \sqrt{1+x^2}\right)$ and

$$\lambda \equiv \frac{s+\zeta}{R} = \frac{s+\sqrt{1+z^2}}{R}. \tag{3.6}$$

A partial fraction decomposition [14] in terms of $\mathrm{sh}\, x$ of the integrand in eq. (3.5) gives

$$\begin{aligned} I &= \frac{1}{R^2} \int_{\mathrm{arcsh}\,\lambda}^{\infty} \frac{\alpha_0 + \alpha_1 \mathrm{sh}\, x + \alpha_2 \mathrm{sh}^2 x + \alpha_3 \mathrm{sh}^3 x}{(1+\mathrm{sh}^2 x)^2} dx \\ &\quad + \frac{1}{R^2} \int_{\mathrm{arcsh}\,\lambda}^{\infty} \frac{\beta_0 + \beta_1 \mathrm{sh}\, x}{(R\mathrm{sh}\, x - s)^2} dx \\ &\quad + \frac{1}{R^2} \int_{\mathrm{arcsh}\,\lambda}^{\infty} \frac{\gamma_0 + \gamma_1 \mathrm{sh}\, x}{A + (R\mathrm{sh}\, x - s)^2} dx \\ &= \frac{I_\alpha + I_\beta + I_\gamma}{R^2}, \end{aligned} \tag{3.7}$$

where λ is defined in eq. (3.6) and the meaning of I_α, I_β and I_γ is obvious.

Notice however that if $A = 0$ (which is the case for at most one R value, for the SIS model it happens at $R = 1$), two of the denominator factors in eq. (3.5) coincide and a different partial fraction decomposition is needed. In the case $s = 0$ the integrand in eq. (3.4) simplifies. One could use the same approach, with a now simplified partial fraction decomposition, however a different substitution is easier. Both these special cases and the previously excluded case $R = 0$ will be treated in Section 3.1.2. Now we focus on the evaluation in the case $R \neq 0, A \neq 0, s \neq 0$.

The integral I_α

The first integral in eq. (3.7) is of trivial evaluation and the result is

$$\begin{aligned} I_\alpha =& \frac{2\alpha_0+\alpha_2}{3} + \frac{\alpha_3}{\sqrt{1+\lambda^2}} - \frac{\alpha_0\lambda}{(1+\lambda^2)^{3/2}} \\ & - \frac{\alpha_3-\alpha_1}{3(1+\lambda^2)^{3/2}} - \frac{(\alpha_2+2\alpha_0)\lambda^3}{3(1+\lambda^2)^{3/2}}, \end{aligned} \tag{3.8}$$

where the α coefficients are given by

$$\begin{aligned} \frac{\alpha_0\alpha_d}{s} =& -17R^8 - 2R^6(11s^2-12A) + R^4(8s^4+19s^2A-9A^2) \\ & + 2R^2(s^2+A)(7s^4+A^2) + s^2(s^2+A)^3, \\ \frac{\alpha_1\alpha_d}{R} =& -6R^8 + R^6(14s^2+15A) + 2R^4(25s^4-4s^2A-6A^2) \\ & + R^2(34s^6+3s^4A+4s^2A^2+3A^3) + 2s^2(2s^6+5s^4A+4s^2A^2+A^3), \\ \frac{\alpha_2\alpha_d}{s} =& -8R^8 + R^6(2s^2+3A) + 2R^4(13s^4+8s^2A+3A^2) \\ & + R^2(s^2+A)(14s^4+9s^2A-A^2) - 2s^2(s^2+A)^3, \\ \frac{\alpha_3\alpha_d}{R} =& -3R^8 + 2R^6(7s^2+3A) + R^4(32s^4+s^2A-3A^2) \\ & + 2s^2R^2(5s^4-A^2) - s^2(5s^2+A)(s^2+A)^2, \end{aligned} \tag{3.9}$$

where

$$\alpha_d = (R^2+s^2)^2[(A+s^2-R^2)^2+4R^2s^2]^2. \tag{3.10}$$

The integral I_β

The β coefficients are given by

$$\beta_0\beta_d = R^4 s, \qquad \beta_1\beta_d = R^3 s^2, \tag{3.11}$$

where

$$\beta_d = A(R^2+s^2)^2. \tag{3.12}$$

Using the standard substitution $y = \mathrm{th}\,(x/2)$ we obtain

$$I_\beta = -\frac{2\beta_0}{s^2}\int_\mu^1 \frac{y^2-2sy/R-1}{(y^2+2Ry/s-1)^2}dy, \tag{3.13}$$

where

$$\mu \equiv \tanh\left(\frac{\mathrm{arcsh}\,\lambda}{2}\right) = \sqrt{1+\frac{1}{\lambda^2}} - \frac{1}{\lambda}. \tag{3.14}$$

It can be easily proved that the two real zeros of the denominator lie outside the integration domain. The standard partial fraction decomposition

technique gives elementary rational integrals and after some simplification we find that the explicit expression is given by

$$I_\beta = \frac{\beta_0}{R}\left(\frac{\sqrt{1+\lambda^2}}{\zeta} - \frac{1}{R}\right). \tag{3.15}$$

The integral I_γ

The third integral is the most complicated one, due to the presence of the parameter A in the integrand. The partial fraction decomposition coefficients in eq. (3.7) for $R \neq 0$, $s \neq 0$ and $A \neq 0$ are given by

$$\begin{aligned}\frac{\gamma_0\gamma_d}{R^2 s} &= -R^6 - 2R^4(s^2 - 3A) - R^2(s^4 - 18s^2A - 3A^2) - 8A(s^2 + A)^2,\\ \frac{\gamma_1\gamma_d}{R^3} &= -R^4(s^2 - 3A) - 2R^2(s^4 + 8s^2A + 3A^2) - (s^2 - 3A)(s^2 + A)^2,\end{aligned} \tag{3.16}$$

with

$$\gamma_d = A[(A + s^2 - R^2)^2 + 4R^2s^2]^2. \tag{3.17}$$

At variance with the integrals I_α and I_β we now have to distinguish the integration procedure as a function of the sign of A. Inspection of eq. (3.7) suggests that an easy factorization of the denominator of I_γ could be obtained in the case $A < 0$. However, as the same procedure cannot be applied to the case $A > 0$ without using complex numbers, we prefer to follow another approach that maximizes the similarity of the treatment in the two cases. We cannot exclude that other approaches exist, leading to an even more direct integration. In the following we describe the approach we deem optimal after several attempts.

The substitution $y = e^x$ gives

$$I_\gamma = \frac{2\gamma_1}{R^2}\int_\nu^\infty \frac{(y^2 + Hy - 1)\,dy}{\Delta(y)}, \tag{3.18}$$

where

$$\Delta(y) = y^4 - \frac{4s}{R}y^3 + \left(\frac{4A}{R^2} + \frac{4s^2}{R^2} - 2\right)y^2 + \frac{4s}{R}y + 1, \tag{3.19}$$

with

$$\nu \equiv e^{\operatorname{arcsh}\lambda} = \lambda + \sqrt{1+\lambda^2} \tag{3.20}$$

and

$$H = 2\frac{\gamma_0}{\gamma_1}. \tag{3.21}$$

In principle, we could use the antisymmetry of $\Delta(y)/y^2$ (after noticing that $y = 0$ is not a zero) to factorize it: it is readily seen that if y_1 is a zero of Δ,

then so is $-1/y_1$. This implies that $\Delta(y)/y^2$ can be written as a quadratic polynomial in $t = y - 1/y$, from which the factorization is immediate. However, if $A > 0$ the two roots of this quadratic polynomial in t are complex conjugates.

In practice this computation is not needed since any quartic polynomial with real coefficients can be factorized into two quadratic polynomials with real coefficients. We found it useful, without loss of generality, to adopt the factorization

$$\Delta(y) = \left[(y - \Delta_+)^2 + \delta_+\right]\left[(y - \Delta_-)^2 + \delta_-\right]. \tag{3.22}$$

Expansion of eq. (3.22) and comparison with eq. (3.19) shows that

$$\Delta_\pm = \frac{s}{R} \pm \sqrt{\frac{s^2}{R^2} + \delta}, \qquad \delta_\pm = \frac{1-\delta}{\delta}\Delta_\pm^2, \tag{3.23}$$

where

$$\delta = \frac{\sqrt{(A + s^2 - R^2)^2 + 4R^2s^2} - (A + s^2 - R^2)}{2R^2}. \tag{3.24}$$

Notice that we always have $\delta > 0, \Delta_+ > 0, \Delta_- < 0$. If $A > 0$, then $0 < \delta < 1$ and hence $\delta_\pm > 0$, making the two quadratic polynomials in eq. (3.22) irreducible over the reals. If $A < 0$, then $\delta > 1$ and hence $\delta_\pm < 0$, compatible with the fact that in this case Δ can be factorized into four linear factors over the reals.

Now we can proceed in the usual way, by a partial fraction decomposition. The coefficients in

$$\frac{y^2 + Hy - 1}{\Delta(y)} = \frac{\eta_+ y + \theta_+}{(y - \Delta_+)^2 + \delta_+} + \frac{\eta_- y + \theta_-}{(y - \Delta_-)^2 + \delta_-} \tag{3.25}$$

are given, after some simplification, by

$$\begin{aligned} \eta_\pm \sigma_d &= \pm\, 2\delta\left(2\delta - \frac{Hs}{R}\right), \\ \theta_\pm \sigma_d &= 2\Delta_\pm\left[\frac{s}{R}(\Delta_+ - \Delta_-) \pm \delta\Delta_\pm(H + 2\Delta_\mp)\right], \end{aligned} \tag{3.26}$$

where

$$\sigma_d = 4(\Delta_+ - \Delta_-)\left(\delta^2 + \frac{s^2}{R^2}\right). \tag{3.27}$$

Note that a few simple algebraic relations link the constants above. They can be used to simplify the final expression of I_γ:

$$\Delta_+^2\delta_- = \delta_+\Delta_-^2\,, \qquad \frac{\eta_+\Delta_+ + \theta_+}{\Delta_+} = \frac{\eta_-\Delta_- + \theta_-}{\Delta_-}. \tag{3.28}$$

Doing so, we finally obtain[1]

$$I_\gamma = \frac{\gamma_1\eta_+}{R^2}\ln\frac{(\nu-\Delta_-)^2+\delta_-}{(\nu-\Delta_+)^2+\delta_+} + \frac{2\gamma_1}{R^2}\frac{\theta_+ + \eta_+\Delta_+}{\sqrt{|\delta_+|}}\times \begin{cases} \arctan\dfrac{\sqrt{\delta_+}(\nu-\Delta_-)-\sqrt{\delta_-}(\nu-\Delta_+)}{(\nu-\Delta_+)(\nu-\Delta_-)+\sqrt{\delta_+\delta_-}} & \text{if } A>0; \\ \operatorname{arctanh}\dfrac{\sqrt{|\delta_+|}(\nu-\Delta_-)-\sqrt{|\delta_-|}(\nu-\Delta_+)}{(\nu-\Delta_+)(\nu-\Delta_-)-\sqrt{\delta_+\delta_-}} & \text{if } A<0. \end{cases} \tag{3.29}$$

We stress again that these formulae cannot be used in their present form to describe the velocity dispersion on the z axis ($R = 0$), on the critical cylinder ($A = 0$), or in the case of a spherical stellar density ($s = 0$). All these cases are treated in Section 3.1.2.

Plots of σ_* in the equatorial plane are shown in Figures 3.1-3.3. Upon comparison of these plots, we can see the role each parameter plays. Comparing the orange and red curves, we see that an increase in q leads to a decrease in σ_*. This effect is important mainly at larger R and the difference diminishes as the Miyamoto-Nagai model gets flatter: the green and blue curves are closer together. In general both the halo contribution and the stellar contribution are larger if s is smaller. The influence of R_h is mainly visible in the central region. The smaller R_h, the larger the halo contribution near the center.

Two-dimensional colour-coded maps of σ_* for various parameter values are given in Figures 3.4-3.7. Notice the spherical symmetry in Figure 3.4. The difference between Figures 3.6 and 3.7 is rather small, one could say that a higher q leads to a lower σ_* far above the equatorial plane. The effect of s is clear: for a less flattened Miyamoto-Nagai model (e.g. $s = 0$), the velocity dispersion σ_* is quite high also away from the equatorial plane (beware that there is a considerable difference in the colour coding between the maps with $s = 0$ and those with $s = 10$).

[1] The addition formulae used to obtain (3.29) are

$$\begin{aligned} \operatorname{arctanh} u - \operatorname{arctanh} v &= \operatorname{arctanh}\frac{u-v}{1-uv}, \\ \arctan u - \arctan v &= \arctan\frac{u-v}{1+uv}, \end{aligned}$$

where for $|x| < 1$, $\operatorname{arctanh} x = \frac{1}{2}\ln\frac{1+x}{1-x}$.

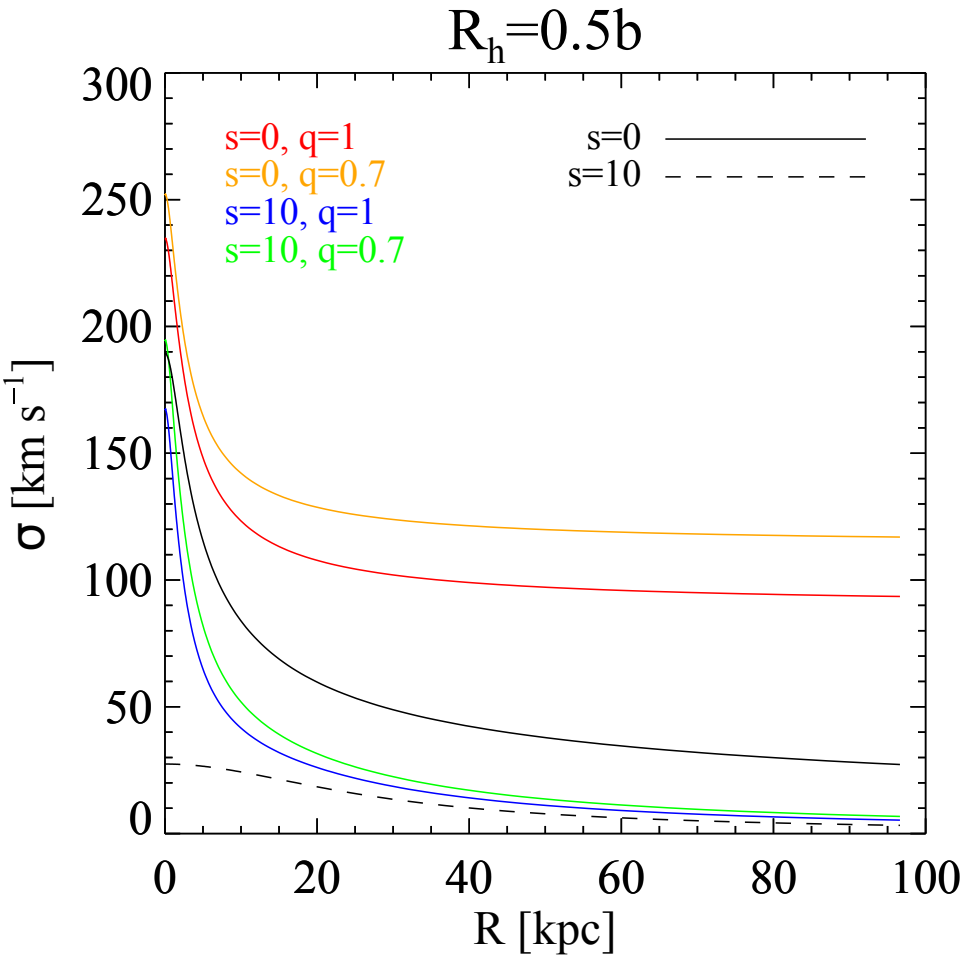

Figure 3.1: σ_* in the equatorial plane ($z = 0$) for our model with $b = 2$ kpc, $M_* = 10^{11} M_\odot$, $v_\mathrm{h} = 200$ km/s, $R_\mathrm{h} = 0.5b$ and varying values of s and q. The stellar contribution is given by the black curves.

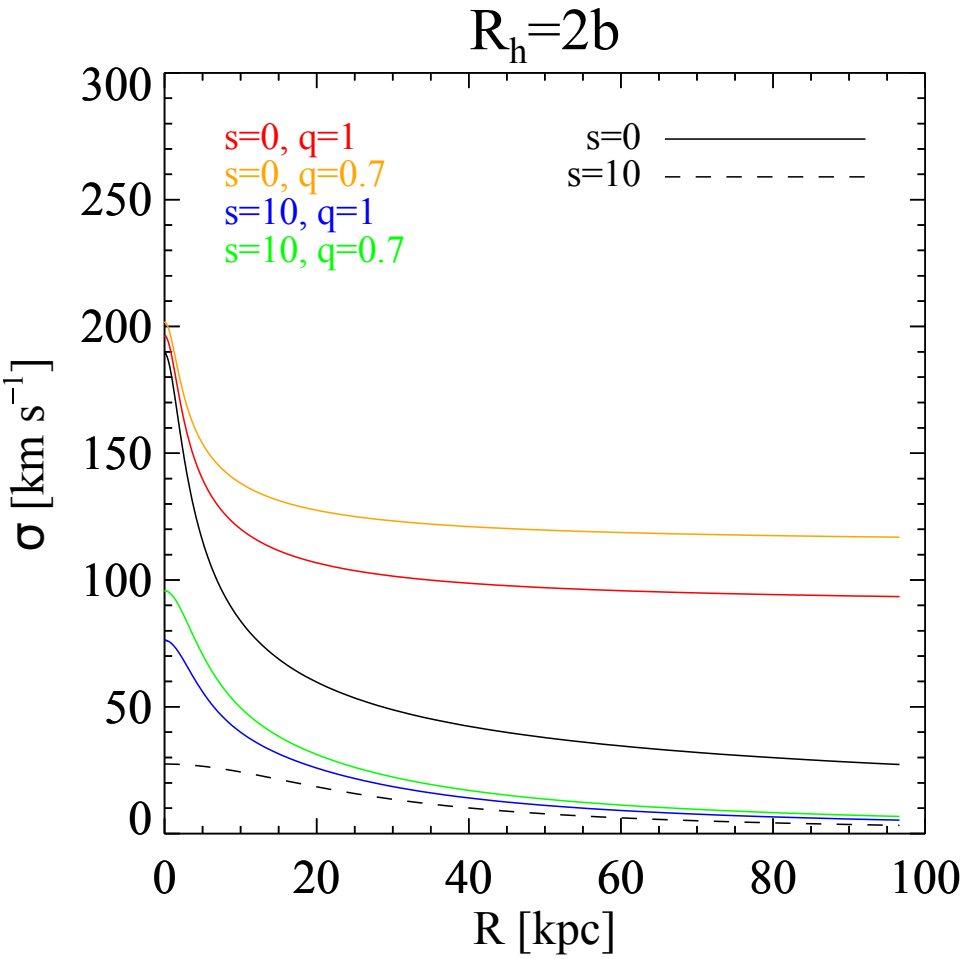

Figure 3.2: σ_* in the equatorial plane ($z = 0$) for our model with $b = 2$ kpc, $M_* = 10^{11} M_\odot$, $v_\mathrm{h} = 200$ km/s, $R_\mathrm{h} = 2b$ and varying values of s and q. The stellar contribution is given by the black curves.

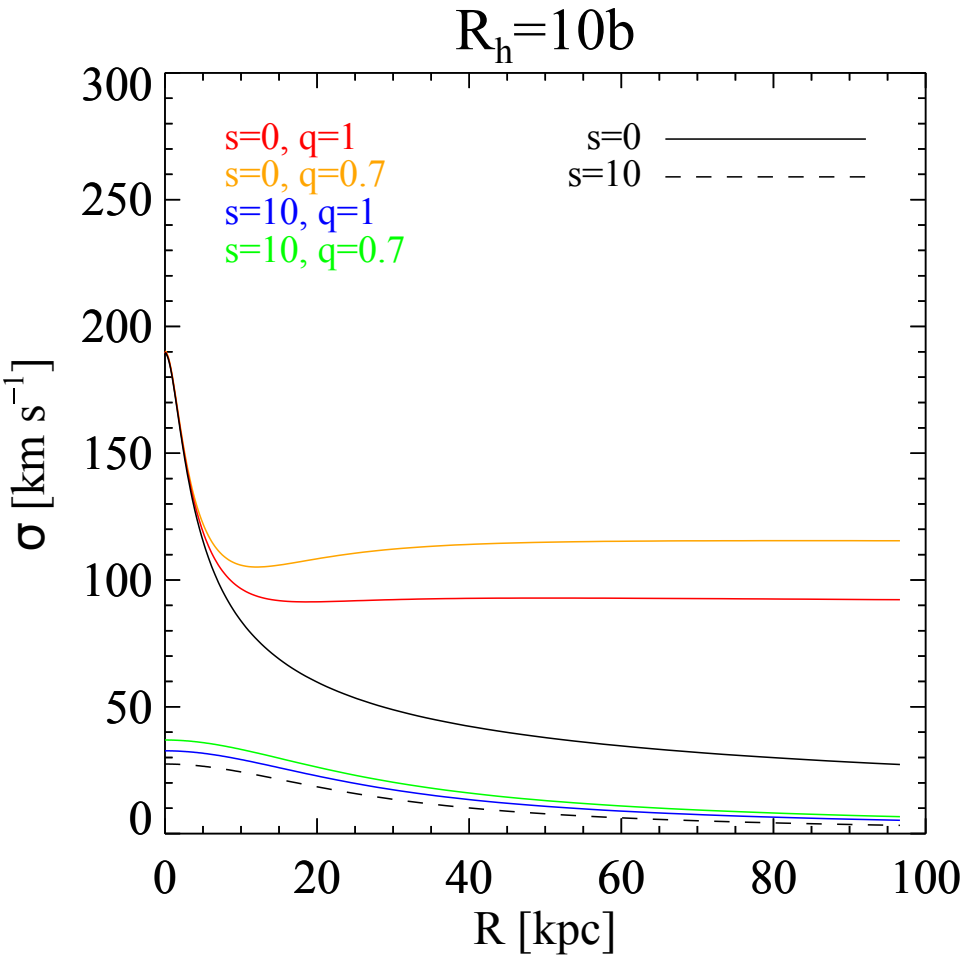

Figure 3.3: σ_* in the equatorial plane ($z = 0$) for our model with $b = 2$ kpc, $M_* = 10^{11} M_\odot$, $v_\mathrm{h} = 200$ km/s, $R_\mathrm{h} = 10b$ and varying values of s and q. The stellar contribution is given by the black curves.

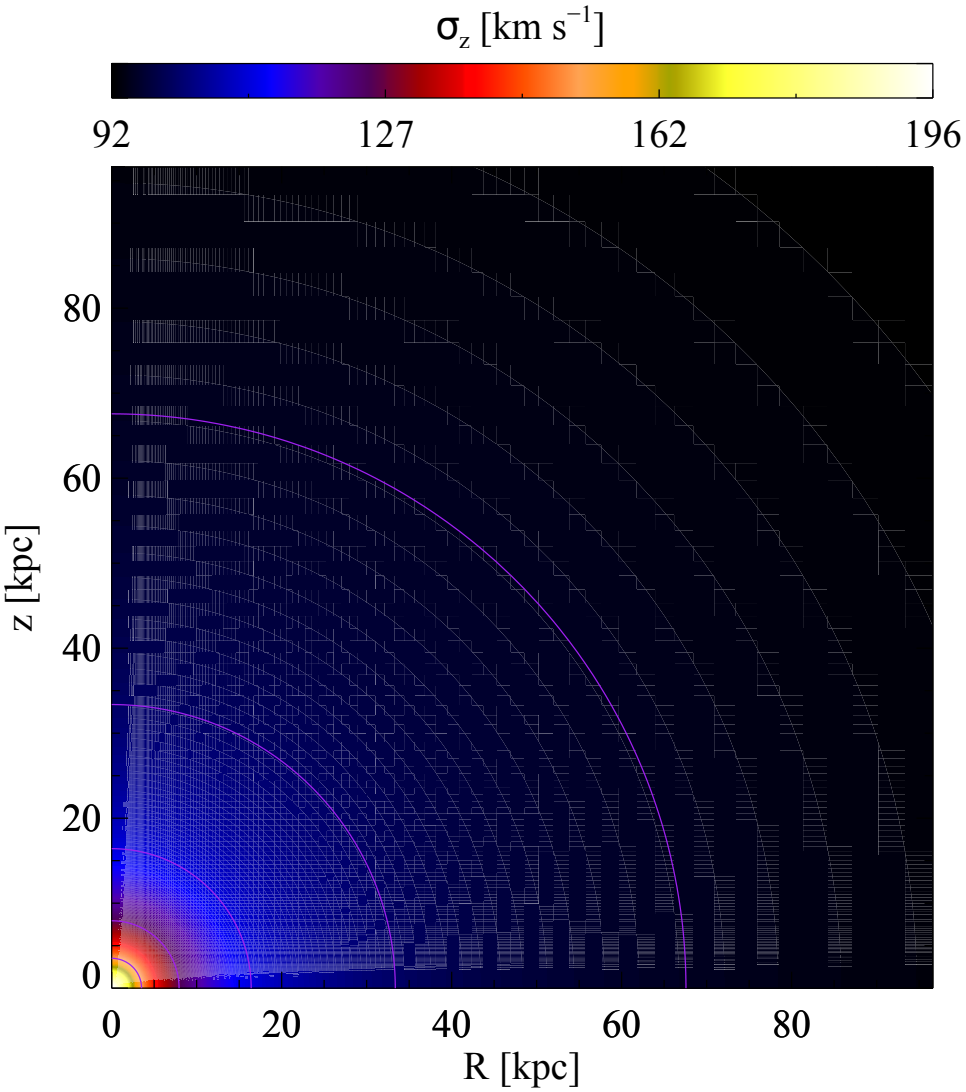

Figure 3.4: σ_* in the full two-dimensional meridional plane for our model with $b = 2$ kpc, $M_* = 10^{11} M_\odot$, $v_\mathrm{h} = 200$ km/s, $R_\mathrm{h} = 2b$, $s = 0$, $q = 1$. Also shown (purple lines) are the isodensity lines for the stellar component.

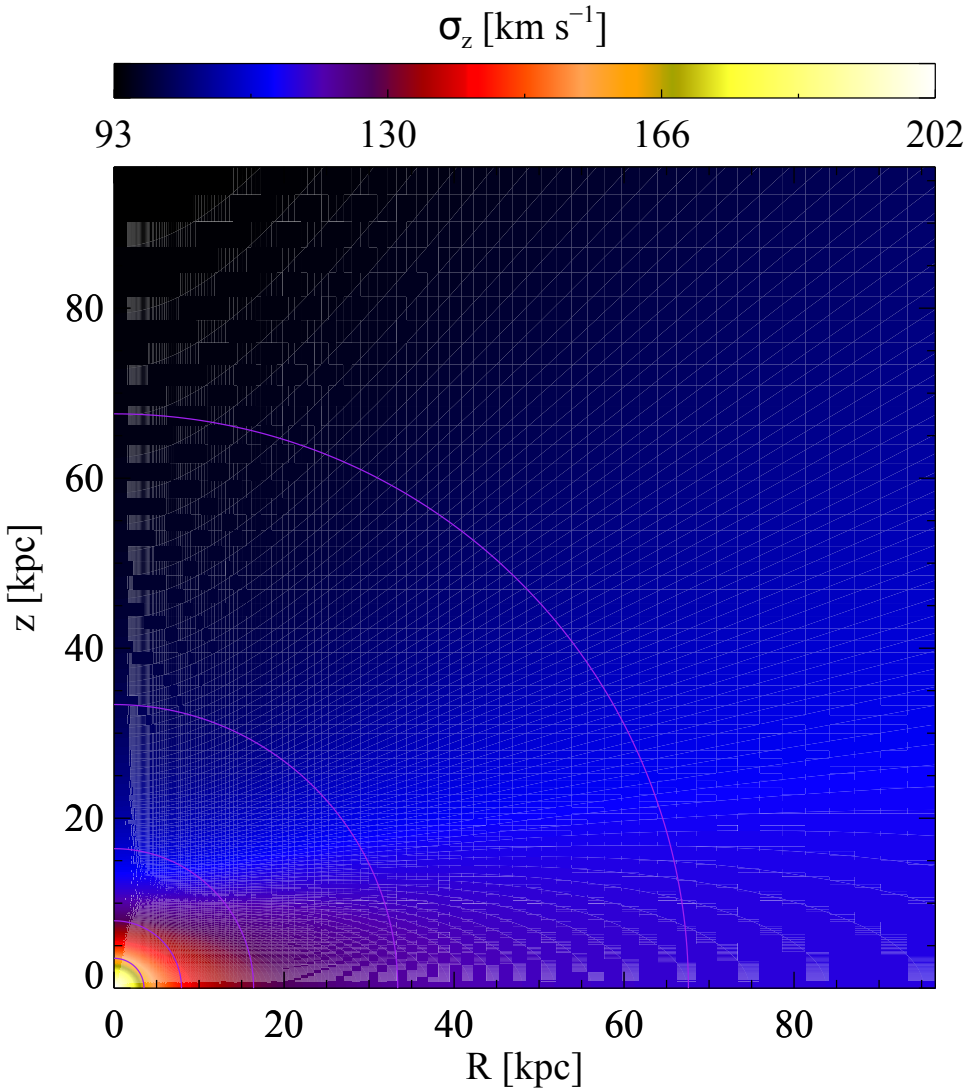

Figure 3.5: σ_* in the full two-dimensional meridional plane for our model with $b = 2$ kpc, $M_* = 10^{11} M_\odot$, $v_\mathrm{h} = 200$ km/s, $R_\mathrm{h} = 2b$, $s = 0$, $q = 0.7$. Also shown (purple lines) are the isodensity lines for the stellar component.

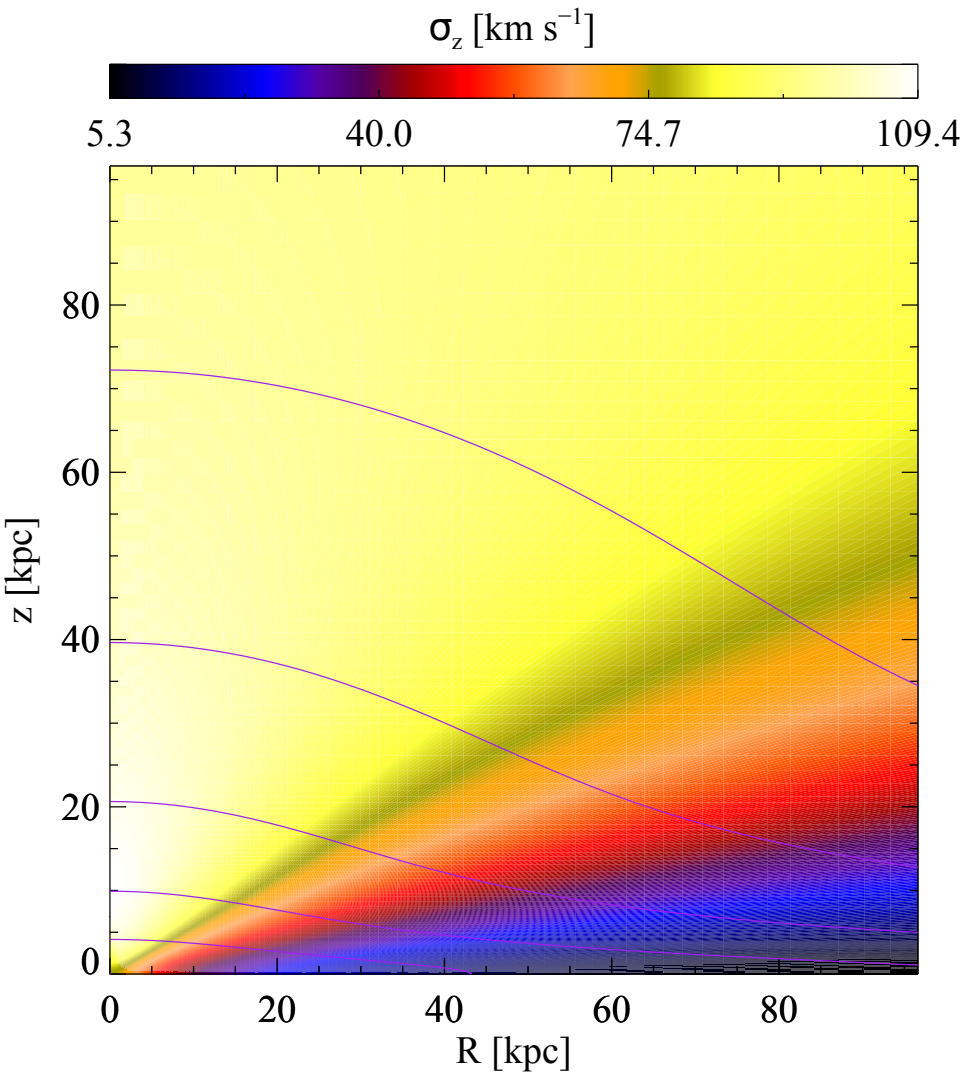

Figure 3.6: σ_* in the full two-dimensional meridional plane for our model with $b = 2$ kpc, $M_* = 10^{11} M_\odot$, $v_\mathrm{h} = 200$ km/s, $R_\mathrm{h} = 2b$, $s = 10$, $q = 1$. Also shown (purple lines) are the isodensity lines for the stellar component.

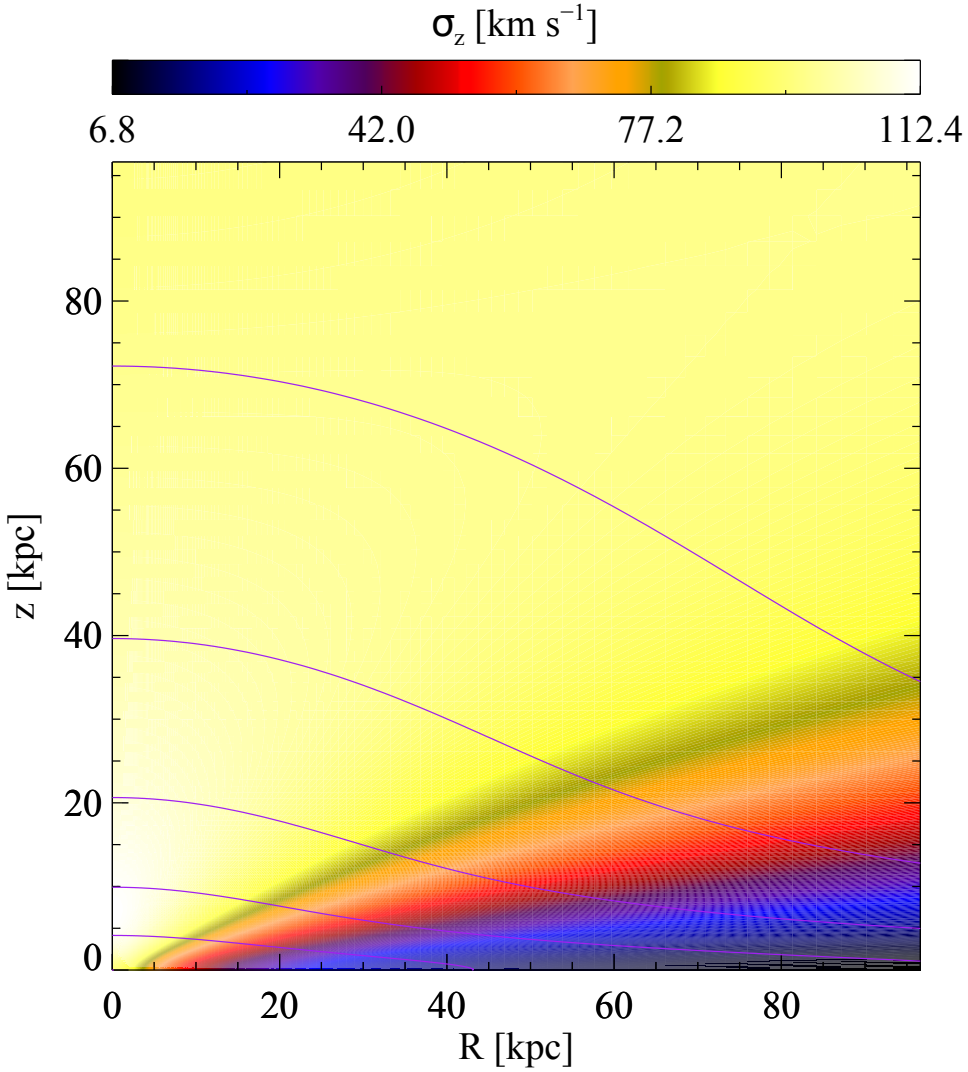

Figure 3.7: σ_* in the full two-dimensional meridional plane for our model with $b = 2$ kpc, $M_* = 10^{11} M_\odot$, $v_\mathrm{h} = 200$ km/s, $R_\mathrm{h} = 2b$, $s = 10$, $q = 0.7$. Also shown (purple lines) are the isodensity lines for the stellar component.

3.1.2 Special cases

In the following we give the explicit solution in the special cases $R = 0$, $A = 0$, $s = 0$. If two or all three of these parameters vanish the following formulae should be used:

- if $A = R = 0$ then eq. (3.31) should be used;
- if $A = s = 0$ then eq. (3.40) should be used;
- if $R = s = 0$ then eq. (3.40) should be used;
- if $A = R = s = 0$ then eq. (3.39) should be used.

Velocity dispersion on the z axis

For $R = 0$, the integral in eq. (3.4) can be easily solved by the standard partial fraction decomposition technique. We obtain

$$I = \frac{1}{As^2\zeta} + \frac{4s}{(A+s^2)^3}\ln\frac{(\zeta+s)^2}{\zeta^2+A} - \frac{A+5s^2}{s^2(A+s^2)^2(\zeta+s)} - \frac{1}{s(A+s^2)(\zeta+s)^2} + \frac{3A^2-6As^2-s^4}{A\sqrt{|A|}(A+s^2)^3}\begin{cases}\arctan\dfrac{\sqrt{A}}{\zeta} & \text{if } A>0;\\ \operatorname{arctanh}\dfrac{\sqrt{|A|}}{\zeta} & \text{if } A<0.\end{cases} \tag{3.30}$$

Note that, by definition, $A \geq -1$ and $\zeta \geq 1$ so that there is no problem with the argument of the arctanh function. Also note that the cases $A = 0$ and $A = -s^2$ should be treated separately: if $A = 0$ then

$$I = \frac{8}{s^5}\ln\frac{\zeta+s}{\zeta} + \frac{s^4+2s^3\zeta-8s^2\zeta^2-36s\zeta^3-24\zeta^4}{3s^4\zeta^3(\zeta+s)^2}. \tag{3.31}$$

If $A = -s^2$ then

$$I = \frac{1}{4s^5}\ln\frac{\zeta+s}{\zeta-s} - \frac{6s^3+10s^2\zeta+9s\zeta^2+3\zeta^3}{6s^4\zeta(\zeta+s)^3}. \tag{3.32}$$

Note that in the latter case $\zeta - s$ cannot be negative since $\zeta \geq 1$ and $A = -s^2 \geq -1$, hence $s \leq 1$.

This gives the solution on the z axis. Notice that this solution is always finite, except in the origin ($z = 0$, hence $\zeta = 1$) in those cases where $A = -1$, which implies that $R_\mathrm{h} = 0$.

Velocity dispersion on the critical cylinder

On the critical cylinder $R^2 = R_c^2 \equiv q^{-2} - R_\mathrm{h}^2$ the parameter A vanishes, and two denominator factors in eq. (3.5) coincide. Note that, if $qR_\mathrm{h} > 1$, there is no critical cylinder since $A > 0$ for every R. If $qR_\mathrm{h} < 1$ then $R_c > 0$, in particular $R_c = 1$ for the SIS model. If $qR_\mathrm{h} = 1$ then the critical cylinder coincides with the z axis and the solution for I is given by eq. (3.31).

The partial fraction decomposition in eq. (3.7) is no longer valid, instead we have that

$$I = \frac{I_\alpha + I_c}{R_c^2}, \tag{3.33}$$

where I_α is as before and I_c can, without loss of generality, be written as

$$I_c = \int_{\operatorname{arcsh}\lambda}^{\infty} \sum_{i=1}^{4} \frac{\theta_i}{(R_c \operatorname{sh} x - s)^i} dx, \tag{3.34}$$

where the coefficients θ_i can be found by the usual partial fraction decomposition technique. The substitution $y = e^x$ transforms the integrals in rational ones:

$$\begin{aligned} \int \frac{dx}{R_c \operatorname{sh} x - s} &= \frac{2}{R_c} \int \frac{dy}{y^2 - 2\frac{s}{R_c} y - 1} \\ &= -\frac{2}{\sqrt{R_c^2 + s^2}} \operatorname{arctanh} \frac{\sqrt{R_c^2 + s^2}}{R_c y - s}. \end{aligned} \tag{3.35}$$

Notice that from eq. (3.34), no singularities are contained in the integration domain. The other integrals are most easily obtained by differentiating with respect to s. The limits of integration for y are ν_c as in eq. (3.20) evaluated at $R = R_c$, and ∞. The final result for I_c obtained in this way can be simplified to

$$\begin{aligned} I_c =& \frac{2R_c^2(3R_c^4 - 24R_c^2 s^2 + 8s^4)}{(R_c^2 + s^2)^{9/2}} \operatorname{arctanh} \frac{\sqrt{R_c^2 + s^2}}{R_c \nu_c - s} \\ &+ \frac{2}{3} \frac{R_c^2 s}{(R_c^2 + s^2)^4} \frac{P_5(\nu_c, R_c)}{(R_c \nu_c^2 - 2s\nu_c - R_c)^3}, \end{aligned} \tag{3.36}$$

where

$$\begin{aligned} P_5(\nu, R) =& 3R^2 s(4R^2 - 3s^2)\nu^5 + R(15R^4 - 54R^2 s^2 + 36s^4)\nu^4 \\ &+ s(-78R^4 + 100R^2 s^2 - 32s^4)\nu^3 + 6R(-4R^4 + 21R^2 s^2 - 10s^4)\nu^2 \\ &+ 3R^2 s(22R^2 - 13s^2)\nu + R^3(13R^2 - 8s^2). \end{aligned} \tag{3.37}$$

A careful treatment shows that in the special case where the critical cylinder coincides with the z axis (i.e. $qR_\mathrm{h} = 1$ and $A = R = 0$), the solution there obtained by eq. (3.33) is indeed the same as the one obtained in eq. (3.31).

Spherical stellar density

The integral (3.4) now simplifies to

$$I = 3\int_{\zeta}^{\infty} \frac{\zeta'}{(R^2+\zeta'^2)^{5/2}(A+\zeta'^2)} d\zeta'. \tag{3.38}$$

The substitution $u = \sqrt{\zeta^2+R^2}$ gives a rational integrand. We have to discern three cases: if $A = R^2$ then

$$I = \frac{3}{5(R^2+\zeta^2)^{5/2}}. \tag{3.39}$$

If $A \neq R^2$ then

$$\begin{aligned} I =& \frac{1}{(A-R^2)(R^2+\zeta^2)^{3/2}} - \frac{3}{(A-R^2)^2\sqrt{R^2+\zeta^2}} \\ &+ \frac{3}{|A-R^2|^{5/2}} \begin{cases} \arctan\sqrt{\dfrac{A-R^2}{R^2+\zeta^2}} & \text{if } A > R^2; \\ \operatorname{arctanh}\sqrt{\dfrac{R^2-A}{R^2+\zeta^2}} & \text{if } A < R^2. \end{cases} \end{aligned} \tag{3.40}$$

3.1.3 An alternative approach

Before using our results for some applications to astrophysical problems, we notice that the integrals that have been calculated so far could (at least for $R > 0$) also be obtained by the Residue Theorem of Complex Analysis. After the change of variable $z = e^x$ in eq. (3.5) we obtain a rational integrand in z, which we call $f_0(z)$. The resulting integration to be performed is in the range $[\nu, \infty[$ and it is trivial to prove that the denominator has no real zeros in this range. The numerator of f_0 has degree 11 and the denominator has degree 16, so that the rational function amply satisfies Jordan's Lemma, see e.g. [30]. In order to use the Residue Theorem we have to modify the integrand so that the contribution after one turn on the circle containing all the poles sums up to be the desired integral. This was done by multiplication of the integrand by $\ln(z-\nu)$. The integration path in the complex plane is qualitatively given in Figure 3.8. At this point the standard method gives

$$I = \int_{\nu}^{\infty} f_0(z)dz = -\sum \mathrm{Res}[f_0(z-\nu)\ln(z-\nu)]. \tag{3.41}$$

The denominator of f_0 is a polynomial of degree 16 in z with real coefficients, which is manifested in the fact that its zeros (hence the poles of f_0) are either real or they come in complex conjugate pairs. The function has both fixed and movable poles. First, there are two fixed quadruple poles at $z_{1,2} = \pm i$. We always have two movable double real poles

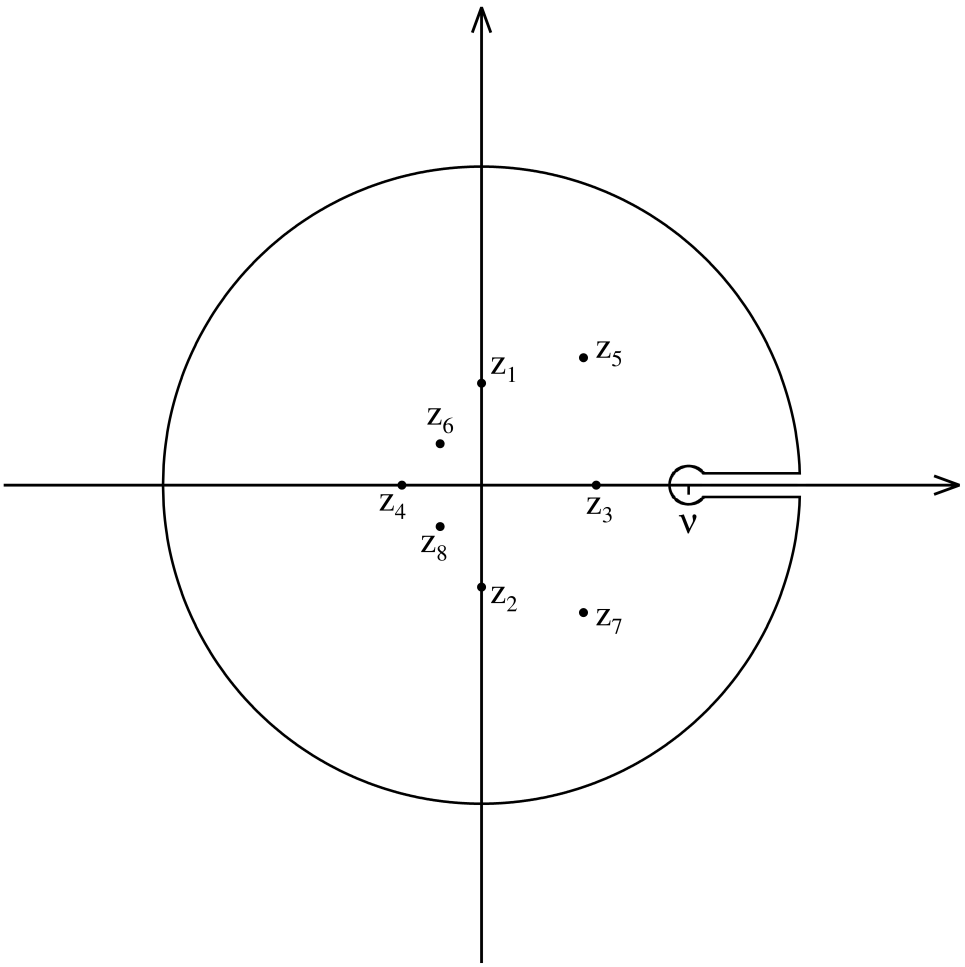

Figure 3.8: The contour in the complex plane. The poles z_1 to z_8 are indicated, the case $A < 0$ is given here.

at $z_{3,4} = (s \pm \sqrt{s^2 + R^2})/R$. Finally we have four movable simple poles at $z_{5,6} = (u \pm \sqrt{u^2 + R^2})/R$ and $z_{7,8} = (v \pm \sqrt{v^2 + R^2})/R^2$, where $u = s + \sqrt{-A}$ and $v = s - \sqrt{-A}$. These four poles are real inside the critical cylinder, outside the critical cylinder they come in two pairs of complex conjugate simple poles. On the critical cylinder they merge with the other double real poles, yielding two quadruple real poles.

We finally notice that despite the elegance of this method and the interesting property that this integration can be performed, we decide not to use this method because the number of poles, their multiplicity and their complex nature does not reduce the amount of work needed to obtain the final (real) results.

3.2 Solution of the second Jeans equation

3.2.1 The general case

In the previous section we gave the solution for the integral I, which solves the first Jeans equation (1.6). For the second Jeans equation (1.7), no further integration is needed: we only need the derivative of I with respect to R. For $R > 0$ one can obtain an explicit expression for dI/dR. The easiest way to do so is to consider eq. (3.5), perform the partial fraction decomposition on the integrand and differentiate with respect to R. The integrals appearing in this way are formally similar to the ones in the previous section and they can be solved with the same techniques.

We differentiate eq. (3.5) with respect to R, taking into account that λ depends on R. This gives

$$\frac{dI}{dR} = -\frac{2I}{R} + \frac{s+\zeta}{R^2\sqrt{1+\lambda^2}} \frac{s + (3R\lambda - 2s)\lambda^2}{(R\lambda - s)^2[A + (R\lambda - s)^2](1+\lambda^2)^2} + \frac{\hat{I}_\alpha + \hat{I}_\beta + \hat{I}_\gamma}{R^2}, \tag{3.42}$$

where

$$\hat{I}_\alpha = \int_{\operatorname{arcsh}\lambda}^{\infty} \frac{\hat{\alpha}_0 + \hat{\alpha}_1 \operatorname{sh} x + \hat{\alpha}_2 \operatorname{sh}^2 x + \hat{\alpha}_3 \operatorname{sh}^3 x}{(1 + \operatorname{sh}^2 x)^2} dx, \tag{3.43}$$

$$\hat{I}_\beta = \int_{\operatorname{arcsh}\lambda}^{\infty} \frac{\hat{\beta}_0 + \hat{\beta}_1 \operatorname{sh} x + \hat{\beta}_2 \operatorname{sh}^2 x}{(R \operatorname{sh} x - s)^3} dx, \tag{3.44}$$

$$\hat{I}_\gamma = \int_{\operatorname{arcsh}\lambda}^{\infty} \frac{\hat{\gamma}_0 + \hat{\gamma}_1 \operatorname{sh} x + \hat{\gamma}_2 \operatorname{sh}^2 x + \hat{\gamma}_3 \operatorname{sh}^3 x}{[A + (R \operatorname{sh} x - s)^2]^2} dx \tag{3.45}$$

and the coefficients are given by

$$\begin{aligned}
\hat{\alpha}_i &= \dot{\alpha}_i \\
\hat{\beta}_0 &= -s\dot{\beta}_0 \\
\hat{\beta}_1 &= R\dot{\beta}_0 - s\dot{\beta}_1 - 2\beta_0 \\
\hat{\beta}_2 &= R\dot{\beta}_1 - 2\beta_1 \\
\hat{\gamma}_0 &= \dot{\gamma}_0(A+s^2) - 2q^2R\gamma_0 \\
\hat{\gamma}_1 &= -2Rs\dot{\gamma}_0 + \dot{\gamma}_1(A+s^2) + 2\gamma_0 s - 2q^2R\gamma_1 \\
\hat{\gamma}_2 &= R^2\dot{\gamma}_0 - 2Rs\dot{\gamma}_1 - 2R\gamma_0 + 2s\gamma_1 \\
\hat{\gamma}_3 &= R^2\dot{\gamma}_1 - 2R\gamma_1
\end{aligned}$$

where the dot denotes differentiation with respect to R. It is clear that $\hat{I}_\alpha$ is formally equal to I_α, hence its solution is

$$\hat{I}_\alpha = \frac{2\hat{\alpha}_0+\hat{\alpha}_2}{3} + \frac{\hat{\alpha}_3}{\sqrt{1+\lambda^2}} - \frac{\hat{\alpha}_0\lambda}{(1+\lambda^2)^{3/2}} - \frac{\hat{\alpha}_3-\hat{\alpha}_1}{3(1+\lambda^2)^{3/2}} - \frac{(\hat{\alpha}_2+2\hat{\alpha}_0)\lambda^3}{3(1+\lambda^2)^{3/2}}. \tag{3.46}$$

We compute $\hat{I}_\beta$ by first performing the substitution $y = \tanh(x/2)$, this leads to

$$\hat{I}_\beta = \frac{2}{s^3}\int_\mu^1 \frac{\hat{\beta}_0 y^4 - 2\hat{\beta}_1 y^3 + (4\hat{\beta}_2 - 2\hat{\beta}_0)y^2 + 2\hat{\beta}_1 y + \hat{\beta}_0}{(y^2+2R/sy-1)^3}dy. \tag{3.47}$$

The quadratic polynomial in the denominator can be factorized as

$$y^2 + \frac{2R}{s}y - 1 = (y-y_+)(y-y_-) \tag{3.48}$$

with

$$y_\pm = -\frac{R}{s} \pm \sqrt{1+\frac{R^2}{s^2}}. \tag{3.49}$$

A partial fraction decomposition then reduces the problem to elementary integrals of the form $\int_\mu^1 (y-y_\pm)^{-n}dy$ with $n = 1, 2, 3$. This decomposition requires the solution of a system of six equations in six variables, which is easily done by standard methods, but we do not give the explicit solutions for the partial fraction decomposition coefficients here since they are quite lengthy.

For $\hat{I}_\gamma$ the substitution $y = e^x$ gives

$$\hat{I}_\gamma = \frac{2}{R^4}\int_\nu^\infty \frac{P(y)}{\Delta^2(y)}dy, \tag{3.50}$$

where $\Delta(y)$ is the polynomial from eq. (3.19) and

$$P(y) = \hat{\gamma}_3 y^6 + 2\hat{\gamma}_2 y^5 + (4\hat{\gamma}_1 - 3\hat{\gamma}_3)y^4 + (8\hat{\gamma}_0 - 4\hat{\gamma}_2)y^3 + (3\hat{\gamma}_3 - 4\hat{\gamma}_1)y^2 + 2\hat{\gamma}_2 y - \hat{\gamma}_3. \tag{3.51}$$

Using the factorisation from eq. (3.22) it is easy to find a partial fraction decomposition of the rational function in the integrand of eq. (3.50), we obtain

$$\begin{aligned}\frac{P(y)}{\Delta^2(y)} =& \frac{\eta_+^{(1)} y + \theta_+^{(1)}}{(y-\Delta_+)^2+\delta_+} + \frac{\eta_-^{(1)} y + \theta_-^{(1)}}{(y-\Delta_-)^2+\delta_-} \\ &+ \frac{\eta_+^{(2)} y + \theta_+^{(2)}}{[(y-\Delta_+)^2+\delta_+]^2} + \frac{\eta_-^{(2)} y + \theta_-^{(2)}}{[(y-\Delta_-)^2+\delta_-]^2}.\end{aligned} \tag{3.52}$$

We do not give the explicit expressions for the numerator coefficients here, since they are too long. They are however easily obtained in the standard way, by multiplying the right-hand side of eq. (3.52) by $\Delta^2(y)$, thus obtaining $P(y)$, and comparing the coefficients with the ones in eq. (3.51). The solution of this linear system of eight equations in eight variables gives the values of the coefficients. The final expression for $\hat{I}_\gamma$ is then easily obtained since only integrals of the following elementary forms remain:

$$\begin{aligned}\int \frac{y-\Delta_\pm}{(y-\Delta_\pm)^2+\delta_\pm} dy =& \frac{1}{2}\ln[(y-\Delta_\pm)^2+\delta_\pm] \\ \int \frac{1}{(y-\Delta_\pm)^2+\delta_\pm} dy =& \frac{1}{\sqrt{|\delta_\pm|}} \begin{cases} \arctan \dfrac{y-\Delta_\pm}{\sqrt{\delta_\pm}} & \text{if } A>0 \\ \operatorname{arctanh} \dfrac{y-\Delta_\pm}{\sqrt{|\delta_\pm|}} & \text{if } A<0 \end{cases} \\ \int \frac{y-\Delta_\pm}{[(y-\Delta_\pm)^2+\delta_\pm]^2} dy =& -\frac{1}{2[(y-\Delta_\pm)^2+\delta_\pm]} \\ \int \frac{1}{[(y-\Delta_\pm)^2+\delta_\pm]^2} dy =& \frac{y-\Delta_\pm}{2\delta_\pm[(y-\Delta_\pm)^2+\delta_\pm]} \\ &+ \frac{1}{2\delta_\pm\sqrt{|\delta_\pm|}} \begin{cases} \arctan \dfrac{y-\Delta_\pm}{\sqrt{\delta_\pm}} & \text{if } A>0 \\ \operatorname{arctanh} \dfrac{y-\Delta_\pm}{\sqrt{|\delta_\pm|}} & \text{if } A<0. \end{cases}\end{aligned} \tag{3.53}$$

Two-dimensional colour-coded maps of σ_φ are given in Figures 3.9 and 3.10. Notice that for $q = 1$ we get quite high values of σ_φ further above the equatorial plane than for $q = 0.7$.

3.2.2 Special cases

We have to distinguish the same special cases as in the previous section, since the obtained formulae do not apply anymore when $sAR = 0$.

On the z axis

Notice that by eq. (3.4) it is clear that I is an even function of R, hence $dI/dR = 0$ at $R = 0$.

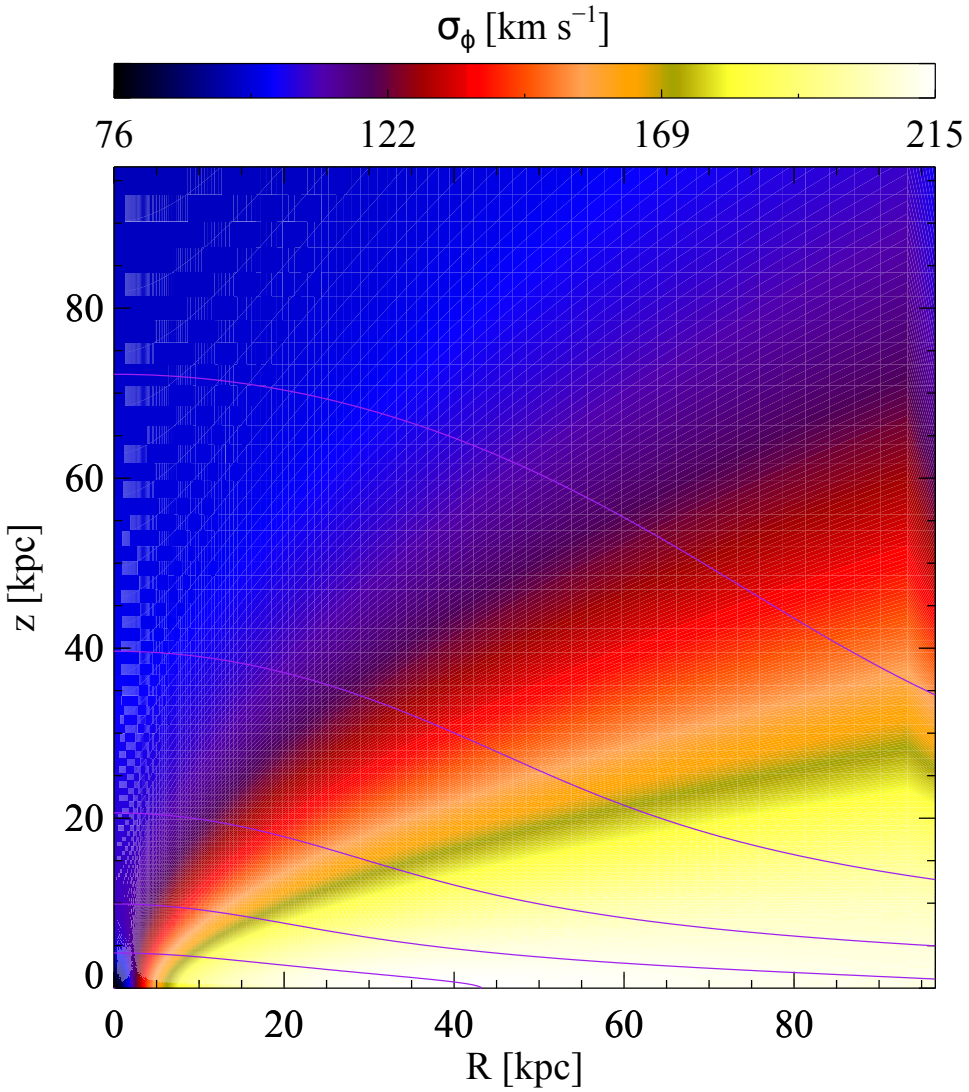

Figure 3.9: $\sigma_{*,\varphi}$ in the full two-dimensional meridional plane for our model with $b = 2$ kpc, $M_* = 10^{11} M_\odot$, $v_\mathrm{h} = 200$ km/s, $R_\mathrm{h} = 2b$, $s = 10$, $q = 1$. Also shown (purple lines) are the isodensity lines for the stellar component.

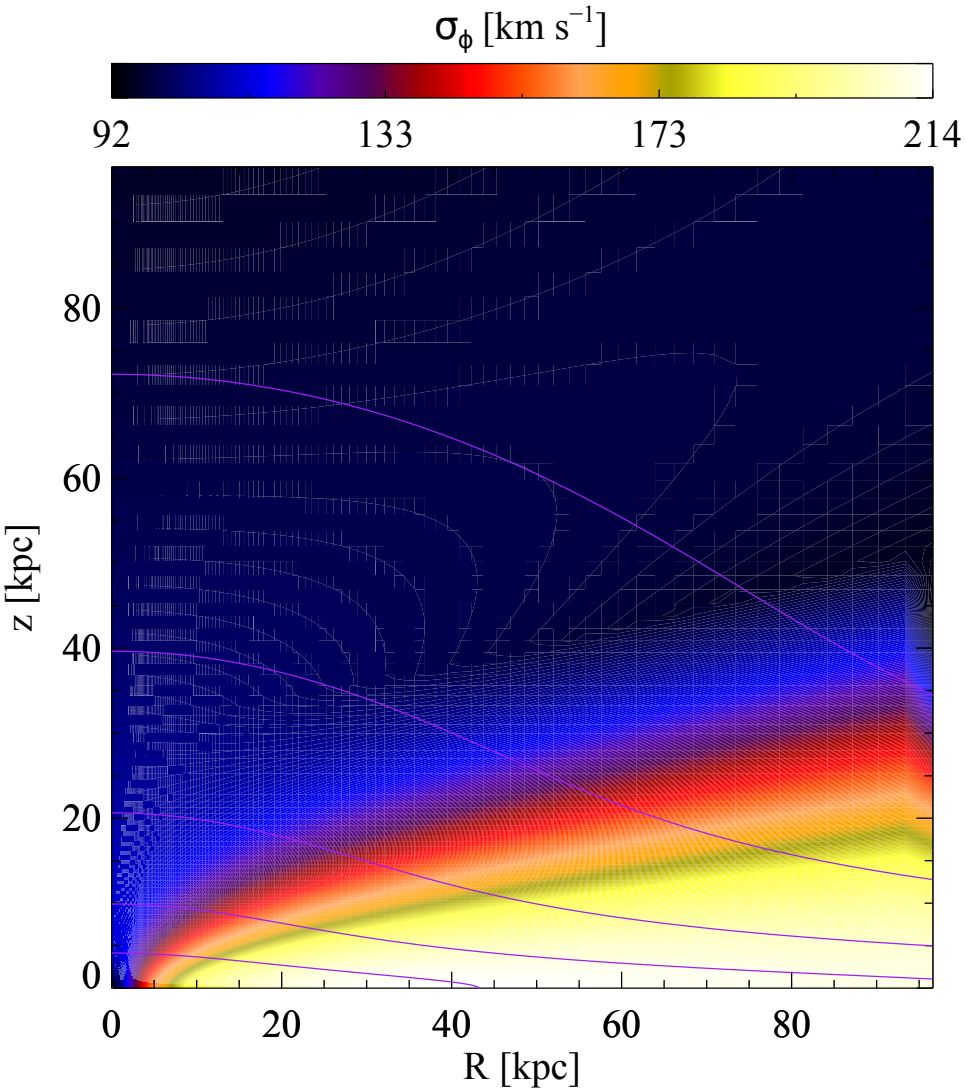

Figure 3.10: $\sigma_{*,\varphi}$ in the full two-dimensional meridional plane for our model with $b = 2$ kpc, $M_* = 10^{11} M_\odot$, $v_\mathrm{h} = 200$ km/s, $R_\mathrm{h} = 2b$, $s = 10$, $q = 0.7$. Also shown (purple lines) are the isodensity lines for the stellar component.

On the critical cylinder

There are several ways to obtain dI/dR on the critical cylinder, i.e. for $A = 0$. Unfortunately, they are all quite complicated. Of course one can take the limit of the general solution for $A \to 0$. In this limit the divergent quantities in $\hat{I}_\beta$ and $\hat{I}_\gamma$ cancel each other. Another approach is to differentiate eq. (3.4) and to evaluate this at $A = 0$. This integral can then be solved in the same way as we solved I in the general case, i.e. with the substitution $\operatorname{sh} x = (s + \zeta)/R$. This leads to

$$\frac{dI}{dR} = \int_{\operatorname{arcsh}\lambda}^{\infty} \frac{P_5(\operatorname{sh} x)}{(R\operatorname{sh} x - s)^6(1 + \operatorname{sh}^2 x)^3} dx, \tag{3.54}$$

where P_5 is a fifth degree polynomial. With an exponential or $\tanh(x/2)$ substitution this transforms in a rational integral, but it is clear that the calculations will be quite cumbersome. Note that obviously differentiating the solution for $A = 0$ with respect to R (which would be considerably less complicated) does not give the desired result, since A depends on R.

Spherical stellar density

If $s = 0$ then we again use eq. (3.38). Differentiating the integrand with respect to R, we obtain

$$\begin{aligned}\frac{dI}{dR} = &-15R \int_\zeta^\infty \frac{\zeta'}{(R^2 + \zeta'^2)^{7/2}(A + \zeta'^2)} d\zeta' \\ &- 3q^2 R \int_\zeta^\infty \frac{\zeta'}{(R^2 + \zeta'^2)^{5/2}(A + \zeta'^2)^2} d\zeta'.\end{aligned} \tag{3.55}$$

Both integrals become rational after the substitution $u = \sqrt{\zeta^2 + R^2}$ and with the standard methods we obtain

$$\frac{dI}{dR} = -\frac{3(5 + 2q^2)R}{7(\zeta^2 + R^2)^{7/2}} \tag{3.56}$$

if $A = R^2$ and else

$$\begin{aligned}\frac{dI}{dR} =& \frac{R(5 - 2q^2)}{(A - R^2)^2(R^2 + \zeta^2)^{3/2}} - \frac{3R(5 - 4q^2)}{(A - R^2)^3\sqrt{R^2 + \zeta^2}} - \frac{3R}{(A - R^2)(R^2 + \zeta^2)^{5/2}} \\ &+ \frac{3q^2 R\sqrt{R^2 + \zeta^2}}{(A - R^2)^3(\zeta^2 + A)} + \frac{15(1 - q^2)R}{|A - R^2|^{7/2}} \begin{cases} \arctan \dfrac{\sqrt{A - R^2}}{\sqrt{R^2 + \zeta^2}} & \text{if } A > R^2 \\ -\operatorname{arctanh} \dfrac{\sqrt{R^2 - A}}{\sqrt{R^2 + \zeta^2}} & \text{if } A < R^2. \end{cases}\end{aligned} \tag{3.57}$$

Chapter 4

Preliminary analysis

The obtained formulae are analytical and simple, yet they are complicated enough to not give an immediate feeling about the behaviour of the model as a function of the parameters. For this reason, as is often done in similar studies, asymptotic formulae are useful, due to their extremely simple algebraic form. In addition, asymptotic formulae are also important because they can be used as a check for the full solutions, by comparing numerical results in the limit cases. Finally, we stress that the obtained formulae have also been tested against the direct numerical solution of the Jeans equations obtained with the numerical code in [24]. The relative errors on the velocity dispersion in a typical region (the central 50 kpc) are of the order of magnitude of 1 in 1000, which is a very satisfactory result. Figures 4.1 and 4.2 show the exact analytical solution for σ and the solution obtained by the numerical code, respectively.

4.1 Influence of the parameters on the derived quantities

Figures 3.1-3.3 show the influence of the various parameters $R_{\rm h}$, s and q on the value of σ_* in the equatorial plane. It is clear that the behaviour in the central regions is mostly determined by the values of $R_{\rm h}$ and s. Indeed, if $R_{\rm h}$ is very small, the dark matter density near the origin is high, which has a big influence on the velocity dispersion near the origin. The more the baryonic matter is in a flat disk (i.e., the larger s), the lower the value of the velocity dispersion everywhere. Also the influence of q is clear: an oblate dark matter halo ($q < 1$) causes a larger velocity dispersion than a spherical ($q = 1$) or a prolate ($q > 1$) halo.

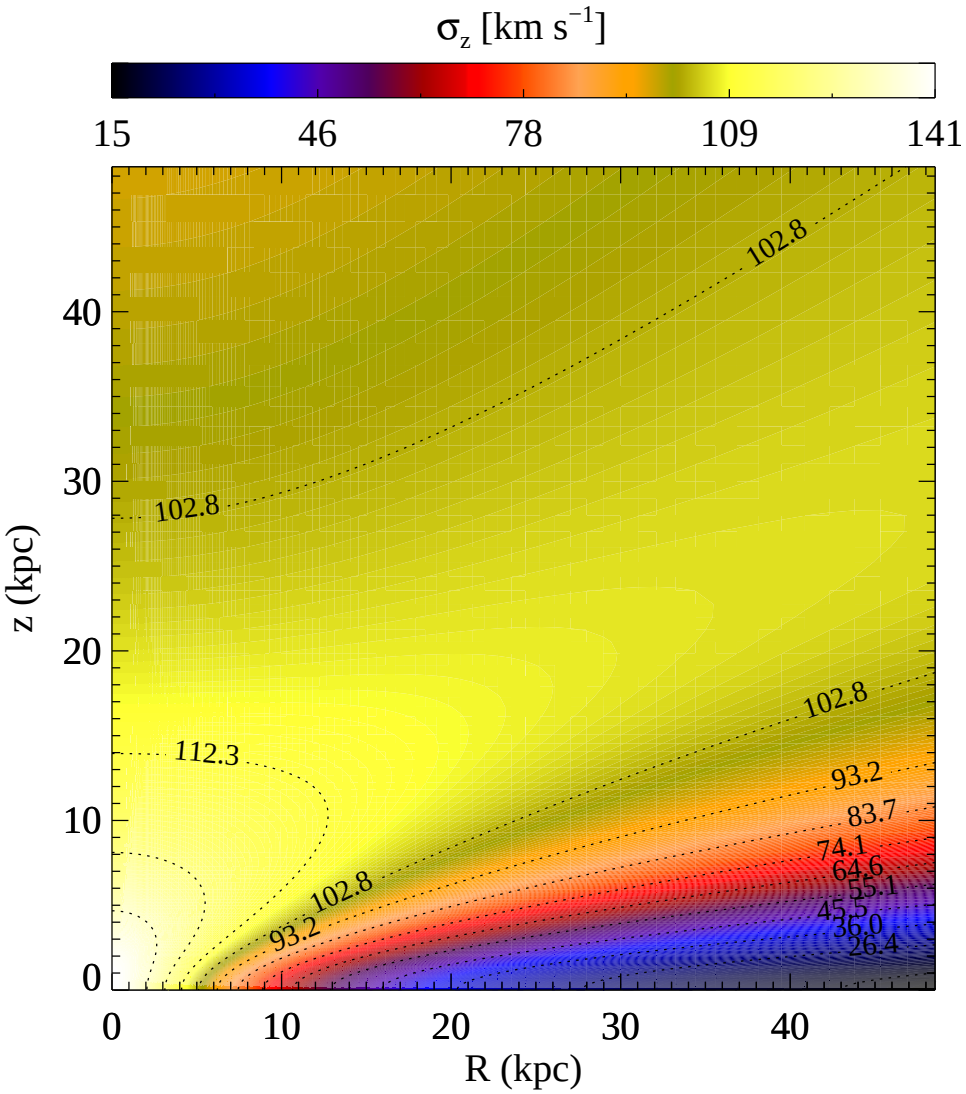

Figure 4.1: σ_z for the inner 50 kpc, based on the obtained (exact) analytical solution with model parameters $b = 2$ kpc, $M_* = 10^{11} M_\odot$, $v_\mathrm{h} = 200$ km/s, $R_\mathrm{h} = 2b$, $q = 0.7$, $s = 1$.

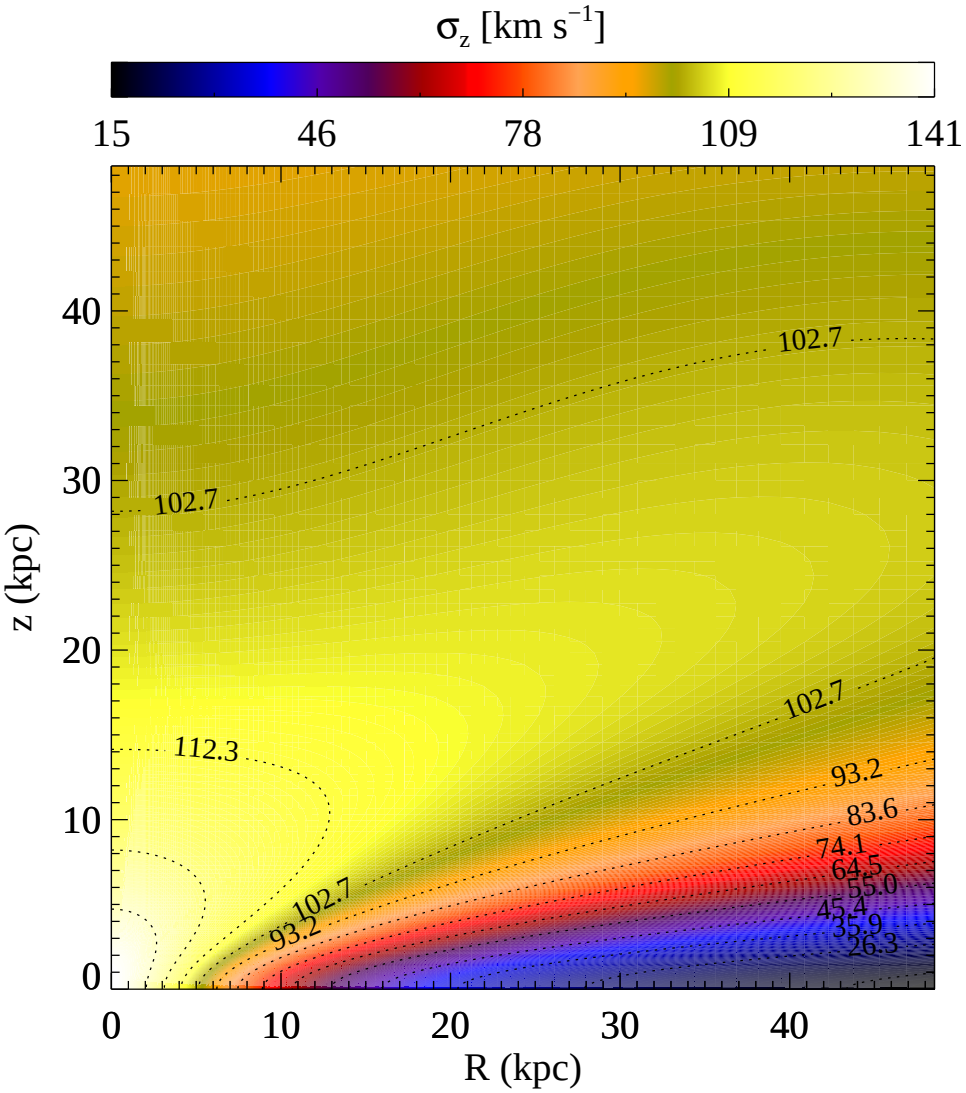

Figure 4.2: σ_z for the inner 50 kpc, based on the numerical solution of the Jeans equations with model parameters $b = 2$ kpc, $M_* = 10^{11} M_\odot$, $v_\mathrm{h} = 200$ km/s, $R_\mathrm{h} = 2b$, $q = 0.7$, $s = 1$.

4.2 Asymptotics

We study, as an example, how the dark matter halo shape and density affect the vertical velocity dispersion and the asymmetric drift of the model, which are two quantities that can be observed. First we give the asymptotic behaviour of the velocity dispersion for the model. The asymptotic expansion of all dynamical quantities of the self-gravitating Miyamoto-Nagai model without halo is trivial and can be obtained directly from the exact expressions given in Chapter 2.

The obtained formulae reported in the text are fully general and they can be easily implemented in numerical codes and in computer algebra systems to explore the behaviour of the model in all cases of interest. However they are sufficiently cumbersome to avoid an immediate reading of their physical contents. For this reason it is helpful to provide asymptotic expansions at selected places in the model. In principle the asymptotic expansions can be obtained by working directly on the obtained expressions, however the asymptotic analysis can also be performed directly on the integral in eq. (3.4). As usual with asymptotic expansions of integrals, some care is needed. As we will see, at all these selected places the velocity dispersion field is dominated at the leading order by the dark matter halo effects.

Recall that all squared velocities such as σ^2 and $v_{\rm h}^2$ are normalized to GM_*/b. We begin with the behaviour near the origin. Two cases must be distinguished: $R_{\rm h} = 0$ and $R_{\rm h} > 0$. In fact, as shown with the aid of a simple ellipsoidal model in Appendix B, in the case $R_{\rm h} = 0$ it is expected that σ_*^2 diverges. Indeed, if $R_{\rm h} = 0$ then

$$\sigma_*^2 = -v_{\rm h}^2 \ln \sqrt{z^2 + q^2 R^2} + \frac{2v_{\rm h}^2 (s+1)^4 \varphi(s) + 1}{2(s+1)(s+3)} + \mathcal{O}(R, z), \tag{4.1}$$

where

$$\varphi(s) = \frac{(s^4 - 6s^2 - 3)\ln 2 + 8s \ln(s+1) - (s^4 - 3s^2 + 6s - 4)}{(s^2-1)^3} \tag{4.2}$$

and $\varphi(1) = \ln(2)/2 - 7/12$. Also $\overline{v_\varphi^2}$ has the same behaviour. If $R_{\rm h} > 0$ then I is finite at the origin (and hence so is σ_*^2) and its value can be obtained by substitution of $z = 0$ into eq. (3.30). As the resulting formulae are trivial to obtain and not illuminating, we do not report them here.

The value of I along the z axis ($R = 0$) is given in Section 3.1.2 (as described at the end of Section 3.1.1, the formulae obtained there are not valid on the z axis). If we let z (and hence ζ) tend to infinity we obtain after an asymptotic expansion

$$\sigma_*^2 = \frac{1}{5} v_{\rm h}^2 + \left(\frac{4s}{45} v_{\rm h}^2 + \frac{1}{6} \right) z^{-1} + \mathcal{O}(z^{-2}) \tag{4.3}$$

as z tends to infinity.

Finally the treatment in the equatorial plane ($z = 0$) for $R \to \infty$ is considerably more complicated than the other two cases. The behaviour in the equatorial plane is given to the first two leading terms, in order to show explicitly the effect of the stellar density. However, this is by far the most interesting application of our models, i.e. the possibility of using kinematic properties in the equatorial plane to infer information about the dark matter halo flattening. The following formula has been obtained both by expansion of the integral and of the explicit formula, and was also verified numerically, thus giving an independent check of the obtained formulae. If $s > 0$ (i.e. the stellar density distribution is not spherical),

$$\sigma_*^2 = \left[\frac{1}{q^2} + \frac{\xi(q)}{s}\right]\frac{v_\mathrm{h}^2}{R^2} + \left[\frac{(s+1)^2}{2s} + v_\mathrm{h}^2\tau(q)\right]\frac{1}{R^3} + \mathcal{O}(R^{-4}), \tag{4.4}$$

where

$$\xi(q) = \frac{q^2-4}{(q^2-1)^2} + \frac{3}{|q^2-1|^{5/2}}\begin{cases}\arctan\sqrt{q^2-1} & \text{if } q > 1\\ \operatorname{arctanh}\sqrt{1-q^2} & \text{if } q < 1\end{cases} \tag{4.5}$$

and $\xi(1) = 3/5$, and

$$\begin{aligned}\tau(q) =& \frac{q^4-3q^2+17}{(q^2-1)^3} - \frac{1}{q^2}\\ &+ \frac{8q^4+8q^2-1}{q^3|q^2-1|^{7/2}}\begin{cases}-\operatorname{arctanh}\dfrac{\sqrt{q^2-1}}{q} & \text{if } q > 1\\ \arctan\dfrac{\sqrt{1-q^2}}{q} & \text{if } q < 1\end{cases}\end{aligned} \tag{4.6}$$

and $\tau(1) = -64/105$. If $s = 0$ however this asymptotic behaviour changes to

$$\sigma_*^2 = \frac{\xi(q)}{3}v_\mathrm{h}^2 + \frac{1}{6R} + \mathcal{O}(R^{-2}). \tag{4.7}$$

Also notice that the parameter choice $q = 1$ and $s = 0$ introduces spherical symmetry to both the stellar and the dark matter component. Hence it is not a surprise that in this case the asymptotic behaviour along the z axis is the same as in the equatorial plane, both near the origin and at infinity.

4.3 Influence of a supermassive central black hole

Consider a black hole with potential

$$\Phi_\mathrm{BH} = -\frac{GM_\mathrm{BH}}{r} = -\frac{\epsilon}{\sqrt{R^2+z^2}} \tag{4.8}$$

where $\epsilon = M_\mathrm{BH}/M_*$ and the same normalizations have been used.

Then the circular velocity contribution is

$$v_{\rm circ}^2(R) = \frac{\epsilon}{R}, \tag{4.9}$$

so that at $R \to \infty$ it ends up in the first term different from $v_{\rm h}^2$, next to a term $1/R$. Since $\epsilon \sim 10^{-3}$ this contribution is very small. Near the origin however, this contribution diverges evidently.

It seems to be impossible to solve the Jeans equations explicitly in the general case. However it is possible to give an asymptotic expansion both near the origin and at large distance, and to solve the Jeans equation (1.1) in the spherical ($a = s = 0$) and isotropic ($\beta = 0$) case: we then get

$$\sigma_{*,\rm BH} = \frac{\epsilon}{3r}\left[-8r(r^2+1)^{5/2} + (r^2+1)(8r^4+12r^2+3)\right]. \tag{4.10}$$

The velocity dispersion component caused by the black hole near the origin is given by

$$\sigma_{*,\rm BH}^2 = \frac{\epsilon}{\sqrt{R^2+z^2}} + \epsilon g(s) + \mathcal{O}(R,z), \tag{4.11}$$

where

$$g(s) = -\frac{2s^4-9s^2-8}{(s+3)(s-1)^3} - \frac{15s}{(s+3)(s-1)^3\sqrt{|s^2-1|}} \begin{cases} \arctan\frac{\sqrt{1-s^2}}{s} & \text{if } s<1; \\ \operatorname{arctanh}\frac{\sqrt{s^2-1}}{s} & \text{if } s>1 \end{cases} \tag{4.12}$$

and $g(1) = -16/7$. The function g is increasing, with $g(0) = -8/3$ and $g(s) \to -2$ as $s \to \infty$. This behaviour is interesting: for very small r the contribution will be stronger than the one caused by the halo (in the divergent $R_{\rm h} = 0$ case). Since ϵ is very small, from a certain r on the halo contribution will dominate. For typical values $q = 1$, $R_{\rm h} = 0$, $\epsilon = 10^{-3}$, $v_{\rm h} = 1$ the leading terms are equal at $r = 10^{-4}$.

In the equatorial plane the velocity dispersion component caused by the black hole depends on s: if $s > 0$ then

$$\sigma_{*,\rm BH}^2 = \epsilon\left(1+\frac{1}{2s}\right)\frac{1}{R^3} + \mathcal{O}(R^{-5}). \tag{4.13}$$

If $s = 0$ then

$$\sigma_{*,\rm BH}^2 = \frac{\epsilon}{6R} + \mathcal{O}(R^{-3}). \tag{4.14}$$

Hence in both cases the black hole only causes a contribution in the second order term, and with a coefficient which contains the very small ϵ.

It is easily checked that the explicit solution for the velocity dispersion in the spherical isotropic case, given above, is consistent with the asymptotic expansions, both at the origin and at infinity.

4.4 The virial quantities

Remarkably, in the SIS halo case it is trivial to prove that the halo contribution in the virial interaction energy, defined by

$$W = -\int \rho_* \langle \mathbf{x}, \nabla \Phi_{\mathrm{t}} \rangle d^3\mathbf{x} = W_{**} + W_{*\mathrm{h}}, \tag{4.15}$$

is given by

$$W_{*\mathrm{h}} = -v_{\mathrm{h}}^2 M_*. \tag{4.16}$$

In the Binney case such an easy result in general does not hold. In that case we have that

$$\begin{aligned} W_{*\mathrm{h}} &= -v_{\mathrm{h}}^2 \int \rho_* \frac{q^2R^2 + z^2}{q^2R^2 + z^2 + q^2R_{\mathrm{h}}^2}\, dV \\ &= -v_{\mathrm{h}}^2 M_* + v_{\mathrm{h}}^2 q^2 R_{\mathrm{h}}^2 \int \frac{\rho_*}{q^2R^2 + z^2 + q^2R_{\mathrm{h}}^2}\, dV. \end{aligned} \tag{4.17}$$

This implies that $W_{*\mathrm{h}}$ is a strictly increasing function of R_{h}. If $R_{\mathrm{h}} = 0$ (so also in the case of a non-spherical halo) then eq. (4.16) holds. If $R_{\mathrm{h}} > 0$ it seems impossible to solve the integral in eq. (4.17) with elementary functions, even if it is possible the formulas will probably be so complicated that they have no practical use.

4.5 A rule of thumb

After verification that all formulae are correct, we can come to these main conclusions:

- There is the influence of the flattening of the baryonic matter on the velocity dispersion: a more spherical distribution gives higher values for σ.
- The role of the parameter R_{h}, which determines the dark matter density in the central regions, is important mainly in these central regions, with increasing σ as R_{h} decreases.
- The halo flattening parameter q (the lower q, the flatter the dark matter halo) is present in the leading term of the asymptotic expansion of σ at large distance. This term is a decreasing function of q.
- As was to be expected, the influence of a central black hole is very much limited to the central regions.

Chapter 5

Three applications

As examples of applications of our new model, we present a few representative cases of the behaviour of the vertical velocity dispersion of stars near the equatorial plane as a function of the dark matter halo flattening, the behaviour of the asymmetric drift and an estimate for the velocity of the radial flow.

5.1 The influence of the halo flattening parameter

From an observational point of view, the influence of the dark matter halo flattening parameter q on the velocity dispersion, is perhaps the most interesting one. The shape of the dark matter halo is the topic of ongoing research, but since all the effects of the dark matter can only be observed indirectly, by the consequences of its gravitational interaction, it is not easy to establish what shape the halo has. Most observations point in the direction of almost spherical haloes, but this is quite a rough estimate: some authors find prolate or triaxial haloes [9], [10], [13], [26].

With these uncertainties in mind, it is interesting to see how the halo flattening parameter q influences observable quantities. Looking back at Figures 3.1-3.3 it is clear that σ in the equatorial plane is a decreasing function of q, where the slope of this function is stronger (i.e. the influence of q is bigger) for more spherical galaxies (i.e. s is small).

Comparing Figures 3.6 and 3.7 we see that in a position high above the equatorial plane and far from the center, for a flatter halo (i.e. $q = 0.7$) we get higher values for σ than for $q = 1$. The same general trend applies to σ_φ, as can be seen by comparing Figures 3.9 and 3.10.

5.2 The asymmetric drift

The circular velocity in the equatorial plane is

$$v_{\rm circ}^2(R) = R\frac{\partial \Phi_{\rm t}}{\partial R} = \frac{R^2}{[R^2+(s+1)^2]^{3/2}} + \frac{v_{\rm h}^2 R^2}{R_{\rm h}^2+R^2}. \tag{5.1}$$

For $R \to \infty$ we can expand this as

$$v_{\rm circ}^2 = v_{\rm h}^2 + \frac{1}{R} - \frac{R_{\rm h}^2 v_{\rm h}^2}{R^2} - \frac{3}{2}\frac{(s+1)^2}{R^3} + \mathcal{O}\left(R^{-4}\right). \tag{5.2}$$

Near the origin we notice that the asymptotic expansion strongly depends on $R_{\rm h}$. If $R_{\rm h} = 0$ then

$$v_{\rm circ}^2 = v_{\rm h}^2 + \frac{R^2}{(s+1)^3} - \frac{3}{2}\frac{R^4}{(s+1)^5} + \mathcal{O}\left(R^6\right), \tag{5.3}$$

but if $R_{\rm h} > 0$ then

$$v_{\rm circ}^2 = \left[\frac{v_{\rm h}^2}{R_{\rm h}^2} + \frac{1}{(s+1)^3}\right] R^2 - \left[\frac{v_{\rm h}^2}{R_{\rm h}^4} + \frac{3}{2(s+1)^5}\right] R^4 + \mathcal{O}\left(R^6\right). \tag{5.4}$$

The asymmetric drift (AD, see [4]) is the phenomenon where there is a difference between the circular velocity $v_{\rm circ}$ and the azimuthal velocity v_φ. We have that

$$v_{\rm circ}^2 - \overline{v_\varphi}^2 = -\frac{R}{\rho_*}\frac{\partial \rho_* \sigma^2}{\partial R}, \tag{5.5}$$

which holds in the case of an isotropic rotator ($k = 1$) and follows immediately from eqs. (1.7) and (1.9). We focus on the difference of the squared velocities because it is of easiest evaluation in our case. Using the asymptotic behaviour obtained before, we see that

$$v_{\rm circ}^2 - \overline{v_\varphi}^2 = \frac{5v_{\rm h}^2}{R^2}\left[\frac{1}{q^2} + \frac{\xi(q)}{s}\right] + \frac{6}{R^3}\left[\frac{(s+1)^2}{2s} + v_{\rm h}^2\tau(q)\right] + \mathcal{O}(R^{-4}) \tag{5.6}$$

if $s > 0$ and

$$v_{\rm circ}^2 - \overline{v_\varphi}^2 = \frac{5}{3}\xi(q)v_{\rm h}^2 + \frac{1}{R} + \mathcal{O}(R^{-2}) \tag{5.7}$$

if $s = 0$ and so in particular AD $\sim v_{\rm h}^2 + 1/R$ in the spherical case where $s = 0$ and $q = 1$. Notice that for fixed s, the leading order term of the expansion is a decreasing function of q. Figures 5.1-5.6 show the AD and the AD as a fraction of the circular velocity as functions of R in the equatorial plane. For these graphs we took the definition of AD as difference of velocities:

$$\text{AD} = v_{\rm circ} - \overline{v_\varphi}, \tag{5.8}$$

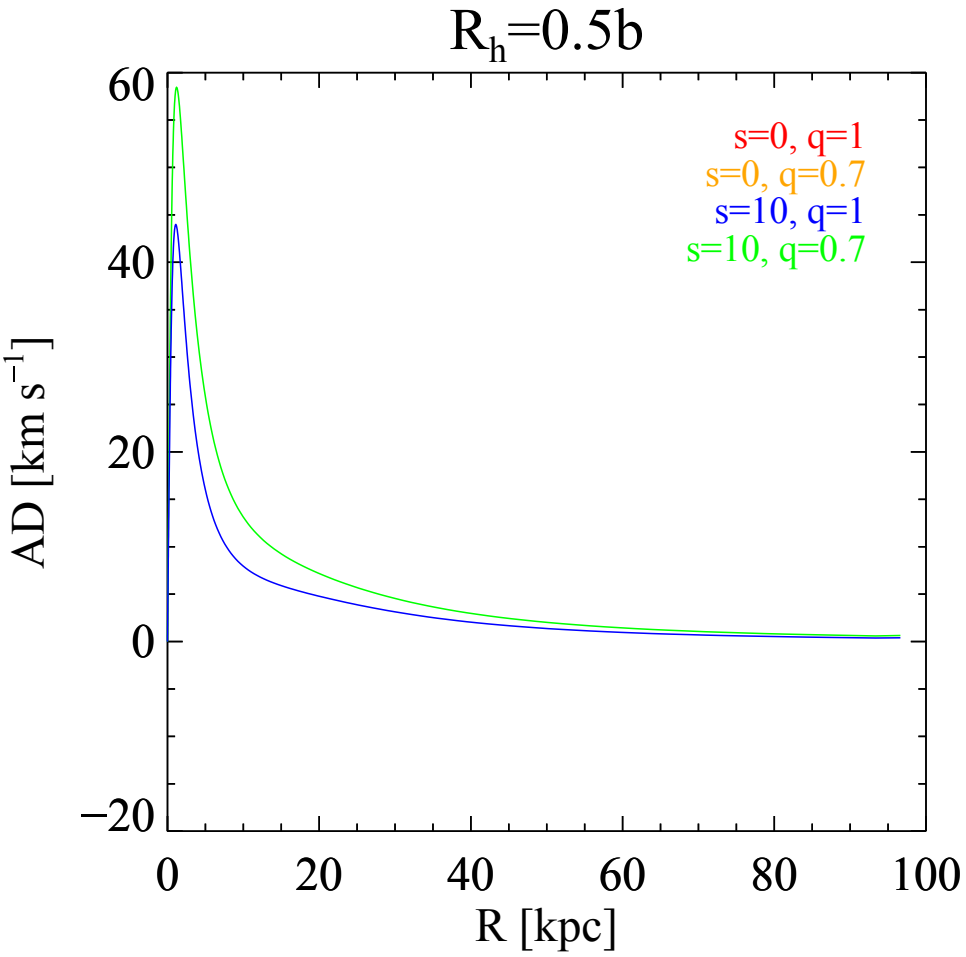

Figure 5.1: The AD in the equatorial plane for our model with $b = 2$ kpc, $M_* = 10^{11} M_\odot$, $v_\mathrm{h} = 200$ km/s, $R_\mathrm{h} = 0.5b$ and different values of s and q.

so that dimensionally the AD is a velocity. Since for $s = 0$ the velocity $\overline{v_\varphi}$ vanishes, we get that AD $= v_\mathrm{circ}$ and the graphs for this case have been omitted. Figure 5.7 shows a map of the AD also outside the equatorial plane. The circular velocity is given in Figures 5.8-5.10, notice that this quantity does not depend on the halo flattening parameter q. The velocity v_φ in the equatorial plane is given in Figures 5.11-5.13, two maps are given in Figures 5.14 and 5.15.

5.3 An estimate for the velocity of the radial flow

In the previous section we discussed the importance of the asymmetric drift in our model. It is clear that radial flows will occur as a consequence of this asymmetric drift. The mechanism at hand is the following: suppose there

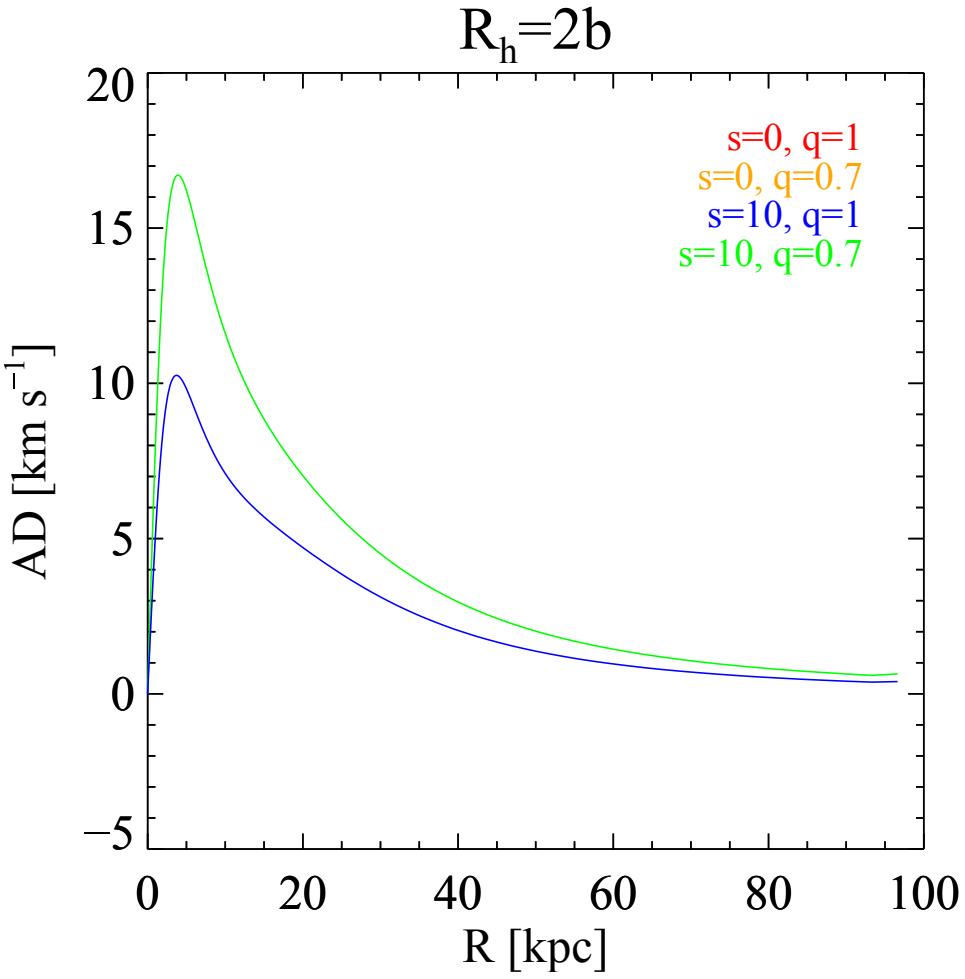

Figure 5.2: The AD in the equatorial plane for our model with $b = 2$ kpc, $M_* = 10^{11} M_\odot$, $v_\mathrm{h} = 200$ km/s, $R_\mathrm{h} = 2b$ and different values of s and q.

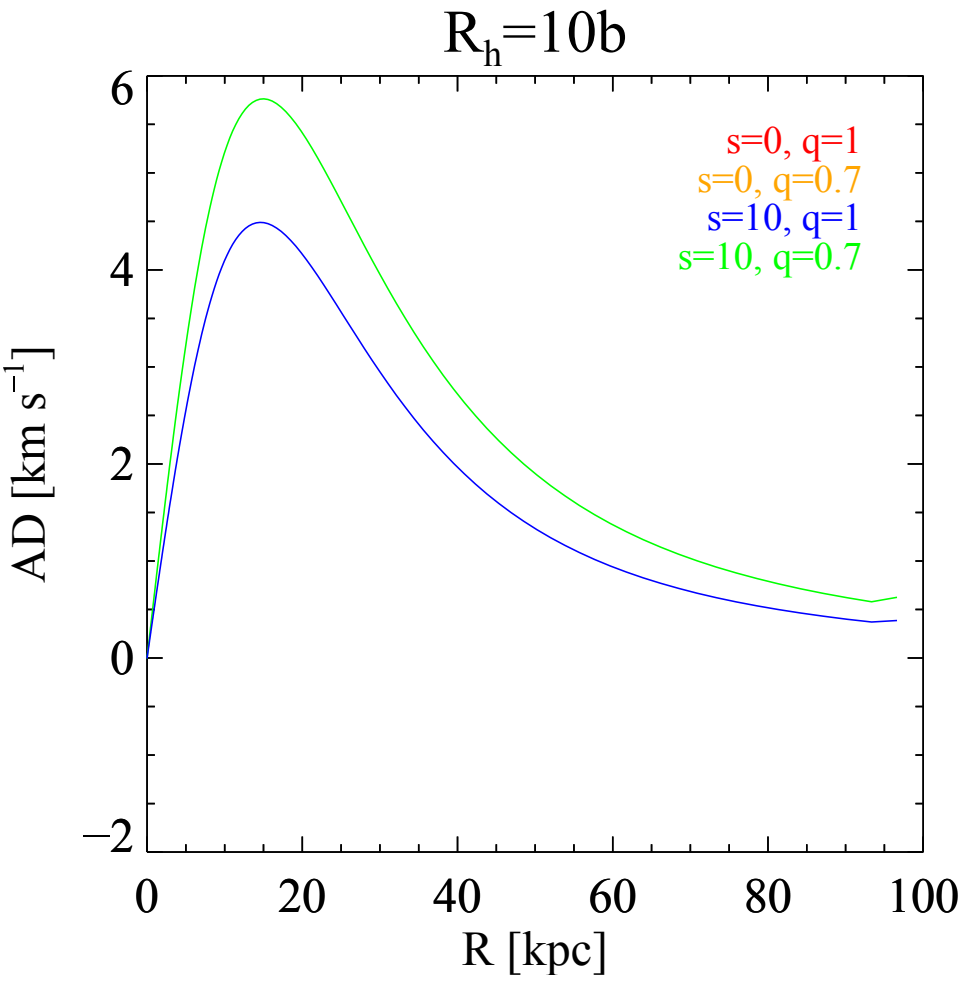

Figure 5.3: The AD in the equatorial plane for our model with $b = 2$ kpc, $M_* = 10^{11} M_\odot$, $v_\mathrm{h} = 200$ km/s, $R_\mathrm{h} = 10b$ and different values of s and q.

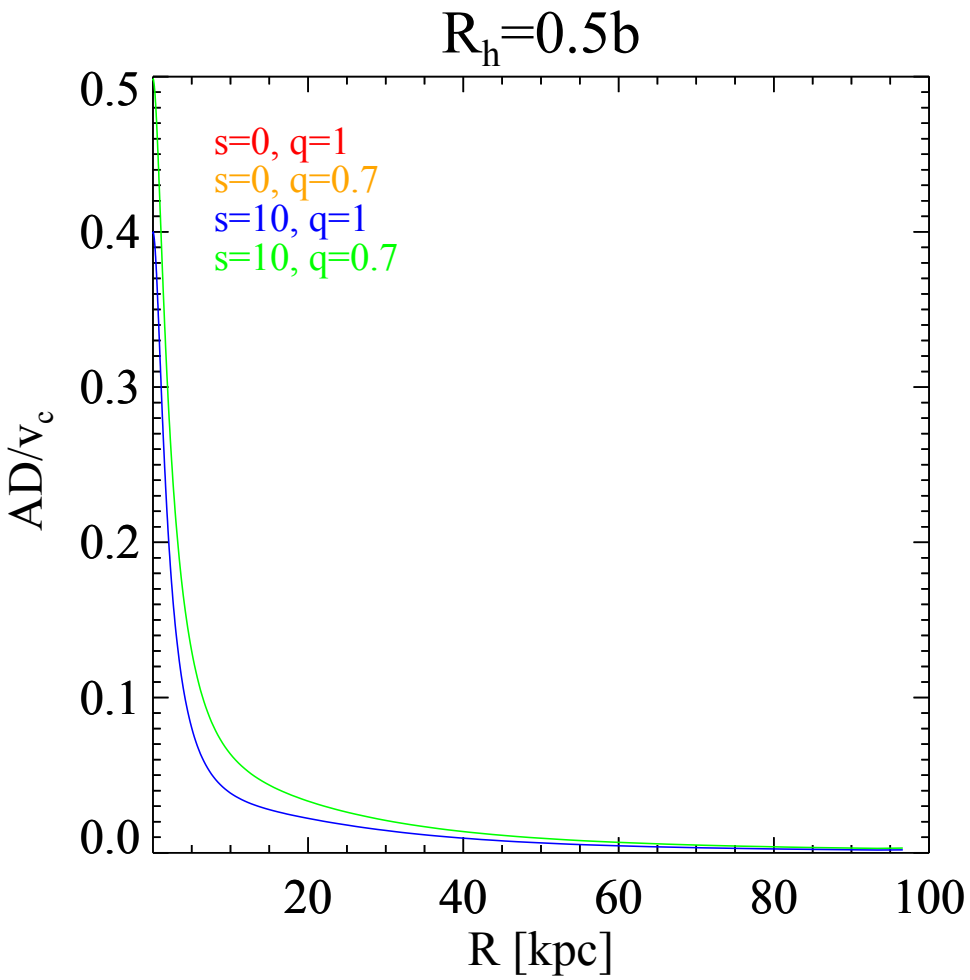

Figure 5.4: The AD/$v_{\rm circ}$ ratio in the equatorial plane for our model with $b = 2$ kpc, $M_* = 10^{11} M_\odot$, $v_{\rm h} = 200$ km/s, $R_{\rm h} = 0.5b$ and different values of s and q.

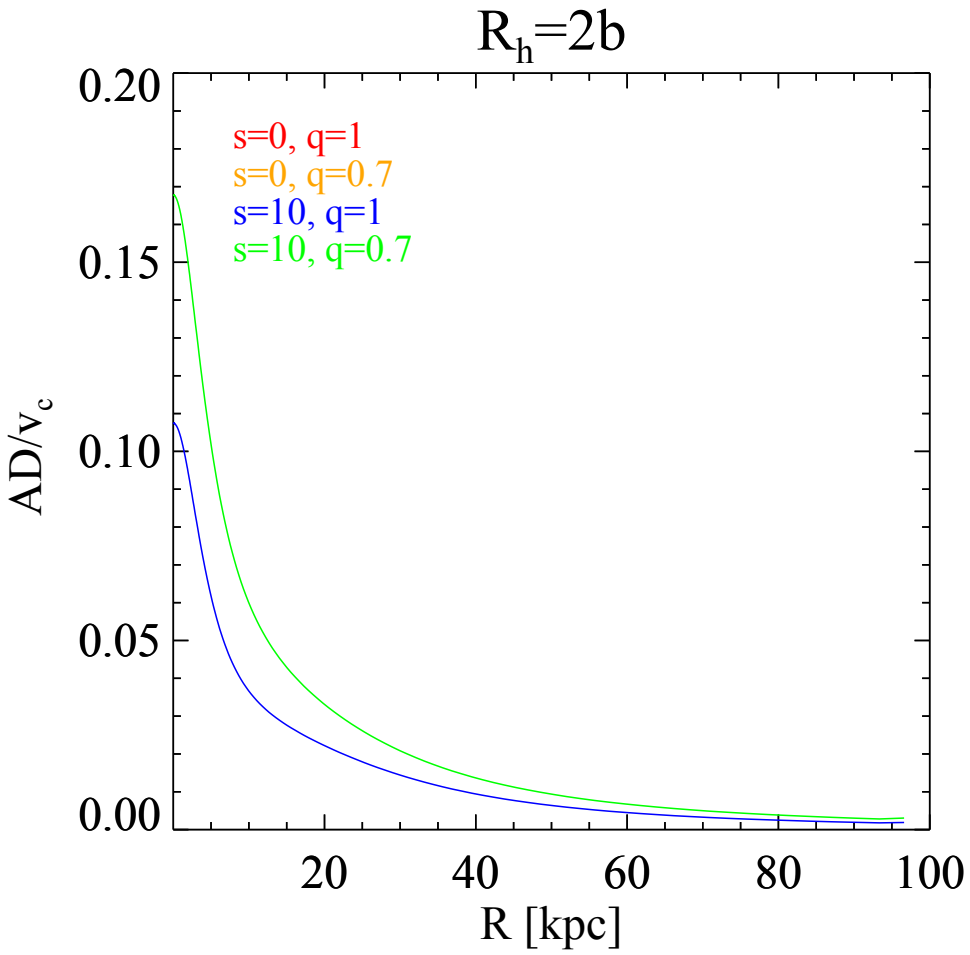

Figure 5.5: The AD/$v_{\rm circ}$ ratio in the equatorial plane for our model with $b = 2$ kpc, $M_* = 10^{11} M_\odot$, $v_{\rm h} = 200$ km/s, $R_{\rm h} = 2b$ and different values of s and q.

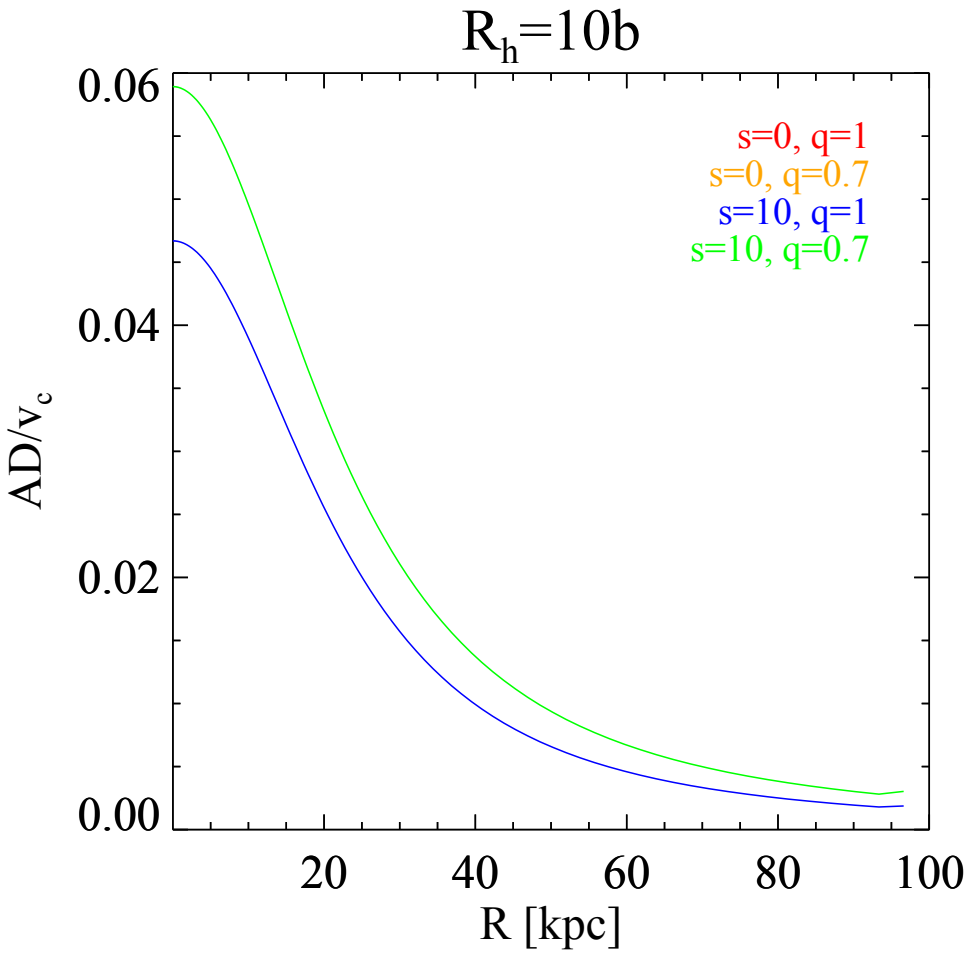

Figure 5.6: The AD/$v_{\rm circ}$ ratio in the equatorial plane for our model with $b = 2$ kpc, $M_* = 10^{11} M_\odot$, $v_{\rm h} = 200$ km/s, $R_{\rm h} = 10b$ and different values of s and q.

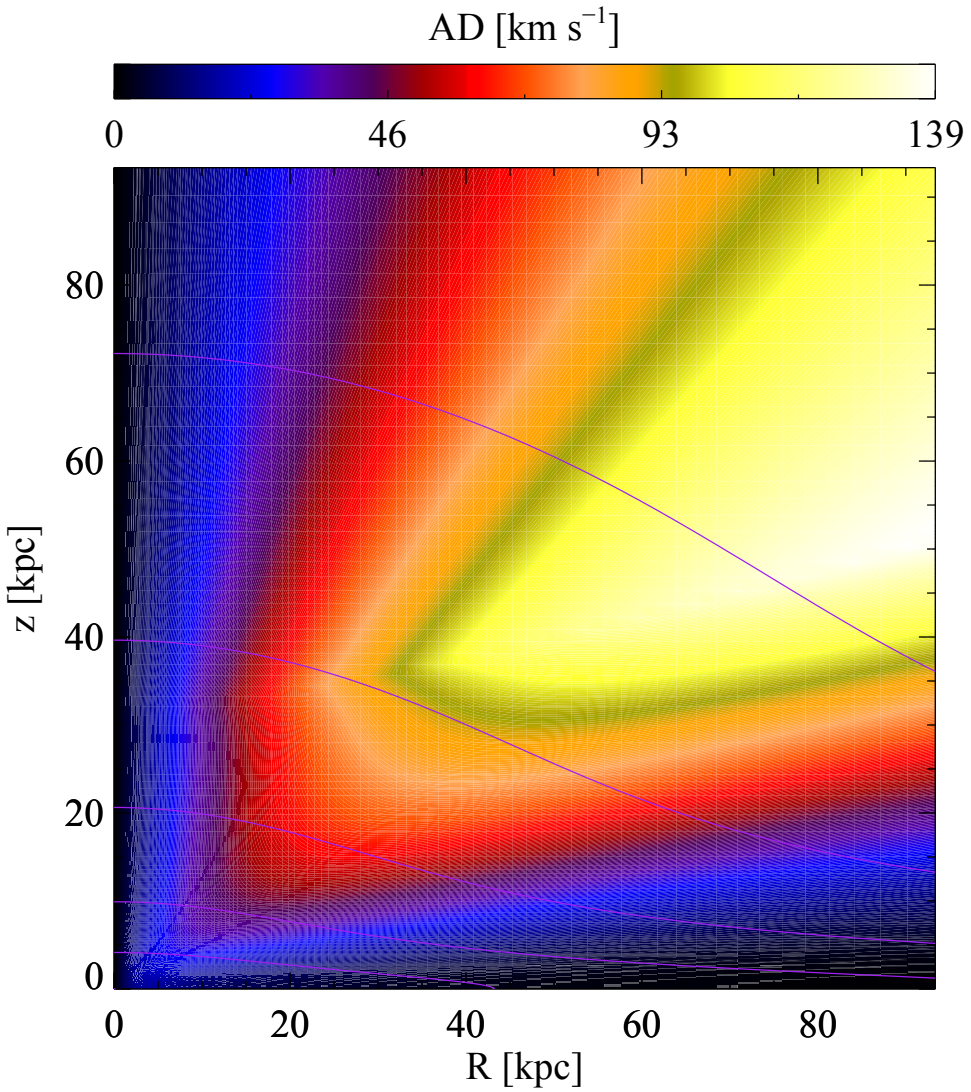

Figure 5.7: The AD in the full two-dimensional meridional plane for our model with $b = 2$ kpc, $M_* = 10^{11} M_\odot$, $v_\mathrm{h} = 200$ km/s, $R_\mathrm{h} = 2b$, $s = 10$, $q = 0.7$. Also shown (purple lines) are the isodensity lines for the stellar component.

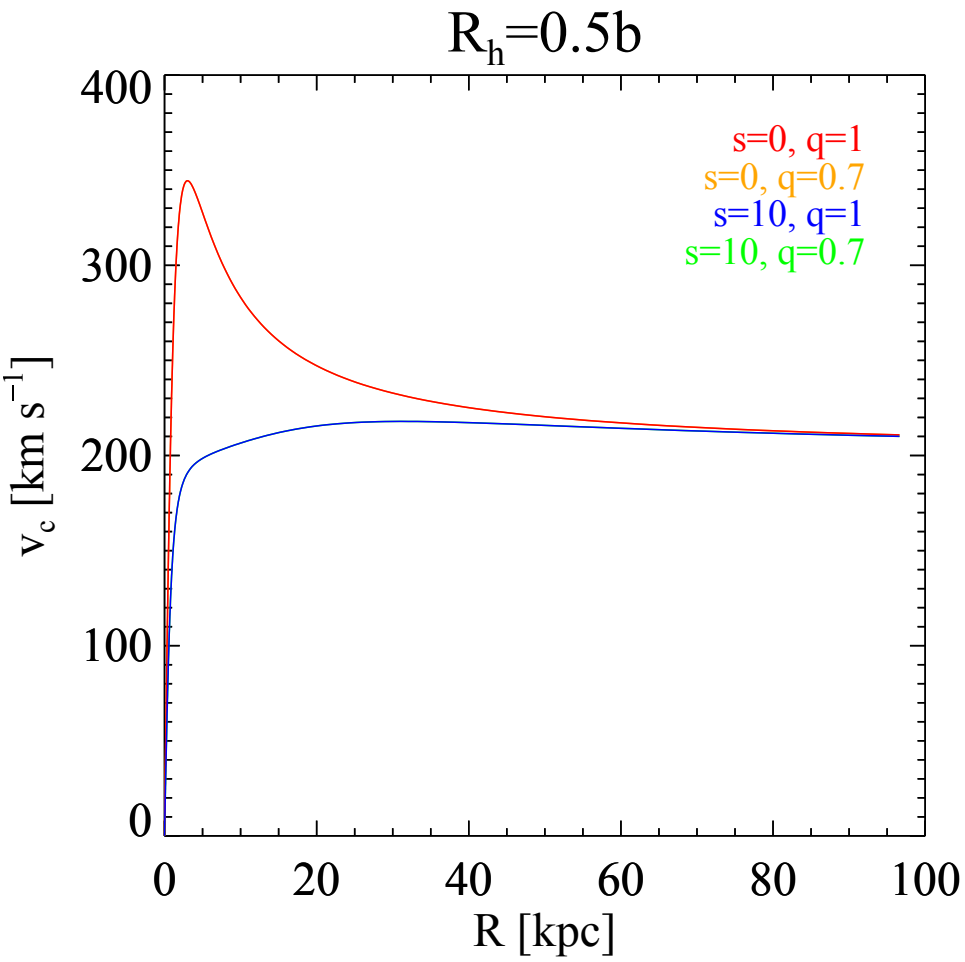

Figure 5.8: $v_{\rm circ}$ in the equatorial plane for our model with $b = 2$ kpc, $M_* = 10^{11} M_\odot$, $v_{\rm h} = 200$ km/s, $R_{\rm h} = 0.5b$ and different values of s and q.

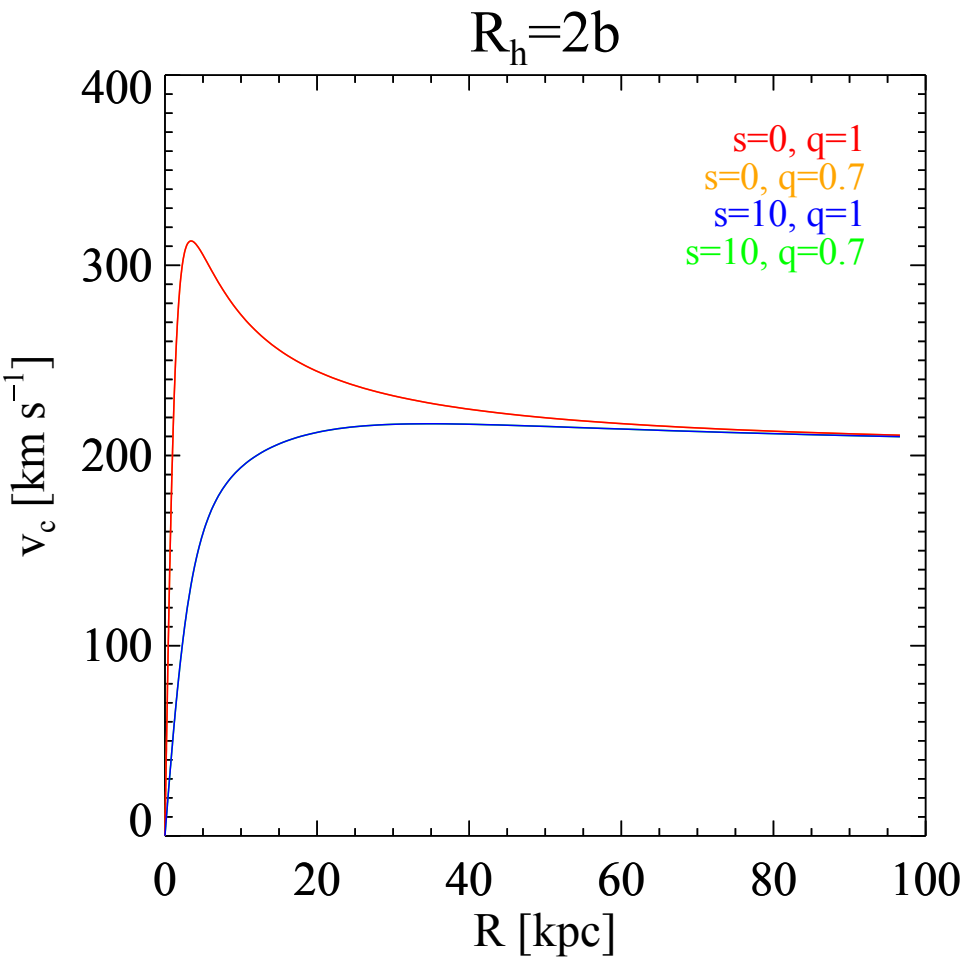

Figure 5.9: $v_{\rm circ}$ in the equatorial plane for our model with $b = 2$ kpc, $M_* = 10^{11} M_\odot$, $v_{\rm h} = 200$ km/s, $R_{\rm h} = 2b$ and different values of s and q.

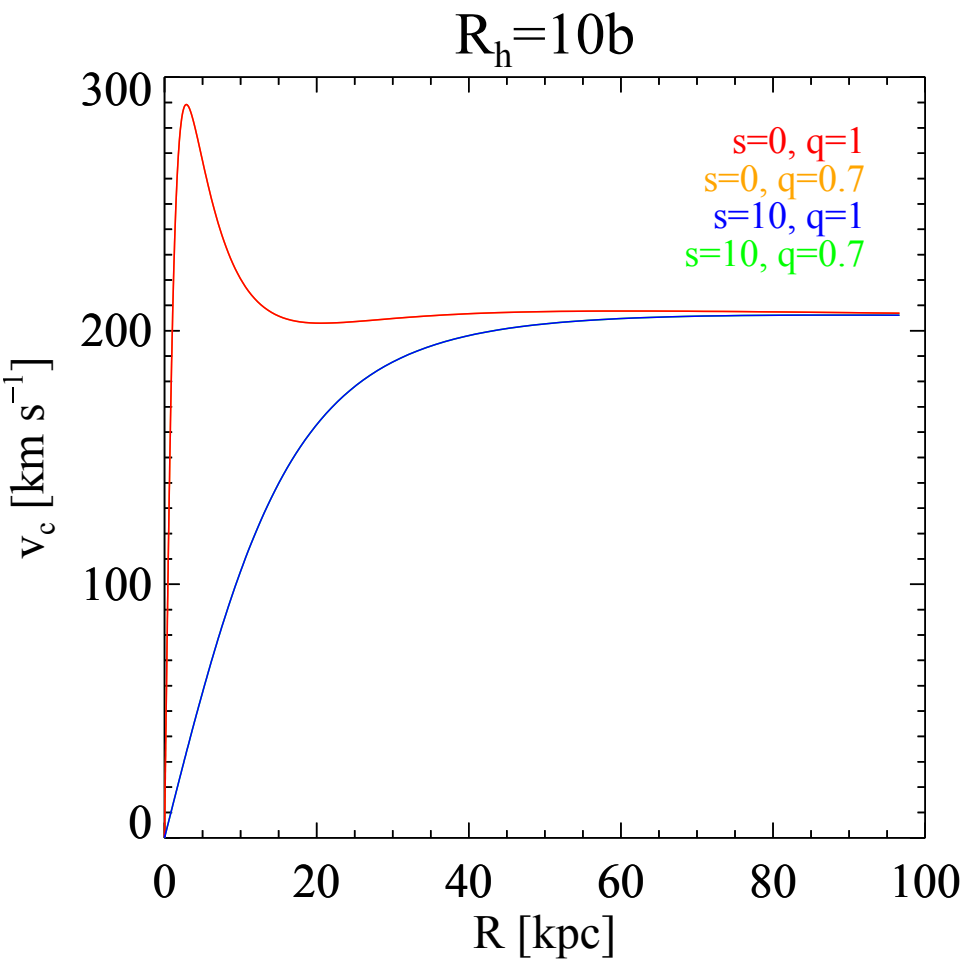

Figure 5.10: $v_{\rm circ}$ in the equatorial plane for our model with $b = 2$ kpc, $M_* = 10^{11} M_\odot$, $v_{\rm h} = 200$ km/s, $R_{\rm h} = 10b$ and different values of s and q.

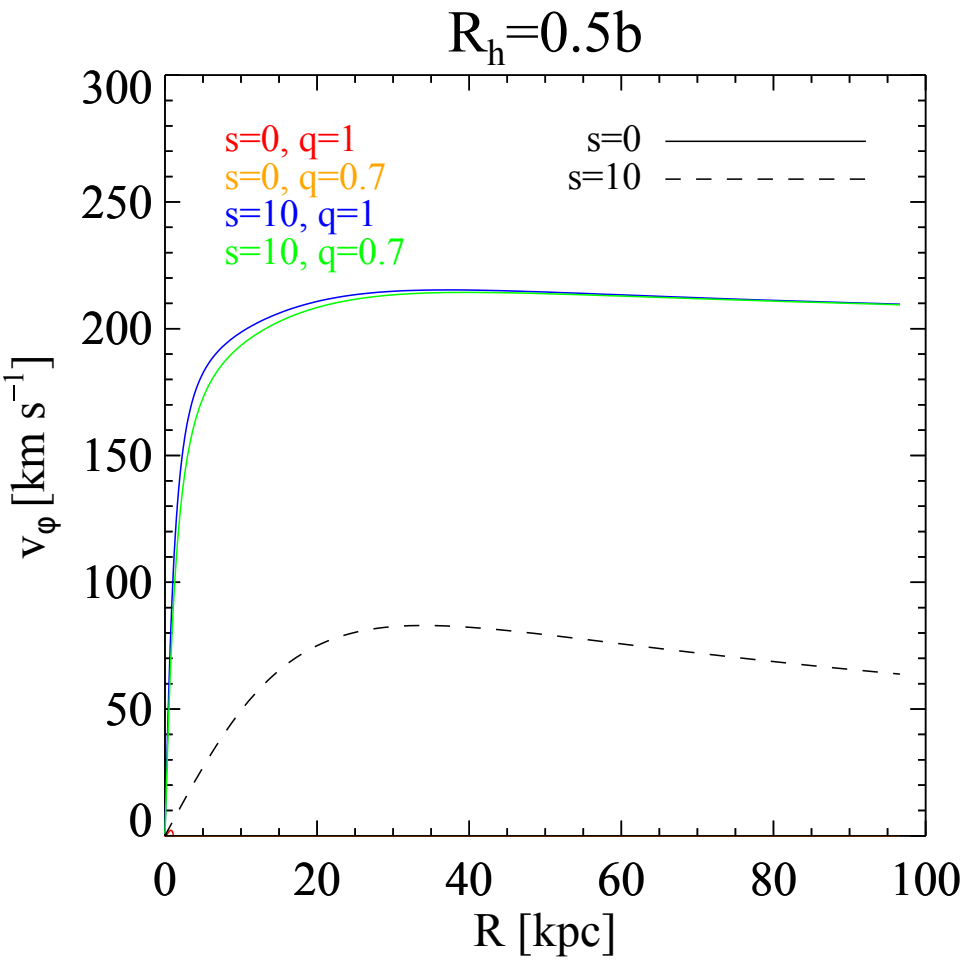

Figure 5.11: v_φ in the equatorial plane for our model with $b = 2$ kpc, $M_* = 10^{11} M_\odot$, $v_\mathrm{h} = 200$ km/s, $R_\mathrm{h} = 0.5b$ and different values of s and q.

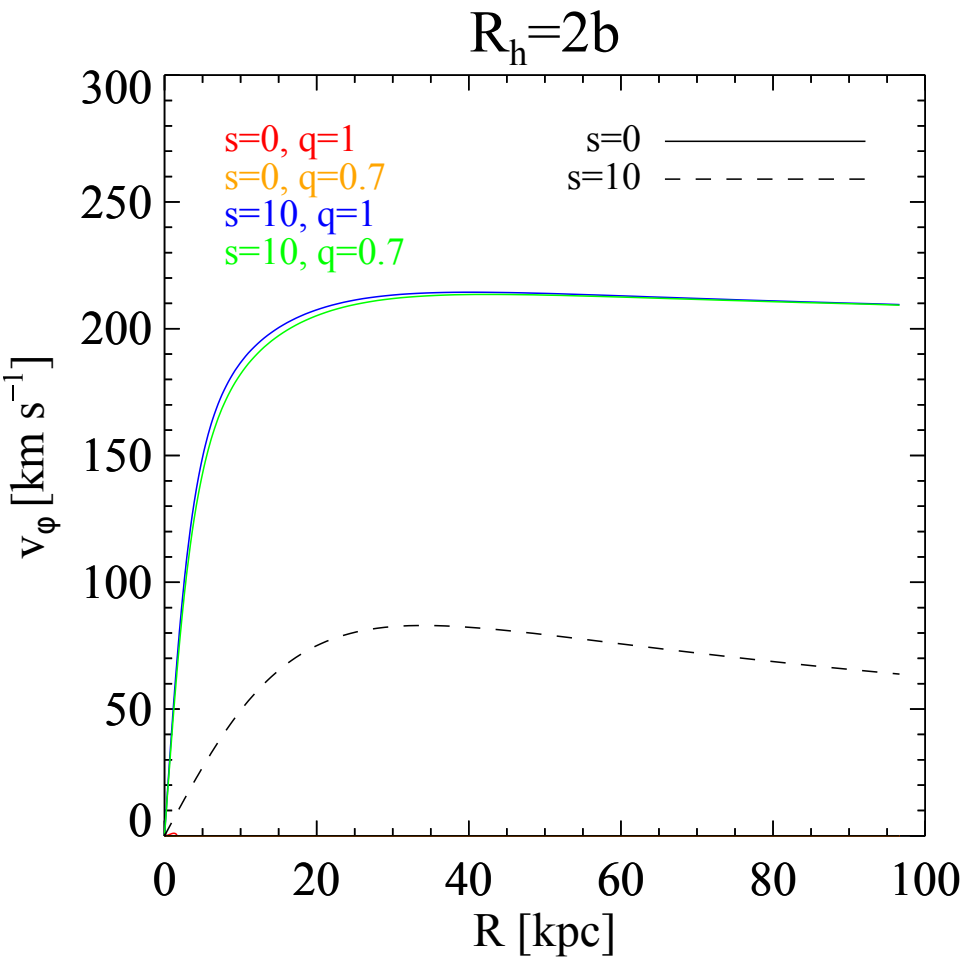

Figure 5.12: v_φ in the equatorial plane for our model with $b = 2$ kpc, $M_* = 10^{11} M_\odot$, $v_\mathrm{h} = 200$ km/s, $R_\mathrm{h} = 2b$ and different values of s and q.

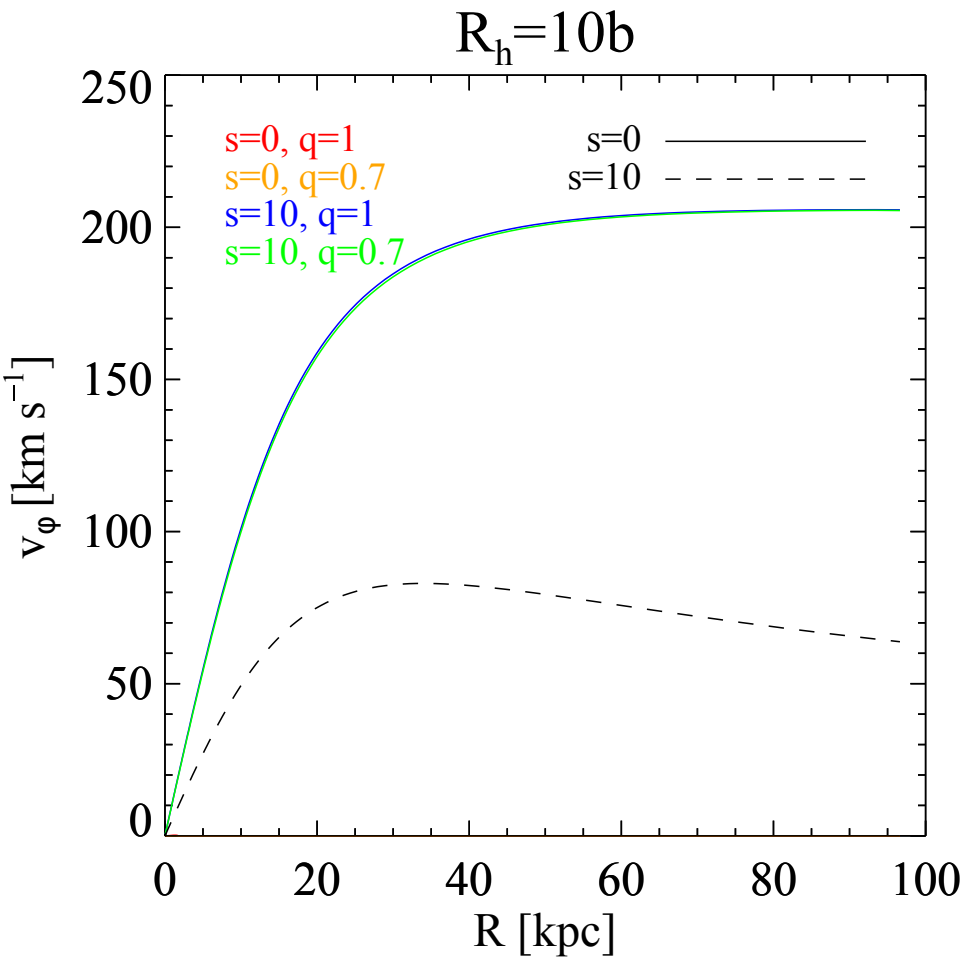

Figure 5.13: v_φ in the equatorial plane for our model with $b = 2$ kpc, $M_* = 10^{11} M_\odot$, $v_\mathrm{h} = 200$ km/s, $R_\mathrm{h} = 10b$ and different values of s and q.

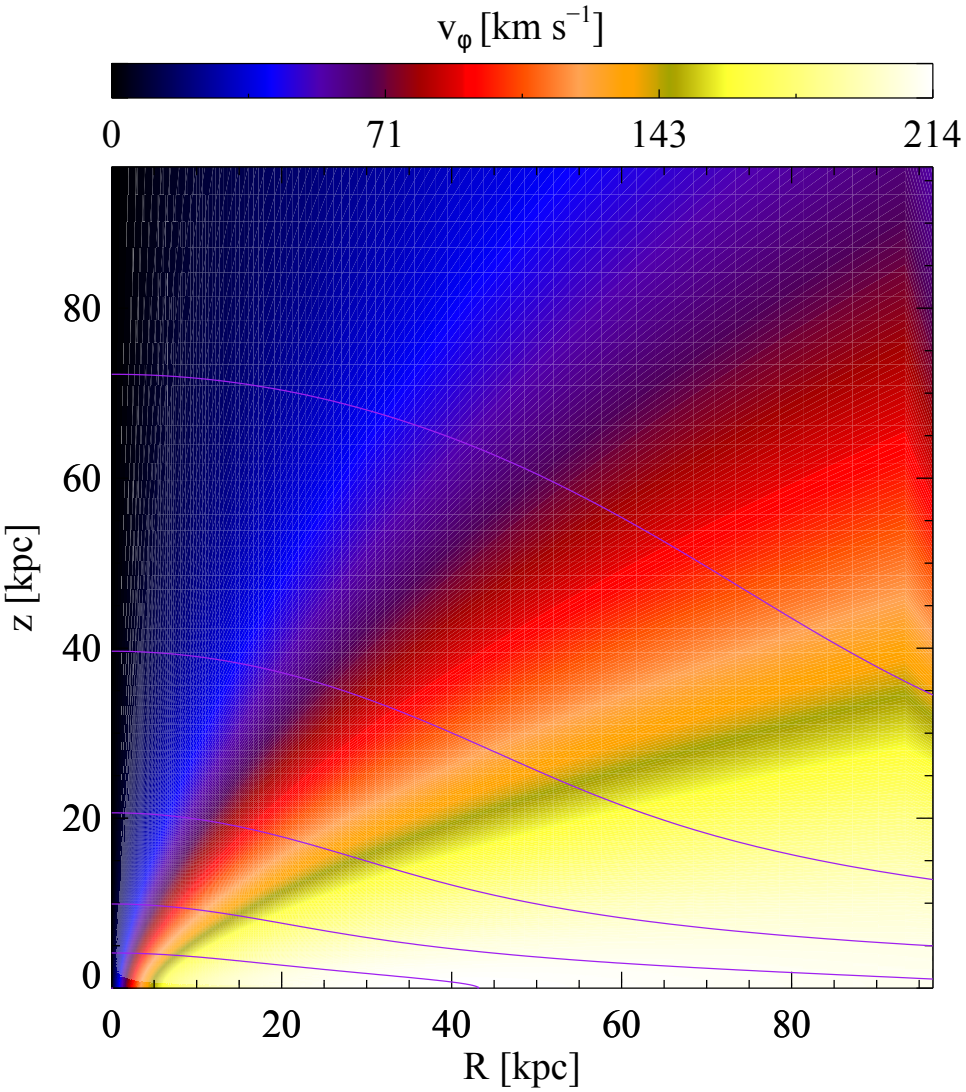

Figure 5.14: v_φ in the full two-dimensional meridional plane for our model with $b = 2$ kpc, $M_* = 10^{11} M_\odot$, $v_\mathrm{h} = 200$ km/s, $R_\mathrm{h} = 2b$, $s = 10$, $q = 1$. Also shown (purple lines) are the isodensity lines for the stellar component.

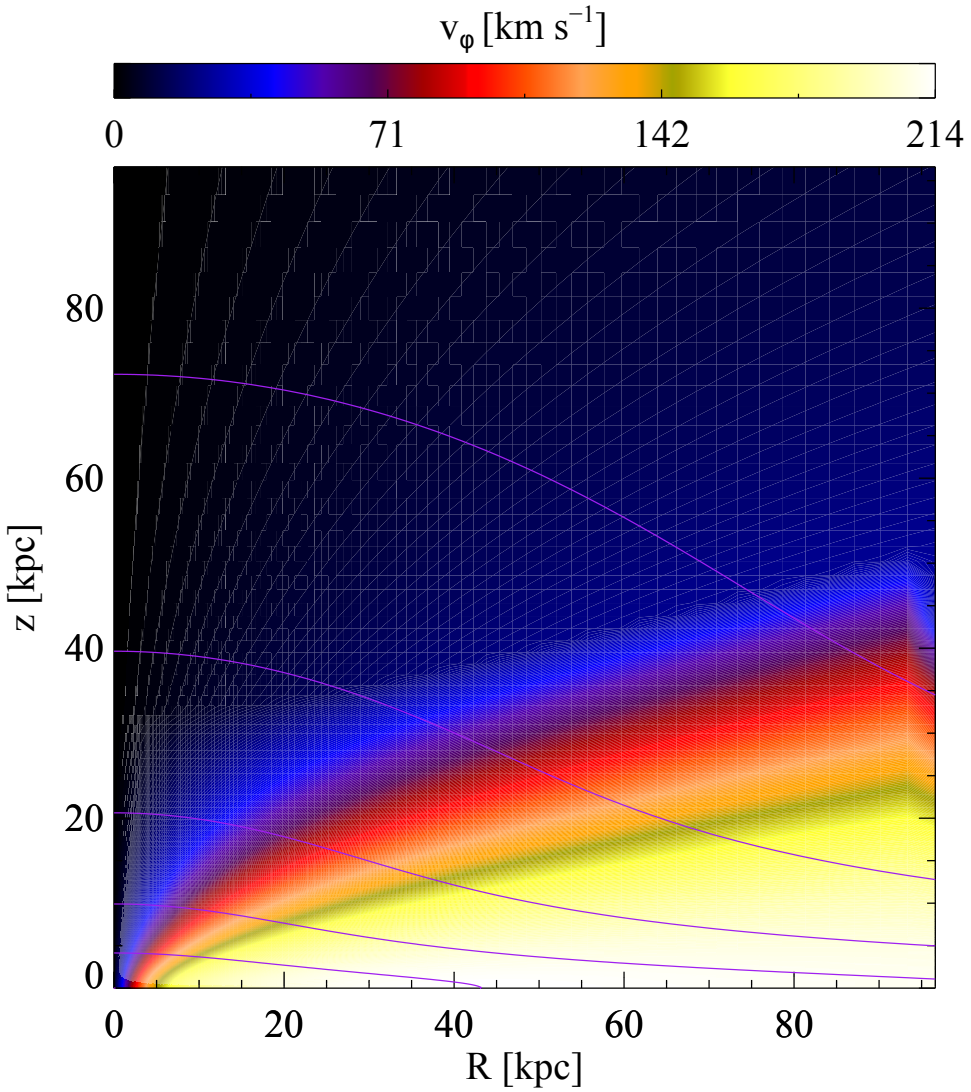

Figure 5.15: v_φ in the full two-dimensional meridional plane for our model with $b = 2$ kpc, $M_* = 10^{11} M_\odot$, $v_\mathrm{h} = 200$ km/s, $R_\mathrm{h} = 2b$, $s = 10$, $q = 0.7$. Also shown (purple lines) are the isodensity lines for the stellar component.

is some cold gas at a distance between R and $R + \Delta(R)$ from the center of the galaxy. For the sake of simplicity, we restrict ourselves to the equatorial plane. This gas follows the galaxy rotation curve.

Then some other gas, coming from stellar feedback, is added into this same region. This new gas has a lower velocity (because of the asymmetric drift) and hence a lower angular momentum. The two components mix and the resulting specific angular momentum will be a weighted average of both initial specific angular momenta.

The result will be that the mixed gas will fall inward. Let us now give an estimate of the velocity of this radial flow. Suppose the superficial density of the cold gas is given by $\sigma_0(R)$. This gas rotates at the circular velocity, hence its angular momentum is given by

$$J_0(R) = 2\pi R\Delta(R)\sigma_0(R) \cdot Rv_{\text{circ}}(R). \tag{5.9}$$

In a time interval Δt the stars inject a certain amount of gas into the interstellar medium, given by

$$M_{\text{in}} = 2\pi R\Delta(R)\dot{\sigma}(R)\Delta(t)Rv_*(R). \tag{5.10}$$

Hence the specific angular momentum after the mixing is given by

$$j(R) = \frac{R(\sigma_0 v_{\text{circ}} + \dot{\sigma}\Delta(t)v_*)}{\sigma_0 + \dot{\sigma}\Delta(t)} = j_0(R) - \frac{\dot{\sigma}\Delta(t)\text{AD}R}{\sigma_0 + \dot{\sigma}\Delta(t)}, \tag{5.11}$$

where $j_0(R) = Rv_{\text{circ}}(R)$ is the specific angular momentum of the cold gas and $\text{AD} = v_{\text{circ}} - v_*$ is the asymmetric drift.

Since AD is a positive quantity, the resulting specific angular momentum will be smaller than j_0, hence there will be inflow: gas flowing towards the more central regions. In order to make an estimate for its velocity, we can look at the first order estimate, valid for small $\Delta(t)$,

$$j(R) = j_0(R) - \text{AD}(R)\frac{R\dot{\sigma}}{\sigma_0}\Delta(t). \tag{5.12}$$

If we evaluate this for a small time step, we obtain that

$$j_0(R + \delta(R)) \sim j_0(R) + j_0'(R)\delta(R) = j_0(R) - \text{AD}(R)\frac{R\dot{\sigma}}{\sigma_0}\delta(t), \tag{5.13}$$

which gives us a formula for the infall velocity:

$$v_{\text{infall}} = -\frac{\text{AD}(R)R\dot{\sigma}}{\sigma_0 j_0'(R)}. \tag{5.14}$$

The magnitude of this effect can be estimated by plugging some typical values into this formula. Let us look at the solar neighbourhood, hence $R = 8\text{kpc}$, and let us take a typical value of $\dot{\sigma}/\sigma_0 = 10^{-9}$. For j_0' we need

the circular velocity, we assume that $v_{\rm circ} = kR^{\alpha}$ where $\alpha = 0$ describes the flat part of the rotation curve. Then $j_0' = (\alpha+1)v_{\rm circ}$. So, for the flat part of the rotation curve the only factor left to estimate is $(v_{\rm circ} - v_*)/v_{\rm circ}$ which we can estimate to be 0.1, as in Figure 5.4. These values lead to a velocity of $v_{\rm infall} \sim 1{\rm km/s}$.

This value is a typical one for this kind of radial velocities. However we want to stress that the inner effect described here cannot be the only one: the observed metallicity gradient and star formation rate strongly suggest that other mechanisms are important as well. Some of these mechanisms are the 'cosmological' radial flow (caused by inflow of extragalactic material and minor mergers) and the radial flow induced by resonance effects with the central bar [11] or with the spiral arms [28].

Chapter 6

Conclusions and discussion

We considered a galaxy density model given by a Miyamoto-Nagai model for the stellar component and a Binney logarithmic halo for the dark matter component. The latter is a generalisation of the Singular Isothermal Sphere, with the notable difference that the SIS model has a singularity at the origin (the density tends to infinity), which is in general not the case in the Binney model.

We focused on the Jeans equations, which in our axisymmetric case are reduced to only two equations. We analytically solved these and gave the asymptotic behaviour of the quantities involved, both at infinity and near the origin. Also some other observable quantities such as the asymmetric drift were discussed and calculated.

Notice that we did not include a black hole in the model. With an extra potential term to describe this black hole it is no longer possible to solve the integrals using only elementary functions. Moreover, since the Miyamoto-Nagai core is flat, the addition of a black hole is physically impossible unless all orbits are circular.

We made plots and studied the asymptotic behaviour of several physical quantities, aiming to clarify the influence of the model parameters. This kind of correlations, such as the one between the dark matter halo flattening parameter q and the asymmetric drift in the central regions, could be of interest for numerical simulations or other galaxy models.

Summarizing, we showed the following.

- We can solve the Jeans equations for the Miyamoto-Nagai model immersed in a generic Binney dark matter halo, which has the SIS as a special case. This was done for all parameter values, thus providing a lot of flexibility, e.g. from a disk galaxy to a spherical one. This model joins the other family of two-component Miyamoto-Nagai models for which the Jeans equations were solved in [6]. We also show that the solution of the Jeans equations for this model can in principle also be obtained with the Residue Theorem.

- The obtained formulae have been tested against their asymptotic expansions and also by solving the Jeans equations with the axisymmetric numerical code in [24]. The latter turned out to give results that are in excellent agreement with each oher: a relative error of the order of magnitude of 1 in 1000 between the exact solution and the solution of the numerical code. Hence this model can also be used as a test for numerical Jeans solvers.

- As a simple preliminary application of our model, we focused on the dependence of the vertical dispersion of stars in the equatorial plane on the dark matter halo flattening parameter q. We showed that the velocity dispersion increases with the flattening of the halo. As is well known, this is relevant for studies of dark matter densities in the solar neighbourhood, see e.g. [12], [4].

- In the same spirit we also investigated the behaviour of the asymmetric drift as a function of the halo properties, finding that it is a decreasing function of q: the flatter the dark matter halo, the higher the value of the asymmetric drift.

- We used our derived values for the asymmetric drift to obtain estimates on a possible new mechanism that could produce radial gas flows in disk galaxies by intrinsic methods due to mass loss of stars near the equatorial plane. Our results show that this mechanism could explain radial flows of the order of 1 km/s.

Of course the applications just mentioned and explored in a very preliminary way are just a few of many other possible applications (e.g. the study of the circular velocity of gas in the equatorial plane, the building of hydrostatic, barotropic and baroclynic models for hot rotating models [2], the setup of numerical simulations of gas flows in early-type galaxies with a proper description of thermalisation and stellar motions,...). We believe that our new model provides a significant addition to the class of known fully analytical axisymmetric models with dark matter haloes. We notice that recently two papers [9], [10] appeared with a new class of axisymmetric dark matter haloes, based on Miyamoto-Nagai-like densities. Even if we did not study the problem in depth, we feel that our method of solving the Jeans equations could work in at least some of these cases as well.

Appendix A

Derivation of the Jeans equations

We start from a general setting and afterwards we turn our attention to the spherical and axisymmetric cases.

Let f be the distribution function for the stellar content of a galaxy. This means that fd^3xd^3v is the stellar mass found at a certain position x with a certain velocity v. This f is normalized to have

$$\int_{R^6} fd^3xd^3v = M_*. \tag{A.1}$$

It follows that the density is given by

$$\rho_*(x) = \int fd^3v, \tag{A.2}$$

where the integration takes place over all velocities. Let the system be described by a Hamiltonian H. The continuity equation

$$\frac{\partial \rho_*}{\partial t} + \frac{\partial}{\partial x} \cdot (\rho_* \dot{x}), \tag{A.3}$$

which expresses the conservation of mass, leads to the collisionless Boltzmann equation

$$0 = \frac{\partial f}{\partial t} + [f, H] = \frac{\partial f}{\partial t} + \frac{\partial f}{\partial q} \cdot \frac{\partial H}{\partial p} - \frac{\partial f}{\partial p} \cdot \frac{\partial H}{\partial q}, \tag{A.4}$$

where (q, p) is any canonical set of coordinates.

A.1 Spherical case

In spherical coordinates, the Hamiltonian is given by

$$H = \frac{1}{2}\left(p_r^2 + \frac{p_\theta^2}{r^2} + \frac{p_\varphi^2}{r^2 \sin^2\theta}\right) + \Phi, \tag{A.5}$$

where

$$p_r = v_r, \qquad p_\theta = r v_\theta, \qquad p_\phi = r \sin\theta v_\varphi \tag{A.6}$$

are the moments and Φ is the total potential (in the most general case it will be the sum of potential terms caused by the baryonic matter, the dark matter and a central black hole). If we consider a steady state system with spherical symmetry, some terms vanish: all time derivatives are zero, as are the angular partial derivatives of Φ and $\partial f/\partial\varphi$. Hence we obtain

$$p_r \frac{\partial f}{\partial r} + \frac{p_\theta}{r^2}\frac{\partial f}{\partial \theta} - \left(\frac{d\Phi}{dr} - \frac{p_\theta^2}{r^3} - \frac{p_\varphi^2}{r^3 \sin^2\theta} \right) \frac{\partial f}{\partial p_r} + \frac{p_\varphi^2 \cos\theta}{r^2 \sin^3\theta}\frac{\partial f}{\partial p_\theta} = 0. \tag{A.7}$$

Now we multiply by p_r and integrate over $dp_r dp_\varphi dp_\theta$. By the divergence theorem, the last term vanishes. In the other terms the integrals can be solved by using the property of the distribution function that

$$v_j \frac{\partial f}{\partial v_i} d^3v = -\delta_{ij}\rho_*. \tag{A.8}$$

Moreover, $\overline{p_r p_\theta} = 0$ since H and J are even functions of v_r and hence so is f. Eventually we obtain

$$\frac{d(\rho\sigma_r^2)}{dr} + \rho\left(\frac{d\Phi}{dr} + \frac{2\sigma_r^2 - \overline{v_\theta^2} - \overline{v_\varphi^2}}{r} \right) = 0. \tag{A.9}$$

This equation is often rewritten as

$$\frac{d(\rho\sigma_r^2)}{dr} + 2\frac{\beta}{r}\rho\sigma_r^2 = -\rho\frac{d\Phi}{dr}, \tag{A.10}$$

where

$$\beta = \frac{2\sigma_r^2 - \overline{v_\varphi^2} - \overline{v_\theta^2}}{2\sigma_r^2} \tag{A.11}$$

is the anistropy parameter, a degree for the radial anisotropy. One can obtain only one such equation, so it is in general not possible to obtain β and σ_r from a known ρ and Φ: the equations are not closed. In the special case of an ergodic distribution function $f(H)$ however, we know that $\beta = 0$ and the equation can be solved for σ_r.

A.2 Axisymmetric case

After spherical symmetry, the next step is axisymmetry. Obviously this case is of interest when one models galaxies, which in general have rather axisymmetric than just spherical symmetry. To handle this case, we first need to

derive the Jeans equations in cylindrical coordinates. The Hamiltonian is given by

$$H = \frac{1}{2}\left(p_R^2 + \frac{p_\varphi^2}{R^2} + p_z^2\right) + \Phi, \tag{A.12}$$

where

$$p_R = v_R, \qquad p_\varphi = Rv_\varphi, \qquad p_z = v_z \tag{A.13}$$

are the moments and Φ is the total potential (in the most general case it will be the sum of potential terms caused by the baryonic matter, the dark matter and a central black hole). If we consider a steady state system with axial symmetry, the partial derivatives with respect to t and φ vanish, leading to

$$p_R\frac{\partial f}{\partial R} + p_z\frac{\partial f}{\partial z} - \left(\frac{\partial \Phi}{\partial R} - \frac{p_\varphi^2}{R^3}\right)\frac{\partial f}{\partial p_R} - \frac{\partial \Phi}{\partial z}\frac{\partial f}{\partial p_z} = 0. \tag{A.14}$$

Now we multiply by p_R and integrate over $dp_R dp_\varphi dp_z$. By the divergence theorem, the last term vanishes. In the other terms the integrals can be solved by using the property of the distribution function that

$$v_j\frac{\partial f}{\partial v_i}d^3v = -\delta_{ij}\rho_*. \tag{A.15}$$

In an analogous way, we can multiply eq. (A.14) by p_φ or by p_z, which gives us two more equations.

This gives three equations for the six second order velocity moments, hence the system is not closed (looking at even higher order moments does not solve this problem since the number of variables increases faster than the number of equations). However, if we assume that the distribution function is of the form $f(E, J_z)$, further simplifications can be made: (1) the velocity dispersion tensor is aligned with the coordinate system, i.e. $\overline{v_R v_z} = \overline{v_R v_\varphi} = \overline{v_\varphi v_z} = 0$; (2) the radial and vertical velocity dispersions are equal, i.e. $\sigma_R = \sigma_z \equiv \sigma$; (3) the only possible non-zero streaming motion is in the azimuthal direction.

This leads to the following two equations, known as the Jeans equations in the axisymmetric case. There are only two because the third one vanishes completely.

$$\frac{\partial \rho_* \sigma^2}{\partial z} = -\rho_*\frac{\partial \Phi_\mathrm{t}}{\partial z} \tag{A.16}$$

and

$$\frac{\partial \rho_* \sigma^2}{\partial R} + \rho_*\frac{\sigma^2 - \overline{v_\varphi^2}}{R} = -\rho_*\frac{\partial \Phi_\mathrm{t}}{\partial R}. \tag{A.17}$$

Appendix B

A simple ellipsoidal model

In order to illustrate the central behaviour of the Miyamoto-Nagai model velocity dispersion as a function of the halo properties, we give here the solution for a simple toy model, obtained by superimposing to the Binney logarithmic halo an ellipsoidally stratisfied beta model with stellar density

$$\rho_* = \frac{\rho_{0*} m_0^\beta}{(R^2 + \frac{z^2}{p^2} + m_0^2)^{\beta/2}}, \tag{B.1}$$

where m_0 is a scale length. Then the first Jeans equation gives

$$\rho_* \sigma_{*\mathrm{h}}^2 = \int_z^\infty \rho_* \frac{\partial \Phi_\mathrm{h}}{\partial z} dz = \rho_{0*} m_0^\beta v_\mathrm{h}^2 p^\beta I. \tag{B.2}$$

This can be solved for general positive β:

$$I = \frac{(z^2 + C)^{1-\frac{\beta}{2}}}{\beta(z^2 + B)} \, {}_2F_1 \left(1, 1; 1 + \frac{\beta}{2}; \frac{B - C}{z^2 + B}\right) \tag{B.3}$$

with

$$B = q^2(R^2 + R_\mathrm{h}^2); \qquad C = p^2(R^2 + m_0^2). \tag{B.4}$$

In specific cases this result can be simplified: if $B = C$ (and so in particular in the singular case where $R_\mathrm{h} = m_0 = 0$) we find that

$$I = \frac{1}{\beta}(z^2 + B)^{-\beta/2}. \tag{B.5}$$

When $B = C$ and $\beta = 3$ we are in the case discussed in [4].

Also if $B \neq C$ but β is an integer the result can be written in elementary functions, e.g. if $\beta = 2$ then

$$I = \frac{1}{2(C - B)} \ln \frac{z^2 + C}{z^2 + B}, \tag{B.6}$$

if $\beta = 4$ then

$$I = -\frac{1}{2(C-B)(z^2+C)} + \frac{1}{2(C-B)^2} \ln \frac{z^2+C}{z^2+B}. \tag{B.7}$$

If $R_{\rm h} = 0$ and $m_0 > 0$ then the behaviour near the origin is given by

$$I \sim -(pm_0)^{-\beta} \ln \sqrt{z^2 + q^2 R^2} \tag{B.8}$$

and hence

$$\sigma^2_{*{\rm h}} \sim -v^2_{\rm h} \ln \sqrt{z^2 + q^2 R^2}, \tag{B.9}$$

reminiscent of the behaviour in eq. (4.1). If $R_{\rm h} > 0$ and $m_0 = 0$ then there is divergence at the origin if $\beta \geq 2$.

Acknowledgments

First of all, I would like to thank my supervisor, prof. Luca Ciotti. Thank you for the support, the interesting discussions, the useful references and so on.

Also many thanks to Silvia Posacki, my co-supervisor for helping me out with the beautiful figures that are vital to this thesis. Good luck with the rest of your PhD!

Of course I also need to thank my fellow students for creating a nice atmosphere and for making me feel accepted, even if I understood only half of your conversations (and that is a mild estimate which could be off for some orders of magnitude). I won't write down your names here, because, as Tiziana taught me, it is quite dangerous if you forget one.

I certainly should not forget the friends at home, former colleagues and former fellow students in the Italian class. It was nice to keep in contact online and at the times I was back in Belgium. But obviously a special mention goes to Klaas and Geertrui for coming to visit me in Bologna, I hope I was able to show you what a nice city it really is.

Nor should I forget the people at the place that was my home for the last two years, the ones with whom I shared my apartment: Federica, Sandro and Aida.

A big thank you certainly goes to my parents, who supported me all the way through this two-year adventure. You probably had some doubts in the beginning, but I am glad I did this, so thanks a lot for being there for me!

And finally, a message to two persons who cannot yet read: my godchildren Jits and Olivia. I certainly hope to see you and your wonderful parents a bit more often in the near future, and perhaps one day I can tell you all about the marvellous universe we live in.

Bibliography

[1] J. Bailin and M. Steinmetz (2005), *Internal and external alignment of the shapes and angular momenta of ΛCDM halos*, The Astrophysical Journal **627**, 647.

[2] M. Barnabè, L. Ciotti, F. Fraternali and R. Sancisi (2006), *Hydrostatic models for the rotation of extra-planar gas in disk galaxies*, Astronomy and Astrophysics **446**, 61.

[3] G. Bertin (2000), *Dynamics of Galaxies*, Cambridge University Press.

[4] J. Binney and S. Tremaine (2008), *Galactic Dynamics (Second Edition)*, Princeton University Press.

[5] L. Ciotti, A. D'Ercole, S. Pellegrini and A. Renzini (1991), *Winds, outflows, and inflows in elliptical X-ray galaxies*, The Astrophysical Journal **376**, 380.

[6] L. Ciotti and S. Pellegrini (1996), *The energetics of flat and rotating early-tipe galaxies and their X-ray luminosity*, Monthly Notices of the Royal Astronomical Society **279**, 240.

[7] J. Dubinski and R. G. Carlberg (1991), *The structure of cold dark matter halos*, The Astrophysical Journal **378**, 496.

[8] N. W. Evans (1993), *Simple galaxy models with massive haloes*, Monthly Notices of the Royal Astronomical Society **260**, 191.

[9] N. W. Evans and A. Bowden (2014), *Extremely flat haloes and the shape of the galaxy*, submitted to Monthly Notices of the Royal Astronomical Society, Arxiv: 1406.3710.

[10] N. W. Evans and A. A. Williams (2014), *A very simple cusped halo model*, submitted to Monthly Notices of the Royal Astronomical Society, Arxiv: 1406.3730.

[11] D. Friedli, W. Benz and R. Kennicutt (1994), *On the influence of bars and star formation on galactic abundance gradients*, The Astrophysical Journal **430**, L105.

[12] G. Gilmore, I. R. King and P. C. van der Kruit (1990), *The Milky Way as Galaxy*, University Science Books.

[13] K. Hayashi and M. Chiba (2014), *The prolate dark matter halo of the Andromeda galaxy*, submitted.

[14] C. Hermite (1872), *Sur l'intègration des fractions rationelles*, Annales de Mathématiques, $2^{\text{ème}}$ série, **11**, 145.

[15] J. H. Jeans (1919), *The configurations of Rotating Compressible Masses*, Philosophical Transactions of the Royal Society A **218**, 157.

[16] G. G. Kuzmin (1956), *Model of the stationary Galaxy allowing three-axial distribution of velocities*, Astronomicheskii Zhurnal **33**, 27.

[17] D. Lynden-Bell (1962), *Exact Solution of the Self-Gravitation Equation*, Monthly Notices of the Royal Astronomical Society **123**, 447.

[18] M. Miyamoto and R. Nagai (1975), *Three-dimensional models for the distribution of mass in galaxies*, Publications of the Astronomical Society of Japan **27**, 533.

[19] R. Nagai and M. Miyamoto (1976), *A family of self-gravitating stellar systems with axial symmetry*, Publications of the Astronomical Society of Japan **28**, 1.

[20] A. Negri, L. Ciotti and S. Pellegrini (2014), *The effect of stellar dynamics on the X-ray emission of flat early-type galaxies*, Monthly Notices of the Royal Astronomical Society **439**, 823.

[21] A. Negri, S. Posacki, S. Pellegrini and L. Cioti (2014), *The effects of galaxy shape and rotation on the X-ray haloes of early-type galaxies - II. Numerical simulations*, submitted to Monthly Notices of the Royal Astronomical Society, Arxiv 1406.0008.

[22] S. Pellegrini (2011), *The Temperature of Hot Gas Halos of Early-type Galaxies*, The Astrophysical Journal **738**, 57.

[23] H. C. Plummer (1911), *On the problem of distribution in globular star clusters*, Monthly Notices of the Royal Astronomical Society **71**, 460.

[24] S. Posacki, S. Pellegrini and L. Ciotti (2013), *The effects of flattening and rotation on the temperature of the X-ray halos of elliptical galaxies*, Memorie della Società Astronomica Italiana **84**, 766.

[25] S. Posacki, S. Pellegrini and L. Ciotti (2014), *The effects of galaxy shape and rotation on the X-ray haloes of early-type galaxies*, accepted for publication in Monthly Notices of the Royal Astronomical Society, Arxiv: 1304.4085.

[26] J. I. Read (2014), *The local dark matter density*, submitted.

[27] C. Satoh (1980), *Dynamical Models of Axisymmetric Galaxies and Their Applications to the Elliptical Galaxy NGC4697*, Publications of the Astronomical Society of Japan, **32**, 41.

[28] J. A. Sellwood and J. J. Binney (2002), *Radial mixing in galactic discs*, Monthly Notices of the Royal Astronomical Society **336**, 785.

[29] C. Smet, S. Posacki and L. Ciotti (2014), *The analytical solution of the two-integral Jeans equations for the Miyamoto-Nagai disk embedded in the Binney logarithmic potential*, in preparation.

[30] E. C. Titchmarsh (1932), *The Theory of Functions*, Oxford University Press.